UNIVERSITY OF CALIFORNIA SAN DIEGO

Dissecting the Role of Theta Oscillations in Memory and in Coordinating Spike Timing of Hippocampus and Medial Entorhinal Cortex

A dissertation submitted in partial satisfaction of the requirements
for the degree Doctor of Philosophy

in

Biology

by

Clare Renee Quirk

Committee in charge:

Professor Stefan Leutgeb, Chair
Professor Brenda Bloodgood
Professor Jill Leutgeb
Professor Mark Mayford
Professor Douglas Nitz

2019

The Dissertation of Clare Renee Quirk is approved, and it is acceptable in quality and form for publication on microfilm and electronically:

Chair

University of California San Diego

2019

DEDICATION

To Matthew Robertson and to Charles, Seamus, and Suzanne Quirk for all of your love and support.
To my beautiful cats, Boycat and Girlcat.

TABLE OF CONTENTS

LIST OF ABBREVIATIONS

AP	Anterior-posterior
CA	Cornu ammonis
CDF	Cumulative density function
DG	Dentate gyrus
DV	Dorsal-ventral
EC	Entorhinal cortex
HD	Head direction
IACUC	Institutional animal care and use committee
lEC	Lateral entorhinal cortex
LFP	Local field potential
LTP	Long term potentiation
mEC	Medial entorhinal cortex
ML	Medial-lateral
MS	Medial septum
MTL	Medial temporal lobe
Ns	Non-significant
PARASUB	Parabubiculum
PFC	Prefrontal cortex
PRESUB	Presubiculum
PV	Parvalbumin
SEM	Standard error mean

SUB Subiculum

SWR Sharp wave ripple

LIST OF FIGURES

LIST OF TABLES

ACKNOWLEDGEMENTS

I would like to thank Matthew Robertson, who has not only been there for me with emotional support but also helped me with every programming problem I came into. He helped write code for me countless times when I felt completely stuck and could not figure anything out. He is the most brilliant person I know. I would not have been able to get through this stage of my life without him. Being able to talk to him every day made me unbelievably happy.

I would also like to thank my parents Charles and Suzanne, my brother Seamus, and my sister-in-law Yun, who have all been there for me. My parents have constantly encouraged me to complete my Ph.D. when it seemed challenging. They have encouraged me to pursue the next stage of my career even though the idea of changing careers away from academia has been difficult. Seamus has been the best brother and my best friend and I'm glad that we get along so well and that I have him in my life. I would also like to thank my uncle, Mark Yeckel, a fellow neuroscientist, who always had great advice.

I would like to thank my advisor, Stefan Leutgeb, who has taught me how to think like a scientist. Stefan has challenged me throughout my Ph.D. to ask tough questions and to do research that no one else was doing because of the difficulty in asking these questions. His encouragement helped me to continue and his support and guidance helped me complete this dissertation. He acted as an ideal scientific role model and always welcomed the results I obtained even when they were contrary to our hypothesis. He also encouraged me to pursue whatever career path I want to take and was always supportive.

I am fortunate to have received not only his guidance, but the guidance of Jill Leutgeb who has been there to ask the difficult questions and always gave her time and full attention to me. She helped shape the research I did with her valuable comments and feedback. I would also like to thank all of my thesis committee members – Douglas Nitz, Mark Mayford, and Brenda Bloodgood for their fundamental role in guiding not only my research projects but also my career.

None of my research would have been possible if I had done this work alone. I had an amazing team of undergraduate and Masters students that were exceptionally intelligent and diligent. I would like to thank Nick Corson, Morgan Wright, Darian Parsey, Ashay Patel, Hongzhe Yu, and Naomie Devico Marciano for all of the work they've done. Their hard work led to the data presented in this dissertation and I could not have done this without them.

I would also like to thank all of the members of my lab who have helped me including Ipshita Zutshi, Sunandha Srikanth, Antonia Schonwald, Siavash Ahmadi, Maylin Fu, Gecelle de Guia, Mark Brandon, Marta Sabariego-Collett, Silvia Viana da Silva, Chris Luong, Gabby Suarez, Kshitij Gaur, and Olivia Hon. I would also like to acknowledge my friends especially Stefania di Costanzo and Lara Labarta Bajo who I met on the first day of grad school and we have been close friends ever since. I would like to thank the people we have collaborated with on other projects – Robert Pulido, Richard Daneman, Anja Payne, and Brenda Bloodgood.

I was fortunate to have received two fellowships during my Ph.D. including the Ruth Stern Graduate Fellowship. I would like to thank Ruth Stern for her generosity that

allowed me to travel to conferences and present my research in Chicago, Austria, and Canada. I would not have been able to have those amazing experiences without this fellowship. I would also like to thank the Biological Sciences program that awarded me with the Cellular and Molecular Genetics Training Grant that provided my funding for several years of my Ph.D. I would especially like to thank the CMG coordinators- Professors Randy Hampton, Amy Pasquinelli, and Debbie Yelon.

I would like to thank Varoth Lilascharoen, Eric Wang, and Byungkook Lim for providing our lab with the viruses that allowed us to successfully perform these experiments. I would like to thank Kiana Miyamoto and Cory Root for helping me by allowing me to use their microscope.

Chapter 2, in full, is material that is unpublished and being prepared for publication. It is coauthored by Quirk, Clare R., Zutshi, Ipshita, Srikanth, Sunandha, Wright, Morgan K., Parsey, Darian F., Devico Marciano, Naomie, Liu, Stanley, Fu, Maylin L., Leutgeb, Jill K., and Leutgeb, Stefan. The dissertation author was the primary researcher and author of this material.

Chapter 3, in full, is material that is unpublished and being prepared for publication. It is coauthored by Quirk, Clare R., Zutshi, Ipshita, Srikanth, Sunandha, Wright, Morgan K., Parsey, Darian F., Devico Marciano, Naomie, Liu, Stanley, Fu,

Maylin L., Leutgeb, Jill K., and Leutgeb, Stefan. The dissertation author was the primary researcher and author of this material.

Chapter 4, in full, is material that is unpublished and being prepared for publication. It is coauthored by Quirk, Clare R., Zutshi, Ipshita, Srikanth, Sunandha, Wright, Morgan K., Parsey, Darian F., Devico Marciano, Naomie, Liu, Stanley, Fu, Maylin L., Leutgeb, Jill K., and Leutgeb, Stefan. The dissertation author was the primary researcher and author of this material.

Chapter 5, in full, is material that is unpublished and being prepared for publication. It is coauthored by Quirk, Clare R., Zutshi, Ipshita, Srikanth, Sunandha, Wright, Morgan K., Parsey, Darian F., Devico Marciano, Naomie, Liu, Stanley, Fu, Maylin L., Leutgeb, Jill K., and Leutgeb, Stefan. The dissertation author was the primary researcher and author of this material.

VITA

2013 Bachelor of Science, University of California Irvine, USA
2019 Doctor of Philosophy, University of California San Diego, USA

PUBLICATIONS

Quirk, C.R., Zutshi, I., Srikanth, S., Wright, M.K., Parsey, D.F., Devico Marciano, N., Liu, S., Fu, M.L., Leutgeb, J.K., Leutgeb, S. (*in prep*). Optogenetic Disruption of Theta Frequency Alters Spike Timing in the Entorhino-Hippocampal Circuit and Impairs Spatial Working Memory.

Pulido, R.S., Munji, R.N., Chan, T.C., Quirk, C.R., Weiner, G.A., Weger, B.D., Elmsaouri, S., Malfavon, M., Gachon, F., Leutgeb, S., Daneman, R. (*in revision*) Neural activity regulates bloodbrain barrier efflux transport through endothelial circadian genes. *Neuron*

FIELDS OF STUDY

Major Field: Biological Sciences
Studies in Biological Sciences, Ph.D.
Professor Stefan Leutgeb

Major Field: Biological Sciences
Studies in Neurobiology, B.Sc.

ABSTRACT OF THE DISSERTATION

Dissecting the Role of Theta Oscillations in Memory and in Coordinating Spike Timing of Hippocampus and Medial Entorhinal Cortex

by

Clare Renee Quirk

Doctor of Philosophy in Biology

University of California San Diego, 2019

Professor Stefan Leutgeb, Chair

Rhythmic oscillations are prominent features of information processing in neuronal circuits that have been linked to cognitive processing. Neuronal oscillations, including theta oscillations (6-9 Hz), have been hypothesized to indicate accurate timing of neuronal activity within and across a system of brain regions including the

hippocampus, medial entorhinal cortex, and prefrontal cortex. Disruption to oscillatory activity has been shown to cause severe disruptions in the ability to form and retrieve memories. This has led to the hypothesis that oscillatory activity and precisely timed neuronal activity is necessary for memory.

Theta (6-9 Hz) oscillations are generated by subcortical pacemaker cells in the medial septum that are GABAergic and express parvalbumin and exhibit rhythmic bursting that is phase-locked to theta. We used optogenetic techniques to target these GABAergic parvalbumin cells in the medial septum in order to precisely manipulate theta frequency. Using this technique, we thoroughly tested how the spike timing of individual cells within the entorhinal-hippocampal circuit is altered when oscillatory activity is modulated. We found that cells within the entorhinal-hippocampal became entrained to the altered theta frequency and also exhibited accelerated oscillatory frequencies that were not seen in baseline conditions.

Damage to the medial septum and its subsequent reduction in theta amplitude results in substantial impairments in hippocampal-dependent memory. However, reductions in theta amplitude by medial septal inactivation also cause large reductions in the firing rates of hippocampus and medial entorhinal cortex neurons. Therefore, it has been difficult to show whether theta oscillations themselves are critical for memory or whether effects on memory are due to other factors such as a reduction in firing rate. We therefore tested whether slightly offsetting the timing of theta oscillations is important for episodic memory and found that even a minor acceleration in theta frequency was sufficient to disrupt memory.

Overall, the results presented in this dissertation provide novel insights into the role of oscillations in controlling the spike timing of cells within the hippocampus and medial entorhinal cortex and directly show a role for oscillatory timing in spatial working memory.

Chapter I.

INTRODUCTION

Anatomy of the medial temporal lobe

The medial temporal lobe (MTL) is composed of several structures including the hippocampus (HC), entorhinal cortex (EC), perirhinal cortex, and the parahippocampal cortices (Amaral and Witter 1989, Squire and Zola-Morgan 1991). The hippocampus proper is further subdivided into distinct subregions: the dentate gyrus (DG), CA1, CA2, and CA3 (van Strien et al 2009). The subicular complex is further subdivided into the subiculum (SUB), presubiculum (PRESUB), and the the parasubiculum (PARASUB).

The hippocampal DG receives a strong projection from EC layers II/III, known as the perforant path (Figure 1.1, Witter 2007). The DG projects to CA3, which projects to CA1. This ECII/III-DG-CA3-CA1 pathway is classically known as the trisynaptic pathway. Stimulation of the EC axons *in vivo* provides simultaneous excitation to DG, CA3, and CA1 (Yeckel and Berger 1990), demonstrating that EC also sends projections to all three subregions. DG granule cells project to CA3 pyramidal cells via the mossy fiber pathway. These CA3 pyramidal cells in turn project back onto CA3 pyramidal cells in a recurrent circuit. CA3 pyramidal cells project to CA1 pyramidal cells via the

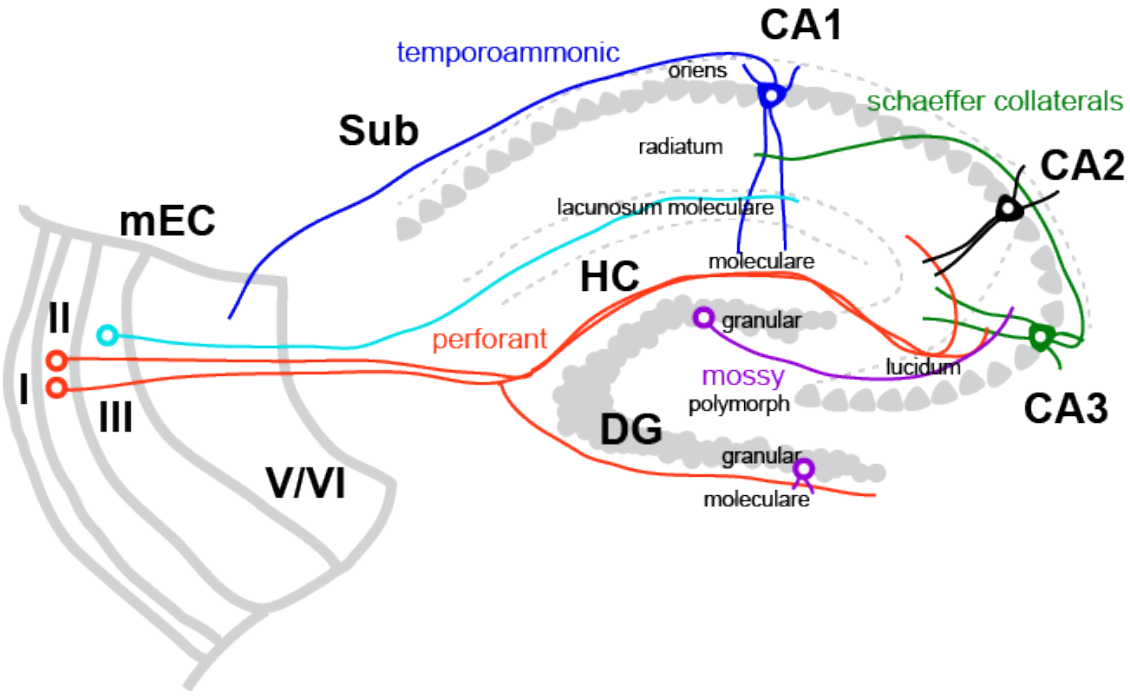

Figure 1.1: Anatomy of the mEC-HC circuit

Schematic drawing of the mEC-HC circuit. Red, mEC layer II cells, light blue, mEC layer III cells, purple, DG granule cells, green, CA3 pyramidal cells, black, CA2 pyramidal cells, dark blue, CA1 pyramidal cells. mEC layer II projects to DG and CA3 via the perforant path (red). mEC layer III cells project to CA1 pyramidal cells. DG cell project to CA3 via mossy fiber pathway. CA3 projects to CA1 pyramidal cells and weakly to CA2 pyramidal cells via schaffer collateral pathway (green). CA1 pyramidal cells project back to subiculum (Sub) and mEC layers V/VI via the temporoammonic pathway (blue).

Schaffer Collaterals. The less-studied CA2 subregion, previously thought to be a transition zone between CA1 to CA3, receives input from ECII and weaker input from CA3 (Chevaleyre and Siegelbaum 2010). EC layer III sends a prominent projection directly to the CA1 subregion (Steward and Scoville 1976, Witter et al 1988).

Types of memory

Memory can be divided into two main categories: declarative and non-declarative memory (Squire and Zola-Morgan 1991, Squire 1992). Declarative memory is defined as any memory that one could declare including memory for information and events, defined as semantic and episodic memory (Tulving 1972). Nondeclarative memory, also called implicit memory, includes memories that are not conscious but can be demonstrated through performance. It was previously believed that declarative memory including episodic memory only existed in humans and could therefore only be studied in humans due to other animal's inability to declare. However, it has been observed that humans and non-human animals, including rodents and primates, share many commonalities in their episodic memory (Eichenbaum et al 2005).

The role of the MTL in episodic memory

Evidence for the HC and other regions in the MTL in human memory first became apparent from examination of human amnesic patients including patients H.M.

and R.B. (Scoville and Milner 1957, Zola-Morgan et al 1986). The first and most famous amnesic patient, H.M., had suffered medically intractable seizures since the age of 10. He had undergone surgery by Dr. William Scoville in 1954 along with nine other patients to undergo tissue resection in the MTL. Patient H.M. had bilateral tissue resection of the MTL and showed severe memory impairments in his ability to form new episodic memories, while maintaining many of his previously formed long-term memories. There was no effect on his personality, intelligence, or motor skills (Scoville and Milner 1957, Penfield and Milner 1958). Overall, these results demonstrate that the hippocampus and the cortical structures surrounding it are critical in the ability to form and retain new memories.

Following the results seen from H.M.'s amnesia, these results were replicated through animal studies performed primarily in monkeys and rodents. Lesions to the hippocampal formation also caused memory impairments in rhesus monkeys. When lesions to the HC were combined with lesions to the amygdala, monkeys had impairments during object recognition (Mishkin 1978).

Lesions to the hippocampus or entorhinal cortex caused deficits in a visual concurrent discrimination task (Moss et al 1981). Hippocampal lesions impaired learning on an associative learning task and an object discrimination retention task (Mahut et al 1982). Hippocampal lesions result in the inability to learn and remember the location of a hidden platform in a pool of water, referred to as the "Morris water maze" (Morris et al 1982). Loss of hippocampal function causeed impairments in a novel object in location task (Parkinson et al 1988). Lesions to the HC also caused deficits in a delayed non-

match to sample (DNMS) task (Beason-Held et al 1999). Damage to the HC impaired memory in a delayed alternation task (Racine and Kimble 1965).

More precise lesions have revealed that each distinct subregion in the HC is critical in episodic memory. Inactivation of CA3 NMDA receptors impaired associative memory recall (Nakazawa et al 2002). Lesions to the DG, but not CA1, showed impairments in pattern separation in a fine discrimination task (Rolls and Kesner 2006).

More recently, the mEC has been more thoroughly examined for its role in episodic memory. Lesions to the mEC disrupt performance in tasks that similarly require intact hippocampal function including the Morris water maze (Hales et al 2014) for both recently and remotely acquired spatial memories (Hales et al 2018), trace fear conditioning (Hales et al 2018), and the delayed spatial alternation task (Sabariego et al 2019). Further, spatial memory in the Morris water maze critically depends on the intact function of the dorsolateral band of the EC (Steffenach et al 2005) for successful memory performance.

Spatial representations in the MTL

In addition to having a role in the formation and retrieval of memory, the MTL, especially the HC and mEC, is composed of numerous spatial and directional cells that are thought to support spatial navigation and memory. Nearly all principal cells in the mEC have some level of spatial coding (Diehl et al 2017). Grid cells within the mEC, PRESUB, and PARASUB fire periodically in a hexagonal lattice forming a grid-like

pattern (Hafting et al 2005, Boccara et al 2010, Fyhn et al 2008). Prior to the discovery of grid cells, spatial representations were observed in mEC (Fyhn et al 2004). Border cells or boundary vector cells fire exclusively along or a certain distance from the boundary of an environment (Solstad et al 2008). Head direction (HD) cells fire when an animals head is facing a particular direction and are found in several brain regions including deep layers of the mEC, the postsubiculum, and the anterior thalamic nucleus (Taube et al 1990, Taube et al 2007, Winter et al 2015). Although the majority of studies on grid cells have been conducted in rodents, grid cells have been identified in humans (Jacobs et al 2013) and monkeys (Killian et al 2012). Neurons in the mEC code for the running speed of the animal, called speed cells, by modulating firing rate with running speed (Kropff et al 2015, Sun et al 2015, Hinman et al 2016).

Place cells are cells that fire exclusively when an animal is in one region of space and are found in all subregions of the HC (O'Keefe 1976, Leutgeb et al 2004, Leutgeb et al 2005). As an animal walks through an environment, place cells will cover the entire environment and organize into precise sequences (Dragoi and Buzsaki 2006) and can be internally generated (Pastalkova et al 2008). Place cells code for non-spatial features of the environment including visual cues by modulating their firing rate, also known as "rate remapping" (Leutgeb et al 2004; Knierim 2002, Fyhn et al 2007). Unlike mEC HD and conjunctive HD cells (Sargolini et al 2006), place cells exhibit little HD coding (Muller et al 1994).

The firing properties of HC and mEC cells also show distinct representations when animals are performing learning and memory tasks. During learning and memory

tasks, where a goal is a critical aspect of performing the task for the animal, place cells shift towards goal locations (Kennedy and Shapiro 2009, Aoki et al 2019) and show both retrospective coding, representation of what previously happened, and prospective coding, the representation of what is about to happen (Ferbinteanu and Shapiro 2003). Hippocampal place cells can code for two different spatial trajectories in the same location on a delayed spatial alternation task (Wood et al 2000). Hippocampal neurons also code for time in a similar fashion as place fields but with time fields. These cells have been called "time cells" (MacDonald et al 2011, Kraus et al 2013). Interestingly, grid cells similarly show coding for elapsed time but only on the order of seconds (Kraus et al 2015, Diehl et al 2019). Interestingly, the transient inactivation of mEC caused a disruption in the precise firing of hippocampal time cells (Robinson et al 2017).

The scale of place fields in the HC increases along the dorsal-ventral axis with dorsal HC cells having the smallest place fields and the ventral HC cells having the largest place fields (Jung et al 1994, Kjelstrup et al 2008). Similarly, grid scale increase along the dorsal-ventral axis with dorsal mEC cells having the smallest grid fields and spacing, and ventral mEC cells having the largest grid fields and spacing (Hafting et al 2005, Brun et al 2008).

Grid cells critically depend on intact excitatory drive from the HC (Bonnevie et al 2013). The spatially periodic firing of grid cells is also dependent on intact function of the MS (Brandon et al 2011, Koenig et al 2011), suggesting grid cells require sustained theta oscillations to maintain their firing patterns. Although grid cells lose their spatial precision during reduced theta oscillations, inactivation of the MS does not disrupt other

spatial or directional firing patterns and does not alter speed cell coding in the mEC (Brandon et al 2011, Koenig et al 2011, Hinman et al 2016). Grid cells are disrupted when the anterior thalamic nucleus, a region responsible for conveying information about HD, is inactivated (Winter et al 2015a). Further, passive transport of an animal disrupts the spatial firing patterns of grid cells (Winter et al 2015b). Grid cells receive recurrent inhibition from parvalbumin (PV) GABAergic neurons in the mEC (Buetfering et al 2014). Grid cells also depend on cholinergic function as demonstrated by experiments that systemically block muscarinic acetylcholine receptors (Newman et al 2014).

Grid cells respond to environmental cues including the symmetry or geometry of the environment (Krupic et al 2015) and the context of similar environments (Diehl et al 2017), similar to hippocampal place cells (Muller and Kubie 1987). Grid cells compress and rescale when the environment is compressed (Barry et al 2007).

Grid cells recorded in the mouse mEC show disrupted spatial firing in the absence of visual input (Chen et al 2016, Perez-Escobar et al 2016). However, in the rat, grid cells do not require visual input (Hafting et al 2005) and persist in complete darkness. However, this may not be due to a difference between mice and rats but due to the extent that non-visual cues can be used. Disrupted firing patterns of grid cells have been correlated with impaired path integration (Allen et al 2014, Gil et al 2018), the ability to navigate a learned environment in the complete absence of visual cues, also known as "dead reckoning" (McNaughton et al 2006a).

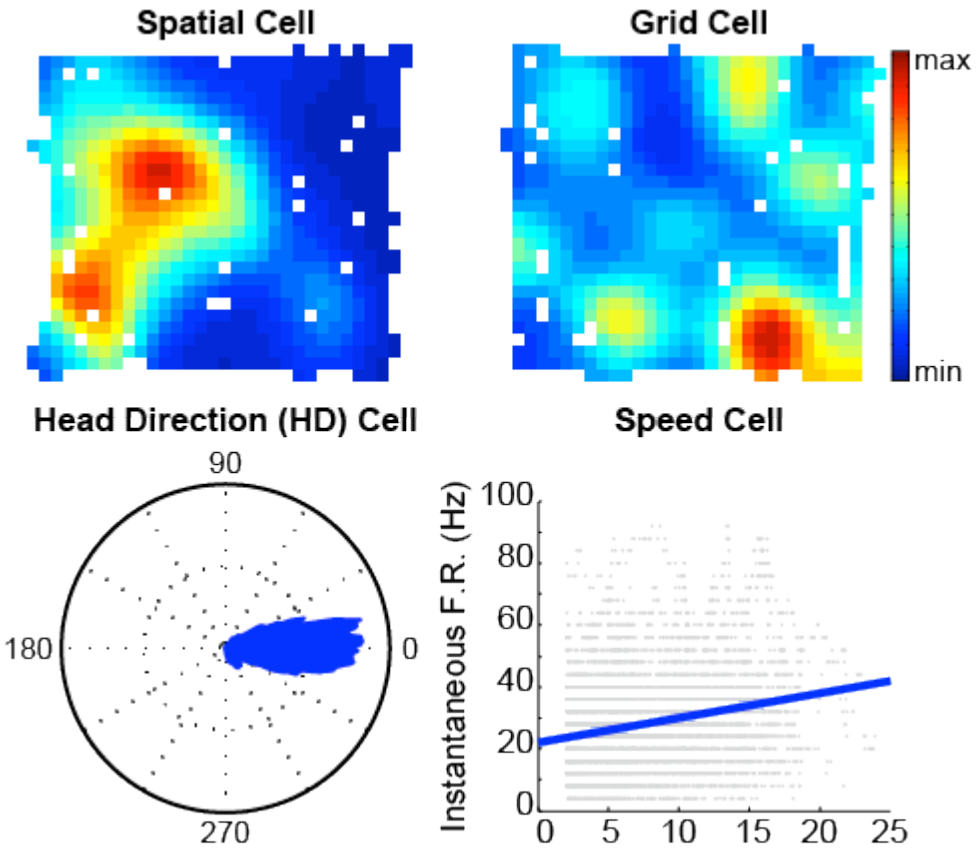

Figure 1.2: Spatial cell types in mEC

Examples of previously described functional cell types in the mEC. Clockwise from top left: spatial non-grid cells, grid cells, head direction (HD) cells, and speed cells. Top row: color corresponds to firing rate with red indicating the max firing rate and blue as the min firing rate.

Multiple models have been put forth that hypothesize the generation of grid cell firing patterns (Giocomo et al 2011). One such model is the oscillatory interference model (Burgess et al 2007, Burgess 2008, Jeewajee et al 2008), which suggests that changes in the frequency of membrane-potential oscillations at two different frequencies is translated into information about speed and direction and is then used to form the spatial periodicity of grid fields. Experimental support for the oscillatory interference model has been observed by the fact that loss of theta rhythm by MS inactivation (Brandon et al 2011, Koenig et al 2011) disrupts the spatial periodicity of grid cells. Other support comes from the finding that the frequency of mEC theta rhythm, especially in the dorsal mEC, is modulated by running speed (Jeewajee et al 2008, Zutshi et al 2018b).

Given that the main input to the HC is the mEC and that multiple spatial and directional cell types in mEC project directly to HC (Zhang et al 2013), it had been previously hypothesized that grid cell function is critical in the function of place cells and had been thought to be the primary source of spatial information for hippocampal place cells. However, the development of place cells (Wills et al 2010) occurs prior to the development of grid cells in the rat (Langston 2010). Further, lesions to the mEC do not completely abolish the existence of place cells in the HC (Hales et al 2014, Schlesiger et al 2015, Sabariego et al 2019). In further support of this, inactivation of the medial septum (MS) results in the disrupted spatial firing patterns of grid cells but not the disrupted spatial coding of hippocampal place cells (Brandon et al 2011, Koenig et al

2011). Overall, these results suggest that the formation of place cells does not critically depend on the intact function of mEC grid cells (Brandon et al 2014).

Anatomy of the medial septum

The MS receives projections from the supramammillary nucleus (Borhegyi et al 1997) and interneurons in the HC and reciprocally sends long-range projections back to the HC and mEC. The MS also sends axonal projections to extrahippocampal cortices including the subiculum, presubiculum, parasubiculum, lateral entorhinal cortex, and retrosplenial coretex (Unal et al 2015). The MS is composed primarily of GABAergic cells that express parvalbumin (PV; Freund 1989), which send projections to interneurons in the HC and mEC (Alonso and Kohler 1984, Freund and Antal 1988, Gonzalez-Sulser et al 2014, Fuchs et al 2016), and cholinergic cells, which send projections to both interneurons and principal cells in the HC and mEC (Dannenberg et al 2015).

GABAergic neurons in the MS send projections to fast-spiking and low-threshold spiking interneurons in all layers of the mEC with the densest projections sent to layers II and V (Gonzalez-Sulser et al 2014). GABAergic neurons in the MS rarely send projections to excitatory cells in mEC (Gonzalez-Sulser et al 2014). Further, these GABAergic projections onto mEC generate inhibitory $GABA_A$ receptor-mediated postsynaptic responses, which can entrain the activity of mEC cells (Gonzalez-Sulser et al 2014). MS GABAergic cells fire coincident with hippocampal CA3 excitation (Joshi et al 2017).

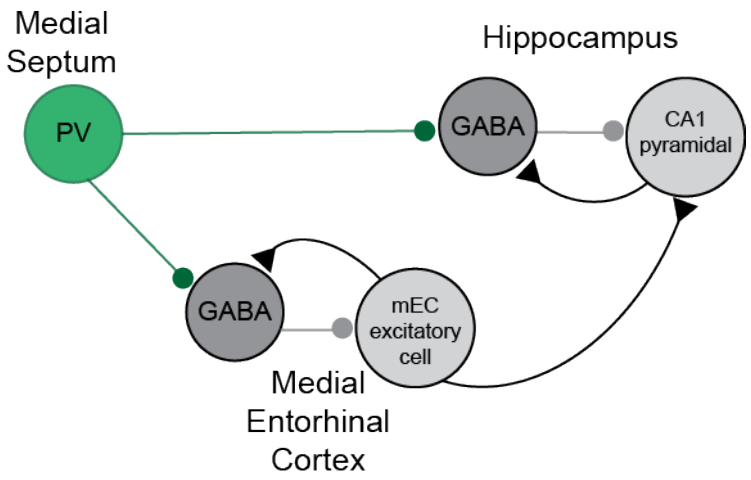

Figure 1.3: Medial septum PV cells project to GABAergic neurons in the HC and mEC

The medial septum is composed primarily of GABAergic PV cells, cholinergic cells, and glutamatergic cells. The medial septum sends long range projections to both the HC and mEC. GABAergic and PV cells in the MS only send projections to interneurons in the HC and mEC.

The GABAergic PV cells in the MS fire rhythmic bursts that are locked to hippocampal theta frequency (Petsche et al 1962; Freund and Antal 1988; Toth et al 1993, Borhegyi et al 2004). Cholinergic cells in the MS are muscarinic and slow firing (Kramis et al 1975), suggesting they do not drive theta frequency. *In vivo* recordings of single units in the MS of freely behaving rats revealed that both putative cholinergic and GABAergic cells fire phase-locked to hippocampal theta oscillations (King et al 1998), although cholinergic cells fired in an irregular fashion. The majority of these rhythmically firing cells also were correlated to the animal's running speed. These findings led to the "pacemaker hypothesis" (Gogolak et al 1968, Stewart and Fox 1990), which suggests that GABAergic MS cells directly drive theta frequency.

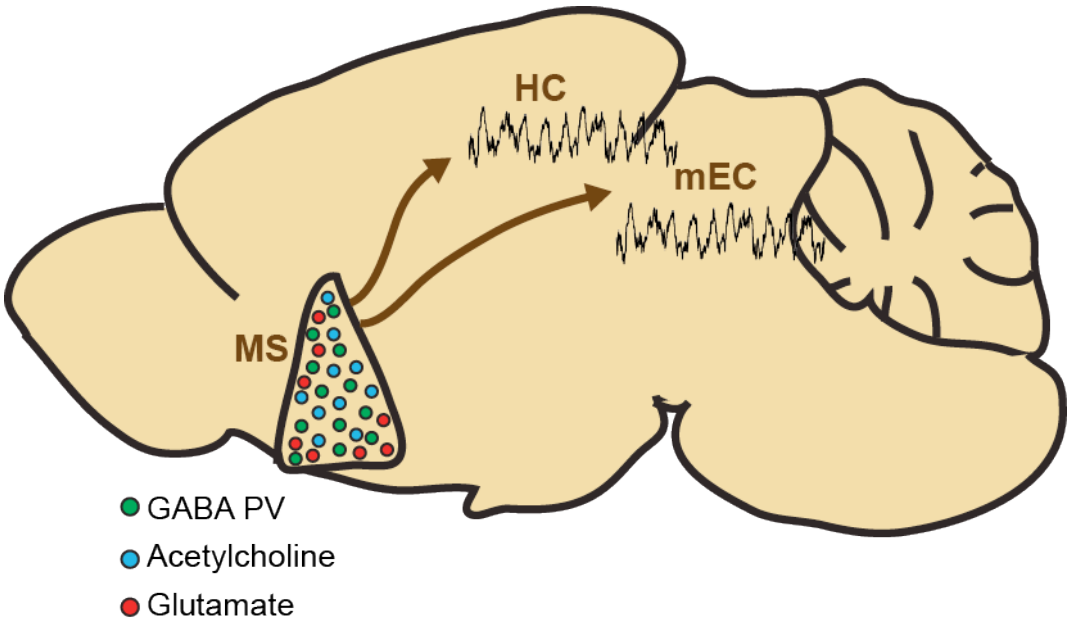

Figure 1.4: Medial septum projects to the hippocampus and medial entorhinal cortex

The medial septum is composed primarily of GABAergic parvalbumin (PV) cells, cholinergic cells, and glutamatergic cells. The medial septum sends long range projections to both the HC and mEC and is critical in generating theta rhythmicity in the mEC and HC.

Oscillations in the MTL

The theta rhythm is an approximately 6-9 Hz oscillation that is detected by local field potential (LFP) recordings in the HC and mEC during periods of both movement and REM sleep (Vanderwolf 1969, Mitchell and Ranck 1980, Buzsaki 2002). Theta oscillations are prominent during memory tasks and have been thought to be important for coordinating the activity of neurons across systems of brain regions including the HC, mEC, and prefrontal cortex (PFC; Buzsaki and Drauguhn 2004, Hasselmo 2005, Benchenane et al 2010, Remondes and Wilson 2013, Hallock et al 2016, Place et al 2016). Theta oscillations are more prominent in the mEC than the lEC (Deshmukh et al 2010). The MS is considered to be critical for theta generation (Mitchell et al 1982), but the exact mechanism that gives rise to the theta rhythm is unknown. The GABAergic PV cells in the MS fire rhythmic bursts that are locked to hippocampal theta frequency (Petsche et al 1962; Freund and Antal 1988; Toth et al 1993). Cholinergic cells in the MS are muscarinic and slow firing (Kramis et al 1975), suggesting they don't drive theta frequency. These findings led to the "pacemaker hypothesis" (Gogolak et al 1968; Stewart and Fox 1990), which suggests that GABAergic MS cells directly drive theta frequency. Individual cholinergic or GABAergic lesions of the MS only partially reduce theta amplitude in the HC (Yoder and Pang 2005). However, combined lesions of both cell types nearly abolish theta. These results suggest that while the pacemaker hypothesis suggests that PV neurons in the MS drive the frequency of theta oscillations, other cell

populations, particularly cholinergic neurons, also contribute to the generation of theta oscillations.

In addition to theta oscillations, which are approximately 6-9 Hz and occur during movement and REM sleep, sharp wave ripples (SWRs) and gamma oscillations are also prominent and are thought to support episodic memory (Colgin and Moser 2010, Colgin 2016). SWRs are irregularly occurring transient (40-100ms) and fast (110-200 Hz) oscillations that occur when animals are in consummatory behaviors such as eating, grooming, and non-REM sleep (Buzsaki 2015). This makes SWRs distinct from theta, which occurs during active movement, exploration, and REM sleep. During an experience, place cells are activated sequentially. During sleep recently following the experience, the place cells, cells that fire exclusively when an animal is in one location of space (O'Keefe 1976), are reactivated in a time-compressed manner during SWR, which is known as "replay" (Skaggs and McNaughton 1996) and has been suggested to be a mechanism for memory consolidation. Disruption of SWRs impairs spatial working memory (Jadhav et al 2012). SWRs and theta occur during different brain states and their occurrence is inversely correlated (Buzsaki 2015). Stimulation of cholinergic cells in the MS results in an increase in theta power and a decrease in SWR frequency (Vandecasteele et al 2014). However, it is unclear if the disruption of SWRs was due to an increase in acetylcholine levels in the HC or due to the increase in theta power. The firing of GABAergic units in the MS are suppressed during SWRs (Dragoi et al 1999), suggesting the possibility that artificially activating these cells may suppress SWRs.

Gamma oscillations represent a wide distribution of frequencies (25-150 Hz) that are closely coupled to theta oscillations (Bragin et al 1995). Slow gamma (25-50 Hz) is synchronized between CA3 and CA1 and occurs at the peak phase of theta (Colgin et al 2009, Schomberg et al 2014). Fast gamma (60-140 Hz) is synchronized between the mEC and CA1 region and is modulated at the trough phase of theta (Colgin et al 2009, Schomberg et al 2014). This suggests that gamma oscillations could represent different routes of information flow and memory processes. Additionally, gamma power and gamma-modulated spiking was higher during successful memory encoding in the macaque HC (Jutras et al 2009). Theta-gamma coupling in the CA3 region of the rat HC has been shown to correlate with memory for associating items with spatial contexts (Tort et al 2009). Theta-gamma comodulation can predict memory for recent spatial episodes (Shirvalkar et al 2010). Fast gamma is also associated with correct execution of spatial working memory (Yamamoto et al 2014) and the encoding of novel object and place pairings (Zheng et al 2016).

Theta modulated spike timing in the MTL

The firing of place cells and grid cells is strongly coupled to theta oscillations (O'Keefe and Recce 1993, Hafting et al. 2005). Inactivation of the MS, which disrupts theta, impairs grid cell spatial tuning without affecting place cell spatial firing (Brandon et al 2011, Koenig et al 2011, Brandon et al 2014). Spatial cells and head direction cells do not lose their spatial or directional tuning during reduced theta oscillations (Brandon

et al 2011, Koenig et al 2011). However, other reports suggest grid cells do not require theta oscillations in other species such as bats (Yartsev et al 2011). Taken together, these findings indicate that while many cell types in the entorhino-hippocampal circuit may be theta-modulated, this does not predict whether that specific cell type is affected by reducing theta oscillations.

A phenomenon that points to a relation between theta and spatial cells is theta phase precession of hippocampal place cells and mEC layer II grid cells. Here, cells always fire at a frequency higher than local theta, causing spikes during consecutive theta cycles to occur at increasingly earlier phases of theta (O'Keefe and Recce 1993, Skaggs et al 1996, Hafting et al 2008). This property can provide information to estimate how far the animal has traversed through the place field based on the phase of theta at which the cell is spiking. Phase precession can additionally order a series of overlapping place fields into a sequence of place cells, known as hippocampal theta sequences. Theta sequences are disrupted during inactivation of the medial septum (Wang et al 2015) while theta phase precession of single place cells remains intact (Schlesiger et al 2015). Optogenetically shifting theta frequency to frequencies higher than the endogenous range (i.e., 10 and 12 Hz) does not disrupt theta phase precession (Zutshi et al 2018a), which implies that the firing frequency of place cells exceeds the stimulation frequency and thus maintains phase precession. There is also no phase precession within the MS itself, whereas spatial cells in the mEC phase precess (Hafting et al 2008). Moreover, lesions to the mEC disrupt phase precession (Schlesiger et al 2015). Taken together, these results suggest that the MS plays a role in setting the base frequency for phase precession.

The role of the MS in memory

Disrupting theta by inactivating or lesioning the MS during hippocampal-dependent memory tasks severely impairs performance (Winson 1978, Chrobak et al 1989, Mizumori et al. 1990, Givens and Olten 1994, Leutgeb and Mizumori 1999, Wang et al 2015). It has been suggested that this deficit is due to alterations in spike timing of cells in the HC and mEC in the absence of theta (Mizumori et al. 1990, Leutgeb and Mizumori 1999, Wang et al 2015). Selective lesions to either the GABAergic or cholinergic cell populations in the MS do not, or only mildly impair spatial memory. Combined lesions of both, however, resulted in a severe memory deficit in hippocampal-dependent memory tasks such as the Morris water maze (Pang et al 2001, Smith and Pang 2005). Other reports suggest that inactivating either cell type is sufficient to cause a memory deficit in a working memory task (Chrobak et al 1992, Bunce et al 2004). The differences seen in these studies is most likely due to differences in methods of inactivations or lesions and which behavioral task was used.

Although silencing the MS is accompanied by severe memory deficits, this deficit can be rescued using electrical stimulation of the MS if the stimulation frequency is theta rhythmic. Inactivation of MS during the Morris water maze impaired learning but could be restored by rhythmic theta stimulation at 7.7 Hz of the fornix (McNaughton et al 2006). In an animal model of traumatic brain injury, rats showed attenuated theta oscillations and deficits in the Barnes maze following lateral fluid percussion that was

rescued by stimulation of the MS at 7.7 Hz one minute prior to training (Lee et al 2013) while non rhythmic stimulation did not improve memory. In a brightness discrimination training task, stimulation at 7 Hz applied five minutes after training improved performance while stimulation of 100 Hz significantly impaired retention of the task (Wetzel et al 1977). Interestingly, theta oscillation frequency is also altered in animal models of Alzheimer's disease (Goutagny et al 2013), which may suggest that memory impairments in Alzheimer's disease may originate in part from altered oscillatory frequency.

Overall, these results strongly point to a role for theta oscillations generated from the MS in hippocampal-dependent memory. However, these experiments also cause drastic changes in the firing statistics of neuronal populations (Brandon et al 2011, Koenig et al 2011, Wang et al 2015), making it difficult to know whether the effect on memory is due to a reduction in theta oscillations or a loss of excitation within the network.

Preview of the dissertation

In chapters II and III we examine the role of oscillatory timing of theta oscillations in the spike timing of HC and mEC cells and the effect on spatial coding. As previously described, many cells within the mEC-HC circuit fired rhythmically in the same frequency range of theta oscillations and showed spatial tuning when exploring an environment. Interestingly, we found that the primary theta modulated input to CA1

originates from the mEC and that mEC cells are more strongly entrained to MS PV stimulation than HC cells were. Both brain regions systematically shifted their peak frequencies toward the stimulation frequency and generated oscillation frequencies that were well outside the endogenous range, which during baseline conditions was generally below 10 Hz, when theta was paced at 10 and 12 Hz.

In chapter IV, we tested whether changes to oscillatory timing in theta oscillations had a role in spatial working memory in a delayed alternation task that has been shown to depend on an intact HC and mEC (Ainge et al 2007, Sabariego et al 2019). We found that shifting theta oscillations to 10 Hz or higher caused a severe memory impairment while stimulating within the endogenous range at 8 Hz did not cause any impairments in memory. Thus, we demonstrated that even a small deviation from the endogenous range ($\leq$ 2 Hz) was sufficient to cause a severe memory impairment. When we further restricted this optogenetically accelerated oscillatory frequency to different periods of the delayed spatial alternation task, we found that only accelerated theta frequency impaired performance on the return arm. These results suggest that the precise timing of theta oscillations is specifically critical during periods of memory encoding during hippocampal dependent tasks.

Importantly, these findings demonstrate a role for theta rhythm in memory that coincides with changes in the spike timing of cells in the mEC-HC circuit. Due to the precise temporal precision of optogenetics used here, we were able to demonstrate that the circuit tolerated a large range of perturbations of oscillatory patterns, such as an increase in amplitude of mEC and increases in gamma amplitude, as long as the

perturbation remained within the endogenous theta range. In particular, we found that even more profound perturbation of oscillatory patterns were without behavioral consequences when limited to behavioral phases during which memory needed to be retained and a choice needed to be selected. While these data confirm a long-hypothesized role for theta in episodic memory encoding, they also show that other aspects of memory processing including memory retrieval are highly tolerant to major disruptions of oscillatory patterns in the mEC-HC circuit.

Taken together, our findings demonstrate that medial septal control of theta oscillations results in stronger changes to the spike timing of cells in the mEC than the HC and that the excessive drive of medial entorhinal and hippocampal oscillatory patterns outside of the endogenous theta range (6-9 Hz) causes selective impairments in the encoding of episodic memories by altering the spike timing of cells within the mEC and HC while leaving spatial, directional, and speed coding intact. This is the first study to demonstrate a direct role for theta oscillation frequency in spike timing in the entorhino-hippocampal network and memory.

Chapter II.

Optogenetic acceleration of theta frequency results in accelerated oscillatory frequencies of hippocampal and medial entorhinal cells

Abstract

Theta oscillations in the medial entorhinal cortex (mEC) and hippocampus (HC) have been hypothesized to coordinate spike timing within the mEC-HC circuit. In this chapter, we tested how rhythmic control of the timing of theta frequency by optogenetic stimulation of medial septum (MS) parvalbumin (PV) cells would alter spike timing within the mEC-HC circuit. We found that MS PV stimulation entrained theta and superseded the endogenous oscillations recorded in both the mEC and HC. We next found that the majority of principal cells in the mEC and HC responded to the stimulation with accelerated oscillation frequencies that were outside the endogenous range and became entrained to the stimulation frequency. We found that principal cells in the mEC became more strongly entrained to optogenetically entrained theta oscillations than cells in the HC. These results demonstrate that the MS sets the oscillatory frequency of theta oscillations in mEC and HC and that cells within these regions shift their spike timing in response to changes in theta oscillation timing.

Introduction

Neuronal oscillations, including theta oscillations, have been hypothesized to reflect accurate timing of neuronal activity within and across a system of brain regions including the hippocampus (HC), medial entorhinal cortex (mEC), and prefrontal cortex (Colgin et al 2009, Benchenane et al 2010, Schomberg et al 2014). Theta (6-9 Hz) oscillations in the HC and mEC (Vanderwolf et al 1969) are generated by subcortical pacemaker cells in the medial septum (MS), which exhibit rhythmic bursting that is phase-locked to theta (Petsche et al 1962, Buzsaki 2015). Juxtacellular recordings suggest these cells correspond to parvalbumin-expressing (PV) neurons (Borhegyi et al 1997), which project to HC and mEC GABAergic interneurons (Freund and Antal 1988, Gonzalez-Sulser et al 2014). Thus, these MS PV cells form a disinhibitory circuit that is well positioned to produce rhythmic potentials in the HC and mEC. These results demonstrate that PV cells within the MS are critical in generating theta rhythmicity within the HC and mEC.

The firing of place cells in the HC and spatial cells in the mEC, including grid cells, is strongly coupled to theta oscillations (O'Keefe and Recce 1993, Hafting et al 2005). A phenomenon that points to a relation between theta and spatial cells is theta phase precession of hippocampal place cells and mEC layer II grid cells. Here, cells always fire at a frequency higher than local theta, causing spikes during consecutive theta cycles to occur at increasingly earlier phases of theta (O'Keefe and Recce 1993, Skaggs

et al 1996, Hafting et al 2008). This property can provide information to estimate how far the animal has traversed through the place field based on the phase of theta at which the cell is spiking. Phase precession can additionally order a series of overlapping place fields into a sequence of place cells, known as hippocampal theta sequences. Theta sequences are disrupted during inactivation of the MS (Wang et al 2015) while theta phase precession of single place cells remains intact (Schlesiger et al 2015). Optogenetically shifting theta frequency to frequencies higher than the endogenous range (i.e., 10 and 12 Hz) does partially disrupt theta phase precession (Zutshi et al 2018a), which implies that the firing frequency of place cells can only in part exceed the artificially accelerated theta frequency, which reduces phase precession. Taken together, these results suggest that the MS plays a role in setting the base frequency for the HC for phase precession.

Most of the evidence for a relationship between oscillations and spike timing in the mEC and HC has remained correlative. Direct evidence for a causal link between oscillations and spike timing has remained sparse due to the fact that it has previously been difficult to manipulate oscillations without altering other firing statistics of neuronal populations. Precise optogenetic manipulation of theta frequency has demonstrated that it is possible to manipulate the timing of theta oscillations (Bender et al 2015, Fuhrmann et al 2015, Blumberg et al 2016, Robinson et al 2016, Justus et al 2017, Zutshi et al 2018a) without causing substantial effects on hippocampal firing rates and place fields (Zutshi et al 2018a). We therefore utilized optogenetic techniques coupled with *in vivo* local field potential (LFP) and single unit recordings in freely behaving mice in order to examine

how altered theta oscillation frequencies alter the spike timing of cells within the mEC-HC circuit.

Methods

Subjects

Fifteen parvalbumin-cre (129p2-Pvalbtm1(cre)arbr/j, Jackson Labs) mice weighing between 25-35 grams were used as subjects. Mice were experimentally naïve and housed individually in Plexiglass cages on an inverse 12 hr light/dark cycle (lights off at 8 am). All training and testing was conducted during the dark phase. Mice were restricted to 85-90% of their *ad libitum* weight and given full access to water. All procedures were conducted in accordance with the University of California, San Diego Institutional Animal Care and Use Committee.

Surgery

Mice were first injected with a viral vector containing the light-driven ion pump, Channelrhodopsin (AAV.EF1α.DIO.ChR2.eYFP) or (AAV.EF1αFLEX.oChIEF.mcitrine). Viral vectors were provided by Dr. Byungkook Lim's laboratory (University of California, San Diego). Mice were anesthetized with isoflurane (induction: 2.5%; maintenance 0.5-2%) and mounted in a stereotaxic frame (David Kopf Instruments, Model 1900). The scalp was cleaned and retracted using a midline incision and the skull was leveled between bregma and lambda. A hole was

drilled over the MS to make a small craniotomy (+1.0mm A/P, -0.7mm M/L) and 750 nL of virus was injected at a rate of 100 nL/min at two locations (400 nL, +1.0mm A/P, -0.7mm M/L, -4.8mm D/V; 350 nL, +1.0mm A/P, -0.7mm M/L, -4.2mm D/V) through a glass pipette using a microsyringe pump (Micro4, UMP3 UltraMicroPump, World Precision Instruments). The pipette was left in place for 5 minutes after the injection before being slowly retracted. Mice were sutured and allowed to recover for a minimum of 7 days.

Mice were implanted with an optic fiber over the medial septal area (MS) and either a four or eight-tetrode microdrive aimed at the medial entorhinal cortex (mEC) or dorsal CA1 region of the hippocampus (HC). Mice were anesthetized with isoflurane (induction: 2.5%; maintenance 0.5-2%). The scalp was cleaned and retracted using a midline incision and the skull was leveled between bregma and lambda.

Five holes were drilled in the skull to attach anchor screws and dental cement to secure the implant. A hole was drilled over the MS (+1mm A/P, -0.7 M/L, -3.7 D/V) and the optic fiber was implanted with a 10° medial-lateral angle. A ground screw was placed over the cortex. The skull was removed using a craniotomy over the HC (-2.25mm A/P, +2.0mm M/L) or MEC (from lambda; -0.9mm A/P, +3.8mm M/L, at an 8° angle anterior-posterior), the dura was removed and tetrodes were placed once they have just entered the brain. The microdrive was then cemented to the rest of the implant.

Postoperative care was administered as needed for five to seven days until mice fully recovered. Any mice in which the shift in peak LFP theta during stimulation was not observed, were not used for analysis.

Behavior

Recordings were done while animals ran 10-14 laps counterclockwise on a rectangular track (150 x 50 cm with a track width of 10 cm) made of grey Plexiglas. Translucent walls were installed as guiderails (3 cm tall). The rectangular track was placed in the middle of a room that had several visual cues throughout and contained a dim light in one corner of the room that served as an orienting landmark. Animals were trained daily on the track for a minimum of two days prior to recording.

Mice were trained to freely forage in a square shaped open field (75 x 75 cm^2) with black walls and a single prominent white cue card along one wall. The open field was placed in the same location for all testing sessions in a room with dim lights and distal cues along all walls. Mice were habituated to the open field for several days before recordings and optogenetic stimulation began. Once mice were trained, each mouse was run for at least three sessions per day: one baseline recording, between one and three stimulation sessions (8 Hz, 10 Hz, or 12 Hz randomized), and one final baseline recording.

Electrophysiological recordings

Local field potential (LFP) signals were recorded using the chronically implanted four-tetrode (bundles of four 17 μm platinum-iridium (90/10%) wires, California Fine Wire Company) microdrives (Anikeeva et al 2012). Tetrodes were stabilized using an optic fiber (200 μm core, Thor Labs, 0.50 NA multimode fiber) that was glued to a

zirconia ferrule (Precision Fiber Products, 230 μm). Electrode tips were plated with platinum to reduce electrode impedances to between 150-250 kΩ at 1 kHz. Recording tetrodes were targeted to the CA1 pyramidal layer or to the dorsal MEC. A preamplifier, tether, and a 32-channel digital data acquisition system (Neuralynx, Inc.) was used. LFP was sampled at 32,000 Hz and filtered between 1 and 1,000 Hz.

Laser stimulation

Light was delivered to the MS using a 473 nm wavelength Blue DPSS Laser System through an optic fiber patch cord (Doric Lenses, MFP_200/240/1100-0.22_10m_FC-ZF1.25(F), 200 μm core, 0.22 NA) to a custom optic fiber implant. The custom fiber optic implant was made using an optic fiber (200 μm core, Thor Labs, 0.50 NA multimode fiber) that was glued to a zirconia ferrule (Precision Fiber Products, 230 μm). The final optic fiber was sanded down to allow maximum light through the fiber and cut to a length of 4 mm. The output intensity was adjusted to between 9.0 and 12.0 mW. Light was delivered at a 50% duty cycle at frequencies of 8, 10, and 12 Hz. Laser stimulation was delivered on alternating laps of the rectangular track for each stimulation condition. The x and y coordinates of the animal's position data were collected using Neuralynx Cheetah Software and was then passed into MATLAB. A custom MATLAB script was used to calculate the median-x and median-y coordinates of the LEDs while the animals were running on the rectangular maze. The script then determined whether the animal was on an alternating lap. Once animals began a stimulation lap, MATLAB would instruct the Neuralynx Cheetah software to turn on the laser stimulation and was

turned off once the MATLAB script determined the animal had finished the lap.

Histological procedures

Mice were perfused with 0.1 M phosphate-buffered saline (PBS) followed by 4% paraformaldehyde in PBS solution. Brains were post-fixed for 24 hours in 4% paraformaldehyde and then cryoprotected in 30% sucrose solution for 2 days. Brains were then frozen and sliced into 40 μm coronal sections for the MS and HC and 40 μm sagittal sections for the MEC on a sliding microtome. Sections were mounted on electrostatic slides and sections of the MS were coverslipped with Fluoroshield with DAPI (Sigma-Aldrich). Sections of the HC or MEC were mounted on electrostatic slides and stained with cresyl violet and coverslipped with Permount (Fisher Scientific, SP15500) to visualize recording locations. Slides were imaged using a virtual slide microscope (Olympus, VS120).

Single unit identification

Single-units were manually isolated offline using MClust (http://redishlab.neuroscience.umn.edu/MClust/MClust.html), on MATLAB 2009b (Schmitzer-Toerbert et al 2005). Neurons were separated in two-dimensional space based on the peak amplitude, peak-to-valley amplitude, and energy of spike waveforms. The same cells was tracked within each day but were not tracked across days. Cells that were not present in all sessions in the day were not included in the analysis. Neurons that were

not separable in cluster space were not included in the analysis. Cluster quality was determined using L-ratio and isolation distance.

Place field characterization

Position on the rectangular track was linearized into 116 bins that were 3.5 cm in size for analysis of spatial properties of HC neurons. Rate maps were computed as the number of spikes per time spent in each spatial bin and were smoothed by a pseudo-Gaussian kernel with a standard deviation of 1 bin. Spatial information was calculated as,

$$I = \sum_{i=1}^{N} p_i \frac{F_i}{F} \log_2 \frac{F_i}{F}$$

where I is the spatial information in bits/spike, p_i is the probability of occupancy in bin I, F_i is the mean firing rate for bin I, and F is the mean firing rate. Rate map stability was determined by calculating the correlation between rate maps for the first half of trials compared to the second half of trials. Place fields were defined as cells that had a peak spatial firing rate greater than 5 Hz that also maintained >20 % of the peak rate for at least 20 cm and less than 140 cm in the field. Cells were classified as principal cells if they had an average firing rate <10 Hz with a peak-valley cutoff of 1.5. Cells were classified as interneurons if their average firing rate exceeded this firing rate threshold and was below the peak-valley cutoff.

Single-cell temporal autocorrelations and frequency

For each cell, spike times were binned at a sampling rate of 500 Hz. The temporal autocorrelation between spike times was then calculated from the resulting vector. The power spectrum of the temporal autocorrelation was obtained via the Chronux function *mtspectrumumc*() in MATLAB using a padding factor equal to six powers of 2 over the sample size. The single-cell frequency was then taken as the frequency with peak power in the 6-14 Hz range.

Statistics

All behavior statistics were done using IBM SPSS Statistics version 23. Details of which tests are used were described with the results. No statistical tests were used for predetermining sample sizes, but our sample size is similar to other studies. For all comparisons between stimulation compared to no stimulation conditions were done using paired comparisons or using repeated-measures. Tests for normality were performed and if normality could be assumed, we used paired two-tailed t-tests. When normality could not be assumed, we used Wilcoxin signed rank tests. For all repeated measures ANOVAs, sphericity was not assumed but accessed using Mauchly's test for sphericity. If sphericity could not be assumed, Greenhouse-Geisser was used.

Results

Optogenetic stimulation of MS PV cells directly controls theta frequency in mEC

To effectively control oscillations during extended behavioral testing, we confirmed that we could control theta oscillations over periods of many minutes. As in previous experiments (Zutshi et al 2018) we expressed channelrhodopsin (ChR2) in PV cells in MS of PV-cre mice and performed local field potential (LFP) recordings in HC, but now also in mEC (Figure 2.1A). We confirmed that ChR2 expression was restricted to the MS (Figure 2.1B) and tetrodes were located in the HC or mEC (Figure 2.1B).

Mice were then trained to run around a rectangular track. Rhythmic stimulation at 8 or 12 Hz was applied to the medial septum on every other lap of the track so neuronal activity could be compared between periods of no stimulation and stimulation (Figure 2.1C). Similar to HC, we found that rhythmic stimulation of PV cells in the MS directly controlled the frequency of theta oscillations (Figure 2.1D) in mEC across a range of frequencies from within the endogenous (6-9 Hz) range at 8 Hz to outside the endogenous range at 10 Hz and 12 Hz (Figure 2.1E). This caused the peak frequency to shift to the stimulation frequency (Figure 2.1E) and superseded the endogenous theta by reducing power in the 6-9 Hz range during stimulation at frequencies of 10 or 12 Hz (Figure 2.1E).

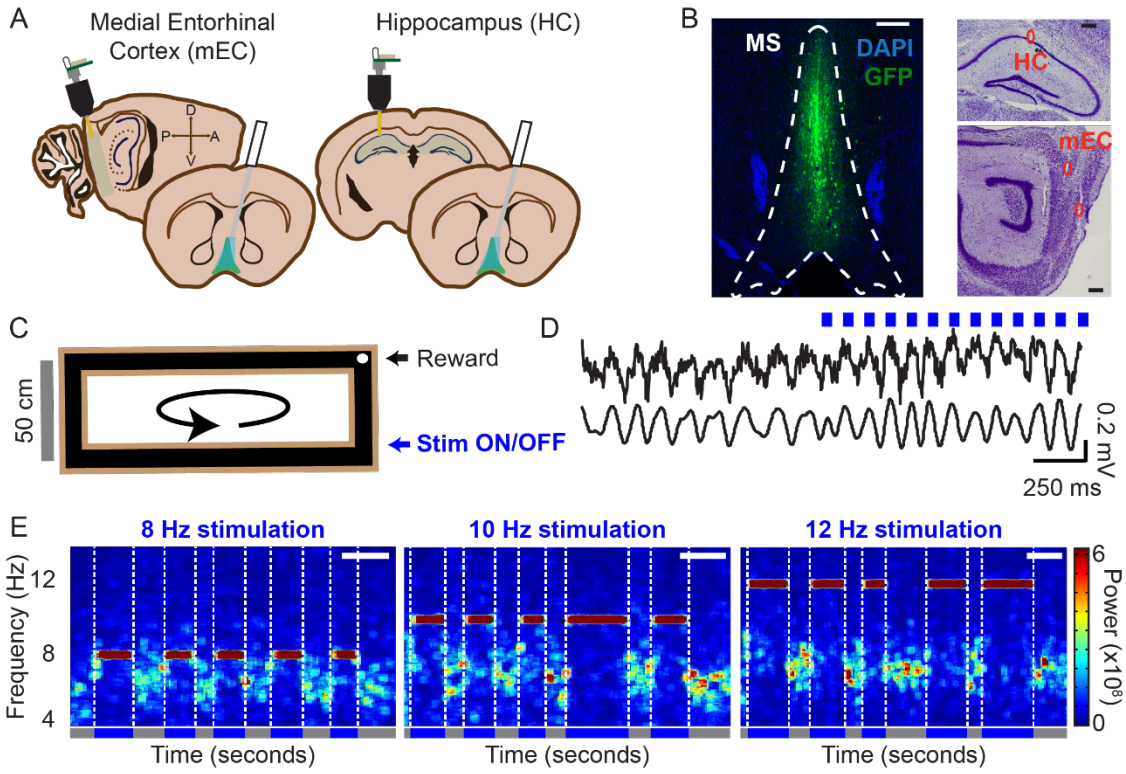

Figure 2.1 Rhythmic optogenetic stimulation of MS PV neurons controls the frequency of theta oscillations in the HC and mEC in freely behaving mice.

(a) PV-cre mice were injected with a viral vector containing ChR2 or oCHIEF (n=6) into the MS. Mice were implanted with an optic fiber over the MS and tetrodes over either the mEC (left) or HC (right). (b) GFP viral expression in the MS (green) counterstained with DAPI (blue). Example tetrode tracks (red circles) in the HC (top) and mEC (bottom). All scale bars are 250 μm. (c) Mice were trained to run counterclockwise on a large rectangular track. MS PV stimulation was performed on alternating laps using constant 8, 10, or 12 Hz stimulation. (d) MS PV stimulation immediately and persistently shifted theta to the stimulation frequency. (e) Example sessions from an individual mouse running on the linear track using 8 Hz and 12 Hz stimulation on every other lap. Theta was shifted to the stimulation frequency during periods of stimulation (blue) and superseded the endogenous (6-9 Hz) oscillation. White scale bars are 50 seconds.

mEC cells became more strongly entrained to the stimulation than HC cells

We next performed single unit recordings in the mEC (N=2 animals, n=127 cells) or HC (N=4 animals, n=181 cells) on the linear track and in the mEC (N=11 animals, n=637 cells) in the open field. To first separate principal cells and interneurons, we calculated the peak/valley ratio and compared that to the firing rate for each cell to calculate a cutoff for mEC on the linear track (cutoff of 15 Hz average firing rate; 8 Hz: n=121 principal cells, n=6 interneurons; 12 Hz: n=121 principal cells, n=6 interneurons; Figure 2.2A), mEC in the open field (cutoff of 10 Hz average firing rate; 8 Hz: n=456 principal cells, n=63 interneurons; 10 Hz: n=165 principal cells, n=28 interneurons; 12 Hz: n=564 principal cells, n=80 interneurons; Figure 2.2B), and HC (cutoff of 10 Hz average firing rate with a peak-valley cutoff of 1.5; 8 Hz: n=181 principal cells, n=18 interneurons; 10 Hz: n=85 principal cells, n=5 interneurons; 12 Hz: n=152 principal cells, n=9 interneurons; Figure 2.2C).

We calculated a pacing efficiency score to estimate the efficacy of the optogenetic stimulation on theta frequency in mEC and HC. We saw that mice in both the mEC and HC showed a shift in frequency at 8 Hz (Figure 2.2D) and 12 Hz (Figure 2.2E). All cells used for the analysis had stable and well-isolated clusters for all sessions (Figure 2.2F) based on L-ratio values (Figure 2.2G, top) and isolation distance (Figure 2.2G, bottom).

Figure 2.2. Single unit recordings.

(a) We calculated the peak-valley ratio and average firing rate (Hz) for each recorded cell in mEC for linear track recording experiments and plotted these two measures against each other. We created a cutoff (dotted line) based on an average firing rate of 15 Hz to separate putative principal cells (blue circles) from putative interneurons (red circles). (b) Same as in (a) but for mEC cells in the open field. A cutoff of 10 Hz was used to separate putative principal cells (blue circles) from putative interneurons (red circles). (c) Same as in (a) but for HC cells on the linear track. We used a rate cutoff of 10 Hz in addition to a peak-valley ratio cutoff of 1.5. Grey cells indicate cells that were not identified as a principal cell or interneuron and were thus excluded from all analysis. (d) We calculated the pacing efficiency for each individual animal during no stimulation (grey bars) and at 8 Hz stimulation (blue bars). (e) Same as in (d) but calculating the pacing efficiency during 12 Hz stimulation sessions. (f) Clusters remained stable in both no stimulation and stimulation conditions. (g) There was no change in the L-ratio (top) or the isolation index (bottom) for any stimulation condition.

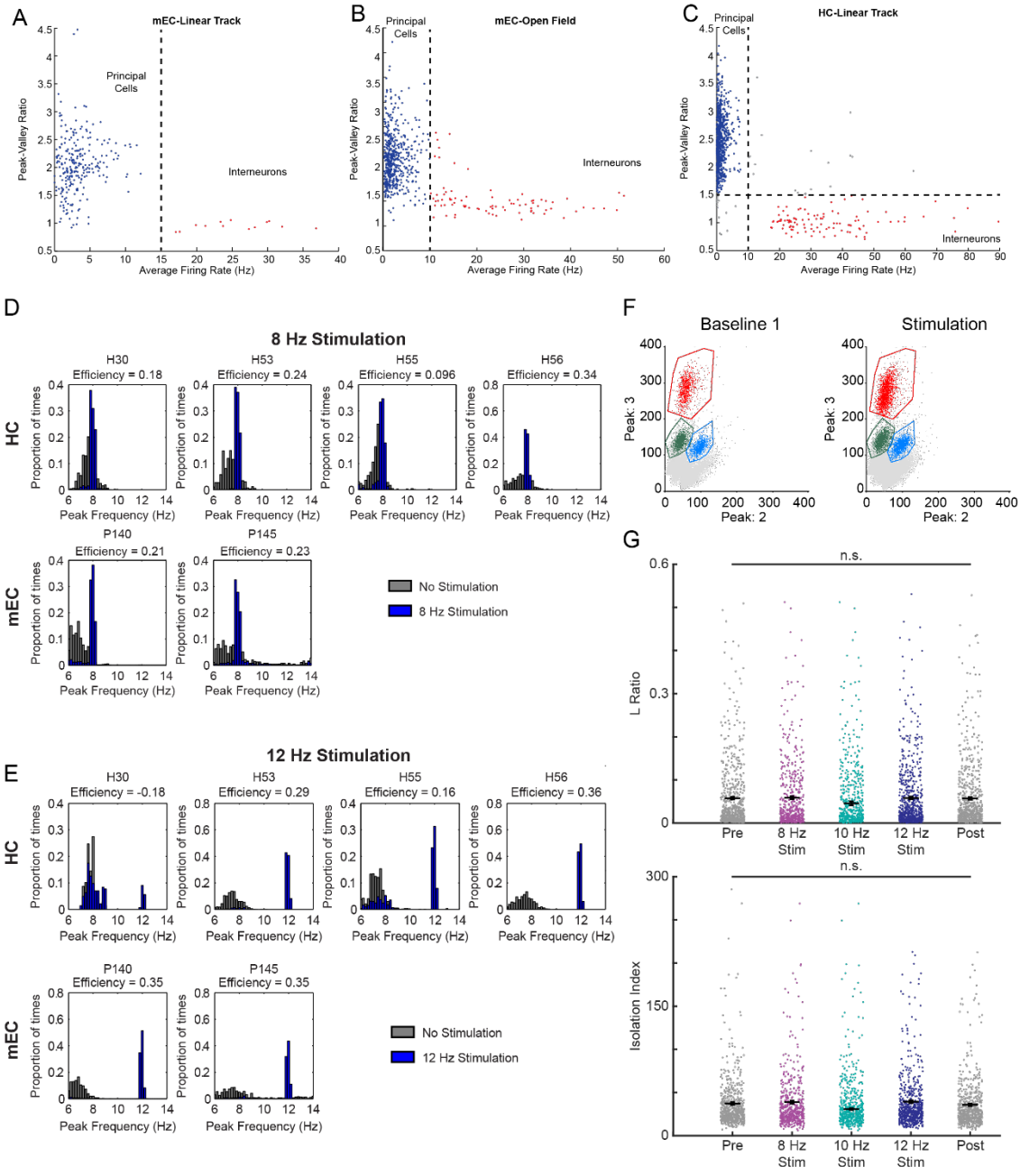
A
mEC-Linear Track
Principal Cells
Interneurons
Peak-Valley Ratio
Average Firing Rate (Hz)
B
mEC-Open Field
Principal Cells
Interneurons
Peak-Valley Ratio
Average Firing Rate (Hz)
C
HC-Linear Track
Principal Cells
Interneurons
Peak-Valley Ratio
Average Firing Rate (Hz)
D
8 Hz Stimulation
HC
mEC
H30
Efficiency = 0.18
H53
Efficiency = 0.24
H55
Efficiency = 0.096
H56
Efficiency = 0.34
P140
Efficiency = 0.21
P145
Efficiency = 0.23
Proportion of times
Peak Frequency (Hz)
No Stimulation
8 Hz Stimulation
E
12 Hz Stimulation
H30
Efficiency = -0.18
H53
Efficiency = 0.29
H55
Efficiency = 0.16
H56
Efficiency = 0.36
P140
Efficiency = 0.35
P145
Efficiency = 0.35
No Stimulation
12 Hz Stimulation
F
Baseline 1
Stimulation
Peak: 3
Peak: 2
G
n.s.
L Ratio
Isolation Index
Pre
8 Hz Stim
10 Hz Stim
12 Hz Stim
Post

We first took the autocorrelation power to measure the extent to which cells alter their rhythmicity in the mEC (Figure 2.2A, left) and HC (Figure 2.2A, right) for no stimulation sessions and stimulation sessions to compare the change in autocorrelation amplitude for each cell (Figure 2.3A) at 8, 10, and 12 Hz stimulation. To examine whether the entire population of cells alters its amplitude during periods of MS PV stimulation, we used a fast-Fourier transform (FFT) to calculate the peak amplitude for each cell and calculate the cumulative distribution function (Figure 2.3B).

We then only included cells that passed a peak amplitude cutoff of 0.1in either the no stimulation or the stimulation condition in order to remove cells that did not show any oscillation amplitude (Figure 2.3C). We then calculated a cumulative distribution function of the autocorrelation power for each stimulation condition in the mEC using the cells that passed this cutoff (Figure 2.3C, left). There was a significant increase in amplitude in the mEC for 8 Hz (ks test, p=2.71e-23), 10 Hz (p=6.74e-5), and 12 Hz (p=3.08e-9). We next calculated the cumulative distribution of cells recorded in the CA1 region of the HC using the same technique described for the mEC (Figure 2.3C, right) and found there was no change in amplitude for 8 Hz (ks test, p=0.78), 10 Hz (p=0.21), or 12 Hz (p=0.43).

Figure 2.3. Principal Cells in mEC are Paced to a Greater Extent Than HC Principal Cells.

(a) Frequency autocorrelations were performed on individual single units that were identified as putative principal cells in the mEC (left) and HC (right) for both no stimulation (grey) and stimulation (blue). The autocorrelation power and frequency were estimated for each cell. (b) Cumulative density function of all single units recorded for each stimulation condition. There was an increase in oscillation amplitude at all stimulation frequencies in the mEC but no change in the HC. (c) We then applied a 0.1 cutoff in either no stimulation or stimulation conditions and calculated the cumulative density function. There was an increase at 8 Hz, 10 Hz, and 12 Hz stimulation in the mEC, but no change for any stimulation in HC.

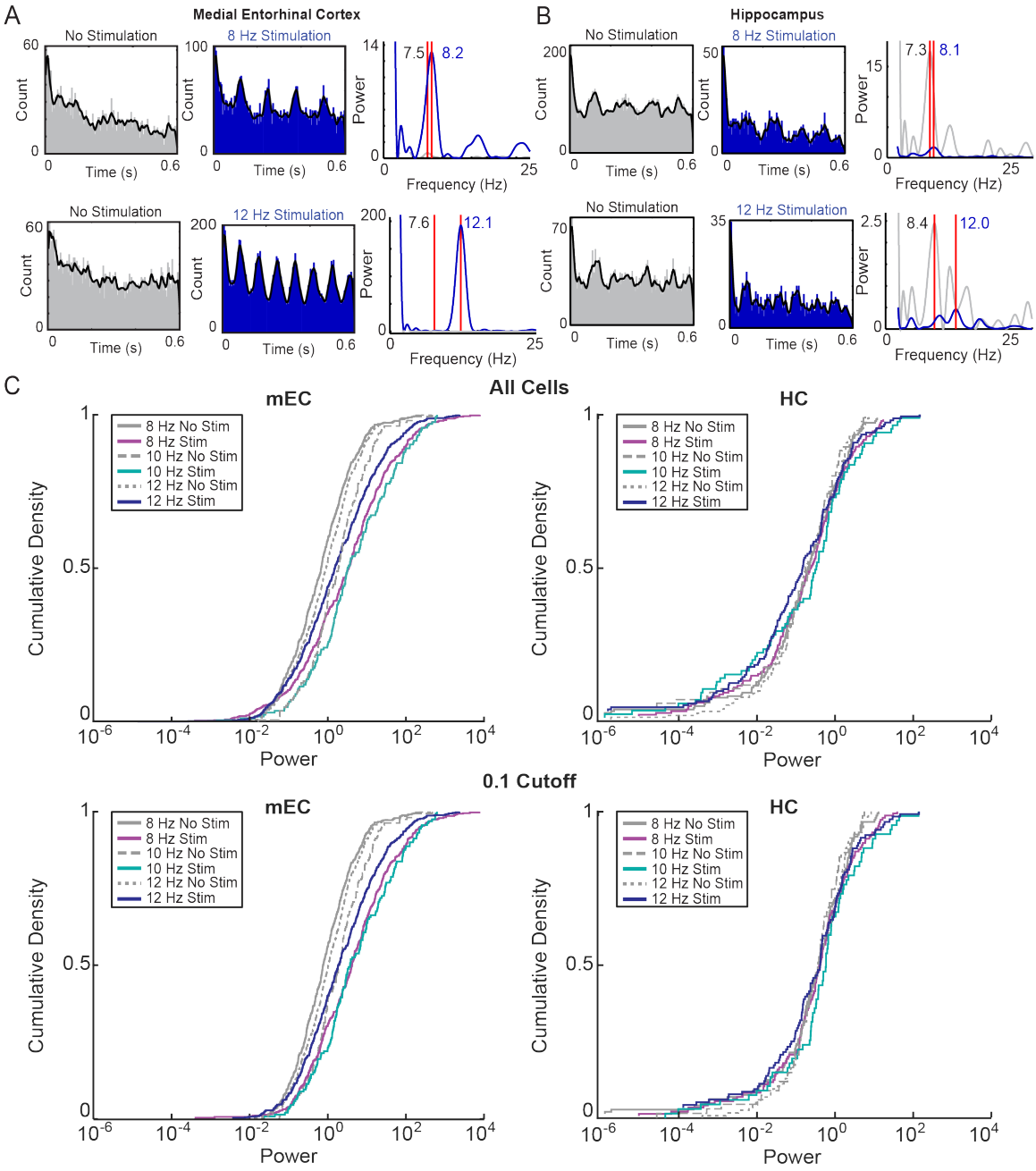
A
Medial Entorhinal Cortex
No Stimulation
8 Hz Stimulation
12 Hz Stimulation
Count
Time (s)
Power
Frequency (Hz)
7.5
8.2
7.6
12.1
B
Hippocampus
7.3
8.1
8.4
12.0
C
All Cells
mEC
HC
8 Hz No Stim
8 Hz Stim
10 Hz No Stim
10 Hz Stim
12 Hz No Stim
12 Hz Stim
Cumulative Density
Power
0.1 Cutoff

Principal cells in the mEC and HC respond with accelerated oscillation frequencies

To next examine to what extent MS PV stimulation controls the rhythmic firing frequency of principal cells in the mEC and HC, we also used the FFT of the temporal autocorrelation to examine the predominant frequency during no stimulation and stimulation (Figure 2.4A). Single cells in the mEC showed a shift in the intrinsic frequency at which they oscillated that approximately matched the shifted LFP frequency (Figure 2.4A-B). During no stimulation conditions, the majority of principal cells recorded in mEC generated oscillations that generally ranged from 6-10 Hz (Figure 2.4B, top). During 8 Hz, 10 Hz, and 12 Hz stimulation, the majority of mEC principal cells were shifted closer to the stimulation frequency (Figure 2.4B, bottom) for 8 Hz, 10 Hz, and 12 Hz stimulation conditions. Accordingly, at 10 Hz and 12 Hz, the majority of cells became shifted to approximately the frequencies that were accelerated compared to the endogenous oscillatory range. Similarly, principal cells in the HC were shifted to the stimulation frequency (Figure 2.4C-D).

We then calculated a cumulative density function for all principal cells that had an amplitude greater than 0.1 (Figure 2.4E-F). We found that the vast majority of these principal cells that passed the amplitude cutoff in the mEC (Figure 2.4E) and HC (Figure 2.4F) shifted in peak autocorrelation frequency in response to optogenetic theta pacing stimulation.

Figure 2.4: The majority of principal cells in mEC and HC shift in frequency during theta pacing.

(a) Color-coded power calculated from the autocorrelation function of principal cells in the mEC during no stimulation sessions (top) with red representing the autocorrelation frequency peak aligned with the peak LFP theta frequency (black dots). During 8, 10, and 12 Hz stimulation sessions (bottom) the majority of principal cells in the mEC became locked to the stimulation frequency. (b) Same as (a) but for principal cells in the HC. Most cells shift to the stimulation frequency at 8, 10 and 12 Hz. (c) Cumulative density function of the peak autocorrelation frequency for each stimulation condition in mEC. Single units shift to frequencies well outside the endogenous range at 10 and 12 Hz. Single units remain within the endogenous range of frequencies at 8 Hz. We then took the difference between the peak LFP frequency and the peak cell autocorrelation frequency (right). The vast majority of cells oscillated within a tight frequency range of the peak LFP frequency during stimulation sessions at all frequencies. (d) Same as in (c) but for cells in the HC. HC principal cells became less tightly coupled to the LFP frequency than mEC principal cells.

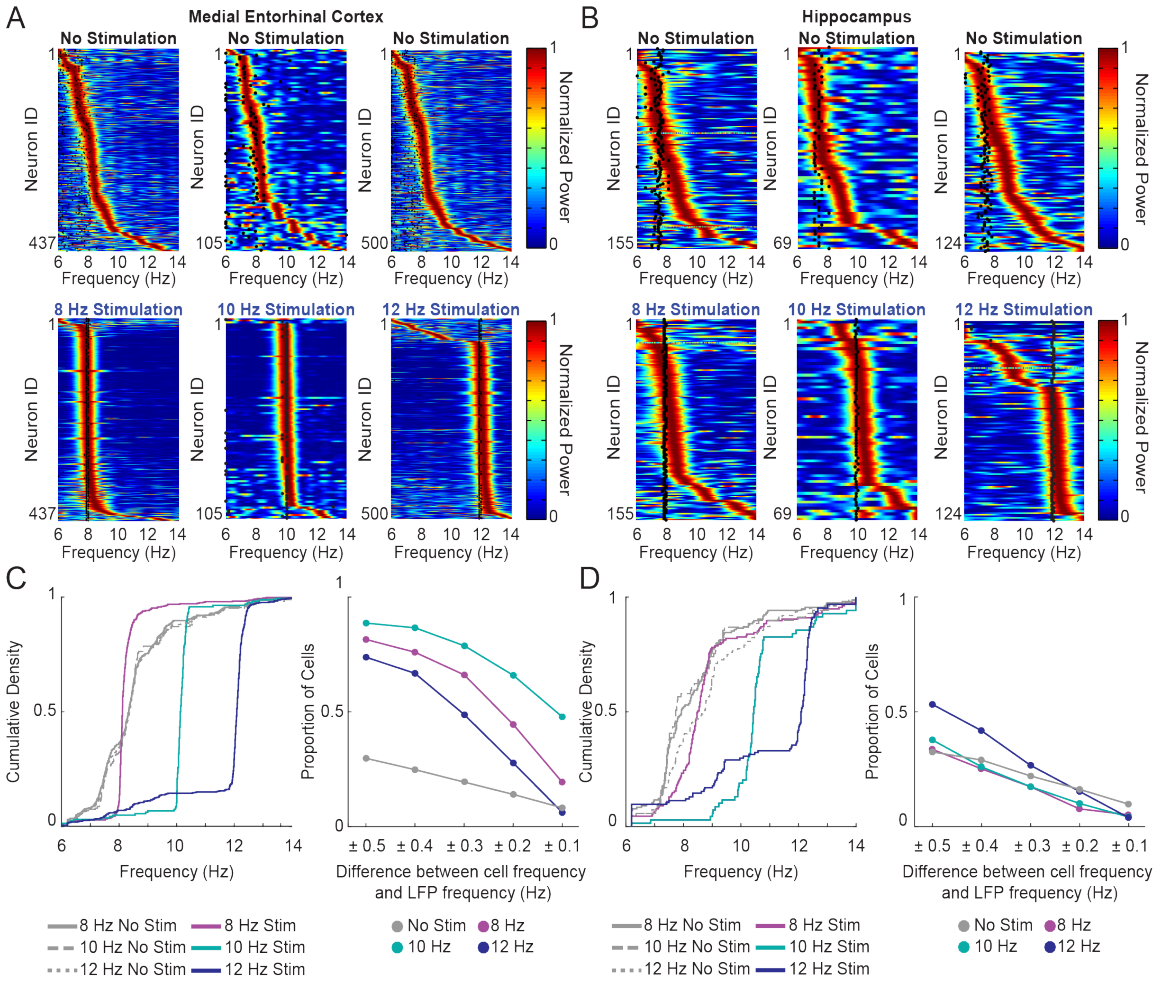
A
Medial Entorhinal Cortex
No Stimulation
No Stimulation
No Stimulation
8 Hz Stimulation
10 Hz Stimulation
12 Hz Stimulation
Neuron ID
Frequency (Hz)
Normalized Power
B
Hippocampus
No Stimulation
No Stimulation
No Stimulation
8 Hz Stimulation
10 Hz Stimulation
12 Hz Stimulation
Neuron ID
Frequency (Hz)
Normalized Power
C
Cumulative Density
Frequency (Hz)
Proportion of Cells
Difference between cell frequency and LFP frequency (Hz)
8 Hz No Stim
8 Hz Stim
10 Hz No Stim
10 Hz Stim
12 Hz No Stim
12 Hz Stim
No Stim
8 Hz
10 Hz
12 Hz
D
Cumulative Density
Frequency (Hz)
Proportion of Cells
Difference between cell frequency and LFP frequency (Hz)
8 Hz No Stim
8 Hz Stim
10 Hz No Stim
10 Hz Stim
12 Hz No Stim
12 Hz Stim
No Stim
8 Hz
10 Hz
12 Hz

Interneurons in the mEC and HC shift in frequency during theta pacing

We next examined whether interneurons in the HC and mEC experience a frequency shift during MS PV stimulation. Individual mEC and individual HC interneurons generated accelerated oscillation frequencies in response to the stimulation frequency (Figure 2.5A-B). While there was a significant increase in amplitude in the mEC during 8 Hz stimulation (Figure 2.5C; ks test, p=5.48e-4), there was no change at 10 Hz (ks test, p=0.17) or 12 Hz (ks test, p=0.40). In the HC, there was a significant increase in amplitude at 8 Hz (Figure 2.5C; ks test, p=0.014) and 10 Hz (ks test, p=0.036) but not at 12 Hz (ks test, p=0.078). The majority of mEC and HC cells shifted in frequency during stimulation sessions (Figure 2.5D).

Figure 2.5: The majority of interneurons in mEC and HC shift in frequency.

(a) Example spike time autocorrelations for interneurons in the mEC for no stimulation and stimulation sessions during 8 and 12 Hz stimulation. (b) Same as in (a) but for interneurons in the HC. (c) Cumulative distribution function of the amplitude for mEC interneurons (left) and HC interneurons (right). (d) Cumulative distribution function of the peak firing frequency of mEC interneurons (left) and HC interneurons (right).The majority of interneurons in both the mEC and HC showed a shift in the peak firing frequency during optogenetic theta pacing. mEC interneurons become more tightly entrained to the stimulation than HC interneurons.

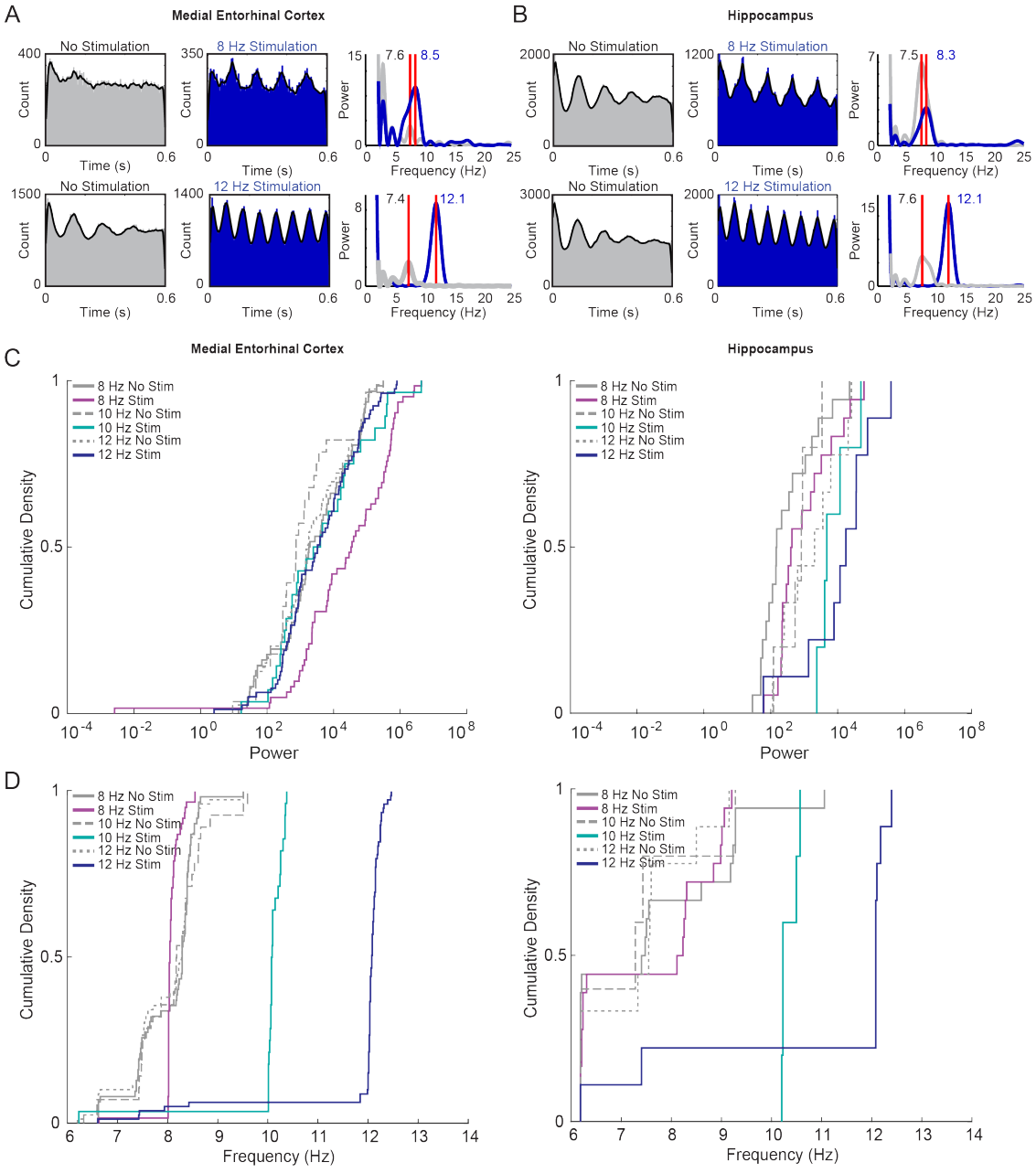
A
Medial Entorhinal Cortex
No Stimulation
8 Hz Stimulation
12 Hz Stimulation
Count
Time (s)
Power
Frequency (Hz)
7.6
8.5
7.4
12.1
B
Hippocampus
7.5
8.3
C
Cumulative Density
Power
8 Hz No Stim
8 Hz Stim
10 Hz No Stim
10 Hz Stim
12 Hz No Stim
12 Hz Stim
D
Frequency (Hz)

Pacing theta oscillations does not alter current source density profile of CA1

To localize the source of theta modulated inputs for endogenous and paced oscillations, we implanted linear silicon probes into CA1 (Figure 2.6A; n=3 mice) and recorded the local field potential at 16 sites spaced 50 μm apart (Figure 2.6B). We analyzed oscillation frequencies within the theta range (6-9 Hz) and also within the sharp wave ripple range (150-250 Hz). We found that the location of sharp wave ripples occurred on the same channels that we could locate in the pyramidal cell layer using the histology to reconstruct the channel locations (Figure 2.6 A-B).

We then performed a current source density (CSD) analysis and calculated the average CSD over every theta cycle for no stimulation, 8 Hz, 10 Hz, and 12 Hz MS PV stimulation (Figure 2.6C). We found that the depth profile did not differ between endogenous and paced oscillations (Figure 2.6C) for any stimulation frequency even though with higher frequency stimulations, theta cycles became shorter. Compellingly, the main sink/source pair during both endogenous and paced oscillations was in the stratum lacunosum moleculare (slm), the main input from the mEC to CA1.

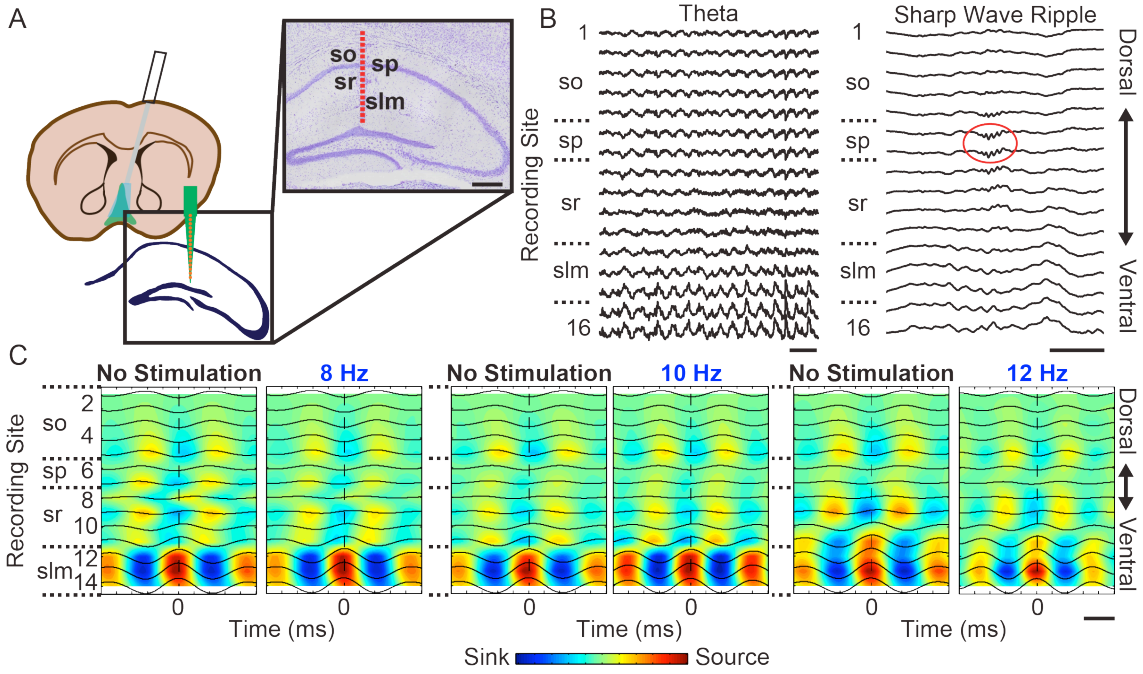

Figure 2.6: The main sink-source pair in CA1 is located in the stratum laconosum moleculare, the main input from mEC

(a) Three mice were implanted with a 16-site linear silicon probe into the CA1 area of HC (n=3). (b) Example LFP traces recorded simultaneously across all silicon probe recording sites ordered from most dorsal (top) to most ventral (bottom). LFP recordings were conducted in freely behaving mice. The location of the maximum amplitude of the sharp wave ripple corresponded to the reconstructed location of stratum pyramidale layer (sp). Scale bar is 250 ms. (c) Average current source density (CSD) analysis across sites 2-15 across CA1. Average CSD profiles were calculated during no stimulation, 8 Hz, 10 Hz, and 12 Hz stimulation. Abbreviations: so-stratum oriens, sp-stratum pyramidale, sr-stratum radiatum, slm- stratum laconosum moleculare. Scale bar is 50 ms.

We repeated this analysis for 3 total mice, which demonstrated that the main sink/source pair was in the slm in all mice (Figure 2.7A-C). These results suggest that the main theta-modulated input to the CA1 region originates from the mEC and we therefore reasoned that the extent of theta pacing in the hippocampus may depend on the control of mEC cells by optic stimulation of MS input.

Figure 2.7. The main sink-source pair in CA1 is located in the stratum laconosum moleculare, the main input from mEC, and is consistent between mice.

(a) Two additional mice implanted with silicon probe electrodes into CA1 in the same design described in Figure 2.6. Sections stained with cresyl violet and reconstruction of each recording site (red line) for all 16 recording locations. (b) Example 2-second LFP recording for each mouse across all 16 electrodes on the silicon probe. (c) Average current source density (CSD) for sites 2-15 for no stimulation, 8 Hz, 10 Hz, and 12 Hz stimulation.

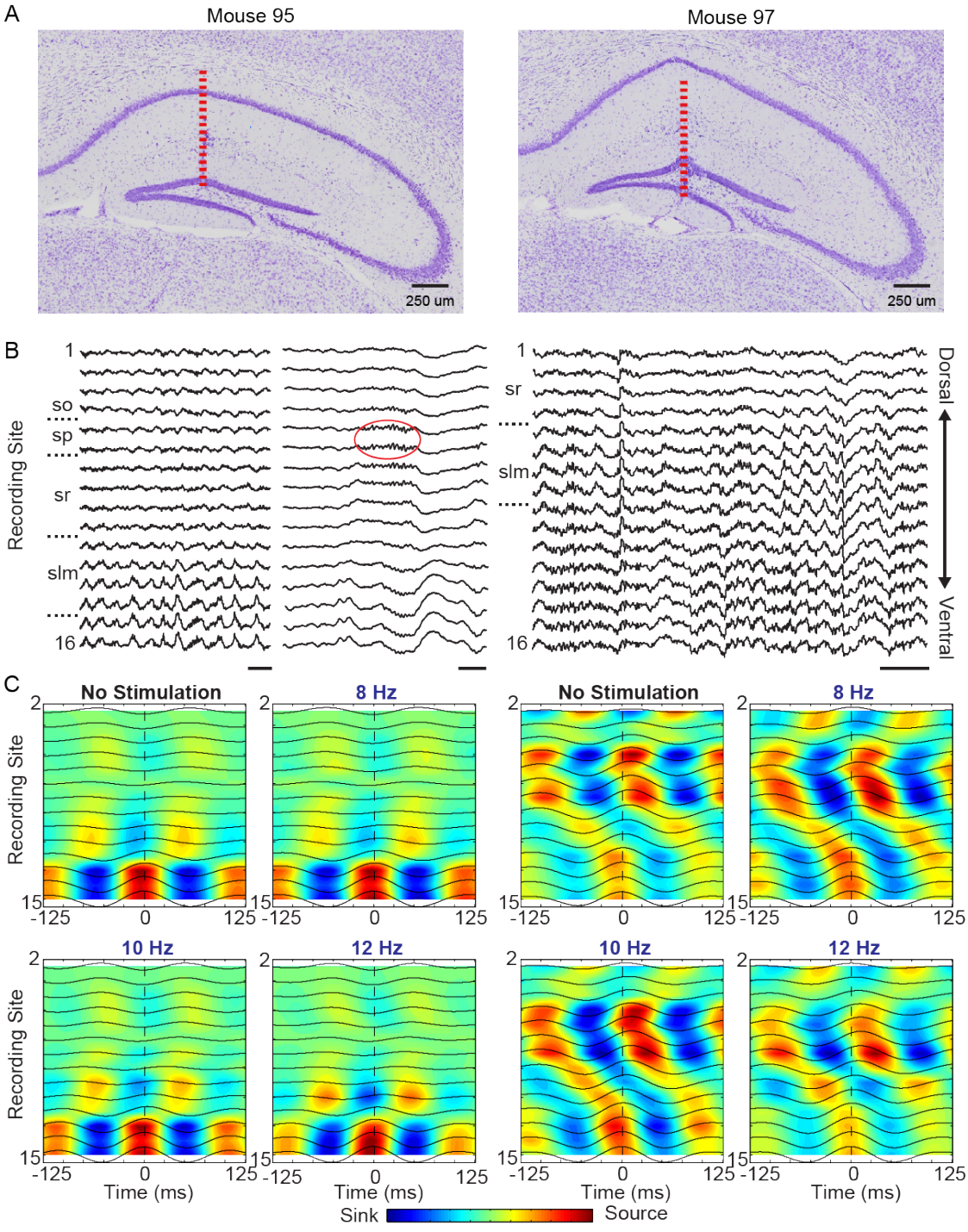
A
Mouse 95
Mouse 97
250 um
250 um
B
Recording Site
1
so
sp
sr
slm
16
Dorsal
Ventral
C
No Stimulation
8 Hz
10 Hz
12 Hz
Recording Site
Time (ms)
-125
0
125
2
15
Sink
Source

Pacing theta oscillations increased phase locking in mEC

We next examined the extent to which mEC and HC principal cells alter their phase related spiking in response to altered theta oscillation frequency and whether there was any change in the extent to which these cells phase lock to the LFP. We looked at the mean phase (degrees) during no stimulation and stimulation sessions and found a significant shift in the mean phase in the mEC (Figure 2.8A) but not in HC (Figure 2.8B). There was a significant change in mean phase in the mEC at 8 Hz (Figure 2.8A, p=1.12e-19), 10 Hz (p=6.36e-6), 12 Hz (p=1.50e-15). There was no change in phase angle in the HC at 8 Hz (Figure 2.8B, p=0.30) or 12 Hz (p=0.083), but there was a small but significant change at 10 Hz (p=0.047). Overall, these results show that MS PV stimulation that directly controls theta frequency has a stronger effect on phase related firing of mEC principal cells than HC principal cells.

We then calculated the mean resultant length as an indication of the extent of phase locking to the local LFP. There was a significant increase in phase locking represented by the mean vector length in the mEC at 8 Hz (Figure 2.8A, p=2.21e-62) and 10 Hz (p=4.55e-5) but not 12 Hz (p=0.24). There was no change in phase locking in the HC at 8 Hz (Figure 2.8B, p=0.52) or 10 Hz (p=0.42) but there was a significant increase at 12 Hz (p=1.74e-9). Overall, these results show that MS PV stimulation that directly controls theta frequency has a stronger effect on phase locking of mEC principal cells than HC principal cells.

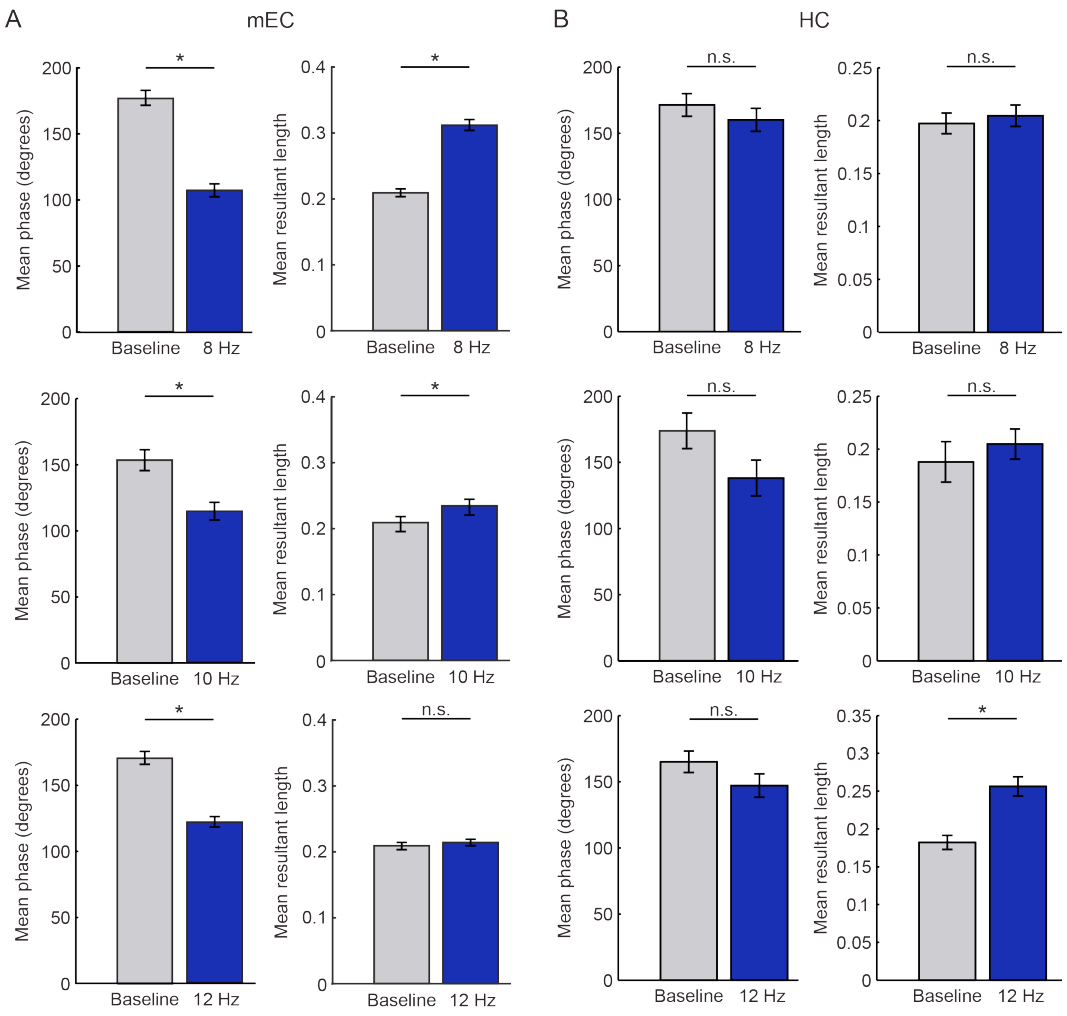

Figure 2.8: mEC principal cells become more phase locked during MS PV stimulation

(a) The mean phase (left) was significantly different between stimulation and no stimulation for mEC principal cells during all stimulation frequencies. There was an increase in the mean resultant length for 8 Hz and 10 Hz in mEC but not 12 Hz. (b) In HC, the mean phase (left) did not differ between no stimulation and stimulation sessions for any stimulation frequency. There was no change in the mean resultant length for 8 Hz or 10 Hz but a significant increase for 12 Hz. *p<0.05.

Discussion

Here, we investigated whether the precise timing of theta oscillatory frequency alters the spike timing of HC and mEC cells. As previously reported (Bender et al 2015, Fuhrmann et al 2015, Justus et al 2017, Zutshi et al 2018), we were able to precisely control the frequency of HC theta oscillations by optogenetically activating MS PV cells and show here that the mEC is not only directly paced by MS PV input, but that the pathway through mEC continues to make a major contribution to hippocampal theta during pacing. The preeminent role of mEC for generating theta oscillations is consistent with a stronger entrainment of mEC cells than HC cells and increased phase locking in response to theta pacing. It is also consistent with the location of the main sink-source pair in the stratum laconosum moleculare, the main input from the mEC to the CA1 region.

The mEC has long been hypothesized to have at least a partial role in generating theta rhythmicity in the HC. It has previously been shown that theta activity in the HC is generated by both feed-forward inhibition coming from MS GABAergic neurons and feed-forward excitation from the entorhinal cortex (Buzsaki et al 1983). In support of this, bilateral lesions to the entorhinal cortex diminish the sink-source pair located in the distal dendrites in CA1 (Bragin et al 1995, Kamondi et al 1998) located in the stratum laconosum moleculare.

Lesions to the mEC also cause a significant reduction to theta amplitude and theta frequency recorded in the CA1 region of the HC (Schlesiger et al 2015). Lesions to the

perforant path reduce theta amplitude in the HC (Yoder and Pang 2005). Lesions to either the GABAergic or cholinergic cell populations in the MS attenuates theta in the HC but does not eliminate it (Yoder and Pang 2005). However, lesions to the GABAergic and cholinergic cell populations in the MS combined with perforant path lesions drastically reduce theta amplitude in the HC (Yoder and Pang 2005). These results suggest that while lesioning the MS reduces theta amplitude in the mEC-HC, the mEC still has a further critical role in generating theta rhythm that is disrupted in the HC following damage to the mEC. Overall these results suggest that medial septal input from GABAergic PV cells may have a stronger drive on oscillatory frequency in the mEC than the HC.

While it has been suggested that theta oscillations contribute to the coordinated spiking that is important for episodic memory, our findings presented here establish a critical role for the MS in regulating the oscillatory timing of cells in the mEC and HC that may play a key role in memory. This is the first study that has demonstrated a direct role for the MS in the oscillatory spike timing of mEC and HC cells.

Acknowledgements

Chapter 2, in full, is material that is unpublished and being prepared for publication. It is coauthored by Quirk, Clare R., Zutshi, Ipshita, Srikanth, Sunandha, Wright, Morgan K., Parsey, Darian F., Devico Marciano, Naomie, Liu, Stanley, Fu,

Maylin L., Leutgeb, Jill K., and Leutgeb, Stefan. The dissertation author was the primary researcher and author of this material.

Chapter III.

Spatial firing patterns are not disrupted during optogenetically paced theta oscillations

Abstract

Cells that exhibit spatial firing patterns in the mEC and HC are tightly coupled to local theta oscillations. Inactivating the MS results in substantial reductions to theta oscillations in the mEC and HC. Reduction in theta amplitude as a result of this inactivation coincides with a reduction in the spatial periodicity of mEC grid cells. Other cells including non-grid spatial cells, head direction (HD) cells, and speed tuned cells in the mEC do not change their spatial, HD coding, or speed coding precision during periods of reduced theta oscillations. Hippocampal place cells do not lose their spatial precision during reduced theta oscillations but do experience a reduction in their average firing rate. However, it remains unclear from these results whether the loss of spatial tuning of grid cells is due to a reduction in oscillatory power or due to a general loss of excitation to mEC principal cells. We therefore examined how manipulations to the oscillatory timing of theta oscillations, which alter the spike timing of principal cells in mEC and HC, change the spatial firing patterns within the mEC-HC circuit.

Introduction

The firing of place cells and grid cells is strongly coupled to theta oscillations (O'Keefe and Recce 1993, Hafting et al. 2005). Inactivation of the MS, which disrupts theta, impairs grid cell spatial tuning without affecting place cell spatial firing (Brandon et al 2011, Koenig et al 2011, Brandon et al 2014). Spatial and head direction cells do not lose their spatial or directional tuning during reduced theta oscillations (Brandon et al 2011, Koenig et al 2011). However, other reports suggest grid cells do not require theta oscillations in other species such as bats (Yartsev et al 2011). Taken together, these findings indicate that while many cell types in the entorhino-hippocampal circuit are theta-modulated, this does not predict whether that particular cell type is effected by reducing theta.

A phenomenon that points to a relation between theta and spatial cells is theta phase precession of hippocampal place cells and mEC layer II grid cells. Here, cells always fire at a frequency higher than local theta, causing spikes during consecutive theta cycles to occur at increasingly earlier phases of theta (O'Keefe and Recce 1993, Skaggs et al 1996, Hafting et al 2008). This property can provide information to estimate how far the animal has traversed through the place field based on the phase of theta at which the cell is spiking. Phase precession can additionally order a series of overlapping place fields into a sequence of place cells, known as hippocampal theta sequences. Theta sequences are disrupted during inactivation of the medial septum (Wang et al 2015) while

theta phase precession of single place cells remains intact (Schlesiger et al 2015) during reduced theta oscillations.

Optogenetically shifting theta frequency to frequencies higher than the endogenous range (i.e., 10 and 12 Hz) does not disrupt theta phase precession (Zutshi et al 2018), which implies that the firing frequency of place cells exceeds the stimulation frequency and thus maintains phase precession. There is also no phase precession within the MS itself, whereas spatial cells in the mEC phase precess (Hafting et al 2008). Moreover, lesions to the mEC disrupt phase precession (Schlesiger et al 2015). Taken together, these results suggest that the MS plays a role in setting the base frequency for phase precession.

However, it remains unknown what the role theta frequency has in regulating spatial firing patterns of HC and mEC cells. In this chapter, we test this question by optogenetically manipulating theta frequency while recording single units in the HC and mEC in freely behaving animals.

Methods

Subjects

Fifteen parvalbumin-cre (129p2-Pvalbtm1(cre)arbr/j, Jackson Labs) mice weighing between 25-35 grams, were used as subjects. Mice were experimentally naïve and housed individually in Plexiglass cages on an inverse 12 hr light/dark cycle (lights off at 8 am). All training and testing was conducted during the dark phase. Mice were

restricted to 85% of their *ad libitum* weight and given full access to water. All procedures were conducted in accordance with the University of California, San Diego Institutional Animal Care and Use Committee.

Surgery

Mice were first injected with a viral vector containing the light-driven ion pump, Channelrhodopsin (AAV.EF1α.DIO.ChR2.eYFP) or (AAV.EF1αFLEX.oChIEF.mcitrine). Viral vectors were provided by Dr. Byungkook Lim's laboratory (University of California, San Diego). Mice were anesthetized with isoflurane (induction: 2.5%; maintenance 0.5-2%) and mounted in a stereotaxic frame (David Kopf Instruments, Model 1900). The scalp was cleaned and retracted using a midline incision and the skull was leveled between bregma and lambda.

A hole was drilled over the MS to make a small craniotomy (+1.0mm A/P, -0.7mm M/L) and 750 nL of virus was injected at a rate of 100 nL/min at two locations (400 nL, +1.0mm A/P, -0.7mm M/L, -4.8mm D/V; 350 nL, +1.0mm A/P, -0.7mm M/L, -4.2mm D/V) through a glass pipette using a microsyringe pump (Micro4, UMP3 UltraMicroPump, World Precision Instruments). The pipette was left in place for 5 minutes after the injection before being slowly retracted. Mice were sutured and allowed to recover for a minimum of 7 days.

Mice were implanted with an optic fiber over the medial septal area (MS) and either a four or eight-tetrode microdrive aimed at the medial entorhinal cortex (mEC) or dorsal CA1 region of the hippocampus (HC). Mice were anesthetized with isoflurane

(induction: 2.5%; maintenance 0.5-2%). The scalp was cleaned and retracted using a midline incision and the skull was leveled between bregma and lambda. Five holes were drilled in the skull to attach anchor screws and dental cement to secure the implant. A hole was drilled over the MS (+1mm A/P, -0.7 M/L, -3.7 D/V) and the optic fiber was implanted with a 10° medial-lateral angle. A ground screw was placed over the cortex. The skull was removed using a craniotomy over the HC (-2.25mm A/P, +2.0mm M/L) or MEC (from lambda; -0.9mm A/P, +3.8mm M/L, at an 8° angle anterior-posterior), the dura was removed and tetrodes were placed once they have just entered the brain. The microdrive was then cemented to the rest of the implant. Postoperative care was administered as needed for five to seven days until mice fully recovered. Any mice in which the shift in peak theta was not observed, were not used for analysis.

Behavior

Recordings were done while animals ran 10-14 laps counterclockwise on a rectangular track (150 x 50 cm with a track width of 10 cm) made of grey Plexiglas. Translucent walls were installed as guiderails (3 cm tall). The rectangular track was placed in the middle of a room that had several visual cues throughout and contained a dim light in one corner of the room that served as an orienting landmark. Animals were trained daily on the track for a minimum of two days prior to recording.

Mice were trained to freely forage in a square shaped open field (75 x 75 cm^2) with black walls and a single prominent white cue card along one wall. The open field was placed in the same location for all testing sessions in a room with dim lights and

distal cues along all walls. Mice were habituated to the open field for several days before recordings and optogenetic stimulation began. Once mice were trained, each mouse was run for at least three sessions per day: one baseline recording, between one and three stimulation sessions (8 Hz, 10 Hz, or 12 Hz randomized), and one final baseline recording.

Electrophysiological recordings

Local field potential (LFP) signals were recorded using the chronically implanted four or eight-tetrode (bundles of four 17 μm platinum-iridium (90/10%) wires, California Fine Wire Company) microdrives (Anikeeva et al 2012). Tetrodes were stabilized using an optic fiber (200 μm core, Thor Labs, 0.50 NA multimode fiber) that was glued to a zirconia ferrule (Precision Fiber Products, 230 μm).

Electrode tips were plated with platinum to reduce electrode impedances to between 150-250 kΩ at 1 kHz. Recording tetrodes were targeted to the CA1 pyramidal layer or to the dorsal MEC. A preamplifier, tether, and a 32-channel digital data acquisition system (Neuralynx, Inc.) was used. LFP was sampled at 32,000 Hz and filtered between 1 and 1,000 Hz.

Laser stimulation

Light was delivered to the MS using a 473 nm wavelength Blue DPSS Laser System through an optic fiber patch cord (Doric Lenses, MFP_200/240/1100-0.22_10m_FC-ZF1.25(F), 200 μm core, 0.22 NA) to a custom optic fiber implant. The

custom fiber optic implant was made using an optic fiber (200 μm core, Thor Labs, 0.50 NA multimode fiber) that was glued to a zirconia ferrule (Precision Fiber Products, 230 μm). The final optic fiber was sanded down to allow maximum light through the fiber and cut to a length of 4 mm. The output intensity was adjusted to between 9.0 and 12.0 mW. Light was delivered at a 50% duty cycle at frequencies of 8, 10, and 12 Hz. Laser stimulation was delivered on alternating laps of the rectangular track for each stimulation condition. The x and y coordinates of the animal's position data were collected using Neuralynx Cheetah Software and was then passed into MATLAB. A custom MATLAB script was used to calculate the median-x and median-y coordinates of the LEDs while the animals were running on the rectangular maze. The script then determined whether the animal was on an alternating lap. Once animals began a stimulation lap, MATLAB would instruct the Neuralynx Cheetah software to turn on the laser stimulation and was turned off once the MATLAB script determined the animal had finished the lap.

Histological procedures

Mice were perfused with 0.1 M phosphate-buffered saline (PBS) followed by 4% paraformaldehyde in PBS solution. Brains were post-fixed for 24 hours in 4% paraformaldehyde and then cryoprotected in 30% sucrose solution for 2 days. Brains were then frozen and sliced into 40 μm coronal sections for the MS and HC and 40 μm sagittal sections for the MEC on a sliding microtome. Sections were mounted on electrostatic slides and sections of the MS were coverslipped with Fluoroshield with DAPI (Sigma-Aldrich). Sections of the HC or MEC were mounted on electrostatic slides

and stained with cresyl violet and coverslipped with Permount (Fisher Scientific, SP15500) to visualize recording locations. Slides were imaged using a virtual slide microscope (Olympus, VS120).

Single unit identification

Single-units were manually isolated offline using MClust (http://redishlab.neuroscience.umn.edu/MClust/MClust.html), on MATLAB 2009b (Schmitzer-Toerbert et al 2005). Neurons were separated in two-dimensional space based on the peak amplitude, peak-to-valley amplitude, and energy of spike waveforms. The same cells was tracked within each day but were not tracked across days. Cells that were not present in all sessions in the day were not included in the analysis. Neurons that were not separable in cluster space were not included in the analysis. Cluster quality was determined using L-ratio and isolation distance.

Place field characterization

Position on the rectangular track was linearized into 116 bins that were 3.5 cm in size for analysis of spatial properties of HC neurons. Rate maps were computed as the number of spikes per time spent in each spatial bin and were smoothed by a pseudo-Gaussian kernel with a standard deviation of 1 bin. Spatial information was calculated as,

$$I = \sum_{i=1}^{N} p_i \frac{F_i}{F} \log_2 \frac{F_i}{F}$$

where I is the spatial information in bits/spike, p_i is the probability of occupancy in bin I, F_i is the mean firing rate for bin I, and F is the mean firing rate. Rate map stability was determined by calculating the correlation between rate maps for the first half of trials compared to the second half of trials. Place fields were defined as cells that had a peak spatial firing rate greater than 5 Hz that also maintained >20 % of the peak rate for at least 20 cm and less than 140 cm in the field. Cells were classified as principal cells if they had an average firing rate <10 Hz with a peak-valley cutoff of 1.5. Cells were classified as interneurons if their average firing rate exceeded this firing rate threshold and was below the peak-valley cutoff.

Single-cell temporal autocorrelations and frequency

For each cell, spike times were binned at a sampling rate of 500 Hz. The temporal autocorrelation between spike times was then calculated from the resulting vector. The power spectrum of the temporal autocorrelation was obtained via the Chronux function *mtspectrumumc*() in MATLAB using a padding factor equal to six powers of 2 over the sample size. The single-cell frequency was then taken as the frequency with peak power in the 6-14 Hz range.

Statistics

All behavior statistics were done using IBM SPSS Statistics version 23. Details of which tests are used were described with the results. No statistical tests were used for predetermining sample sizes, but our sample size is similar to other studies. For all

comparisons between stimulation compared to no stimulation conditions were done using paired comparisons or using repeated-measures. Tests for normality were performed and if normality could be assumed, we used paired two-tailed t-tests. When normality could not be assumed, we used Wilcoxin signed rank tests. For all repeated measures ANOVAs, sphericity was not assumed but accessed using Mauchly's test for sphericity. If sphericity could not be assumed, Greenhouse-Geisser was used.

Results

Spatial firing patterns were preserved during paced theta oscillations

After confirming that MS PV stimulation reliably resulted in the pacing of theta oscillations in both mEC and HC, we next examined the spatial coding responses to individual principal cells in mEC and HC during altered theta oscillations. We optogenetically stimulated the MS PV cells on alternate laps of a rectangular track to compare the same cells between light-on and light-off laps (Figure 3.1A, D). We performed a lap-by-lap analysis of spatial maps, which showed a reversible reorganization between light-on and light-off laps in both mEC and HC cells (Figure 3.1B, E). This effect is similar to previous findings in HC (Zutshi et al 2018) in which a reversible reorganization was seen in both GFP and ChR2 animals, suggesting the reorganization was due to light stimulation rather than the pacing of theta oscillations.

We next compared laps during light-on and light-off conditions and found that spatial coding was largely intact during each condition. This suggests that although the

spatial maps reorganized between light-on and light-off conditions, the maps remained stable during stimulation. In the mEC, there was no change in average firing rate (p_{8Hz}=0.81, p_{12Hz}=0.73; Figure 3.1B) or peak firing rate (p_{8Hz}=0.16, p_{12Hz}=0.21; Figure 3.1B) while there was a decrease in both average firing rate (p_{8Hz}<0.001, p_{12Hz}=0.014) and peak firing rate in the HC (p_{8Hz}<0.001, p_{12Hz}<0.001; Figure 3.1E). There was a decrease in the number of fields per cell at 12 Hz in the mEC (p_{8Hz}=0.08, p_{12Hz}<0.001; Figure 3.1B) and at both 8 Hz and 12 Hz in the HC (p_{8Hz}<0.001, p_{12Hz}<0.001; Figure 3.1E). While there was no change in spatial information in the HC at any stimulation frequency (p_{8Hz}=0.82, p_{12Hz}=0.59; Figure 3.1E), there was a significant increase in spatial information in the mEC at both 8 Hz (p_{8Hz}<0.001) and 12 Hz (p_{12Hz}=0.023; Figure 3.1B).

We next looked at the population spatial coding and saw that in no stimulation conditions, cells collectively covered the entire extent of the track in both mEC (Figure 3.1C) and HC (Figure 3.1F). The cells showed a reorganization of the spatial firing patterns relative to the no stimulation laps.

Figure 3.1. Spatial firing patterns are not altered in either the HC or mEC on the linear track during paced theta oscillations.

(a) Example mEC cells recorded during no stimulation and stimulation laps at 8 Hz stimulation (left) and 12 Hz stimulation (right). (b) Mean (±SEM) stability of rate maps. Within light-off and within light-on stability was higher than stability between light-off and light-on conditions. The mean firing rate was not altered between no stimulation and stimulation conditions for both 8 Hz (top) and 12 Hz (bottom). Other firing properties including peak firing rate, the number of fields per cell, and spatial information) showed significant differences between no stimulation and stimulation. * $p<0.05$. (c) The positions of the spatial fields of mEC principal cells were recorded along the linear track and ordered according to position independently between no stimulation and stimulation. (d) Same as in (a) but for HC principal cells. (e) Within light-off and within light-on conditions was higher than between light-on and between light-off conditions. Same as in (b) but for HC principal cells. * $p<0.05$. (f) Same as in (c) but for hippocampal principal cells. Place fields in the HC collectively covered the entire linear track in both conditions.

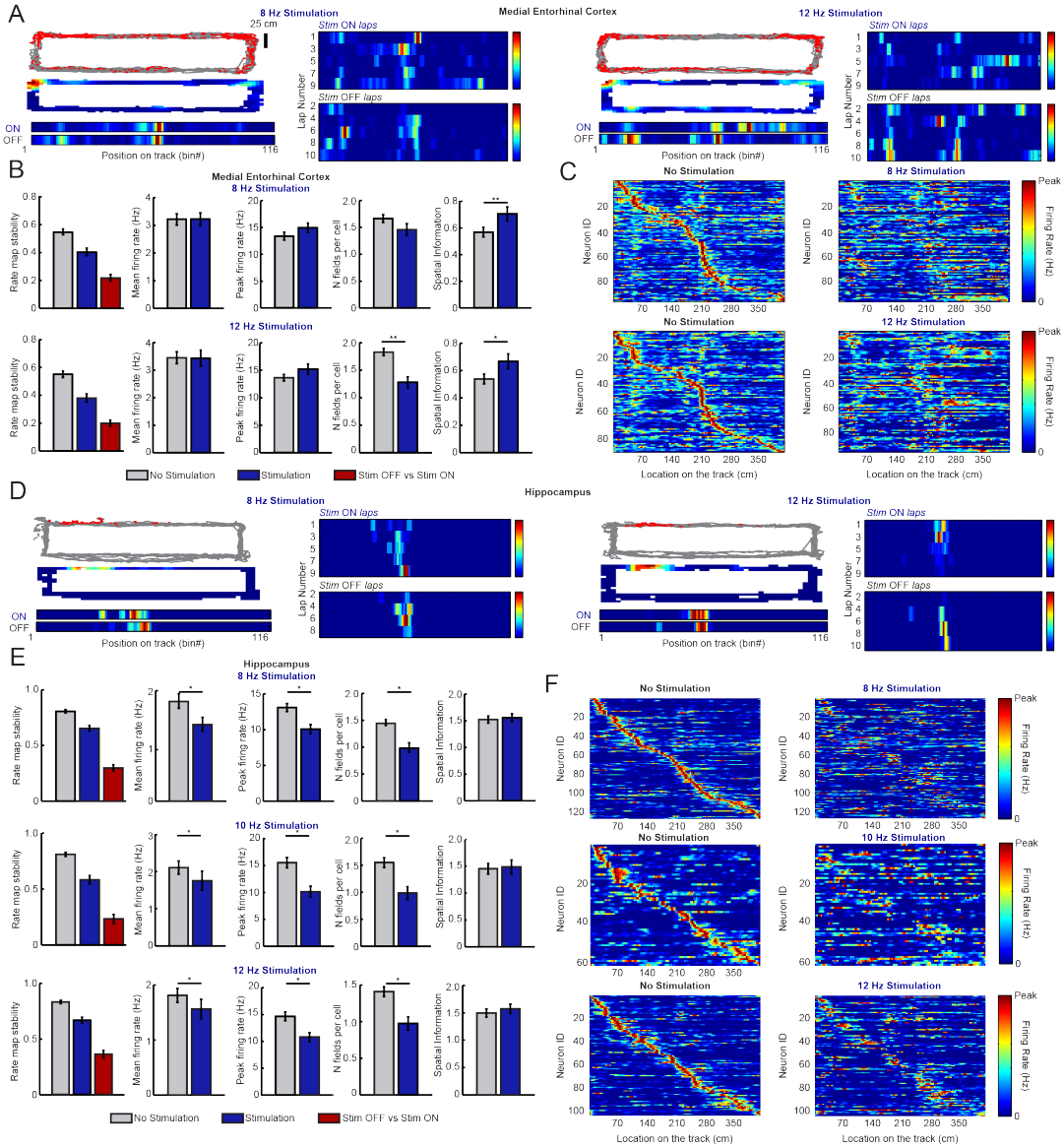
A
8 Hz Stimulation
25 cm
Stim ON laps
Stim OFF laps
Lap Number
ON
OFF
Position on track (bin#)
Medial Entorhinal Cortex
12 Hz Stimulation
B
Medial Entorhinal Cortex
8 Hz Stimulation
12 Hz Stimulation
Rate map stability
Mean firing rate (Hz)
Peak firing rate (Hz)
N fields per cell
Spatial Information
No Stimulation
Stimulation
Stim OFF vs Stim ON
C
No Stimulation
8 Hz Stimulation
12 Hz Stimulation
Neuron ID
Peak
Firing Rate (Hz)
Location on the track (cm)
D
Hippocampus
8 Hz Stimulation
12 Hz Stimulation
E
Hippocampus
8 Hz Stimulation
10 Hz Stimulation
12 Hz Stimulation
F
No Stimulation
8 Hz Stimulation
10 Hz Stimulation
12 Hz Stimulation

Spatial coding in the mEC is not altered during optogenetic theta pacing

We next examined whether medial septal pacing altered spatial coding, speed coding, or head direction (HD) coding while animals randomly foraged in an open field during baseline conditions without optical stimulation and during optical stimulation at 8, 10, or 12 Hz (Figure 3.2A). There was no change in the average firing rate for principal cells (Figure 3.2B; $F_{(4,220)}$=1.52, P=0.22) but a decrease in the average firing rate of interneurons (Figure 3.3A; $F_{(4,36)}$=2.68, P=0.047). The peak firing rate decreased for both principal cells (Figure 3.3B; $F_{(4,220)}$=4.55, P=0.002) and interneurons (Figure 3.3C; $F_{(4,36)}$=3.66, P=0.046).

We next examined whether there was any alteration to spatial coding in mEC principal cells (Figure 3.2C).We looked at spatial non-grid cells and there was no change in spatial information (Figure 3.2D left; $F_{(4,144)}$=1.36, P=0.26) or the within-session correlation in which the rate map from the first half of the session in correlated to the second half of the session (Figure 3.2D right; $F_{(4,168)}$=0.81, P=0.52).

Interestingly, there was no change to the spatial periodicity of grid cells (Figure 3.2E) in terms of gridness (Figure 3.2F left; $F_{(4,20)}$=0.24, P=0.91), spatial information of grid cells (Figure 3.2F right; $F_{(4,20)}$=0.66, P=0.63), or the spacing of grid cells (Figure 3.3D; $F_{(4,20)}$=1.28, P=0.31).

Table 3.1. mEC open field cell numbers.

Number of cells for each identified cell type for each stimulation condition. A total of 637 unique cells from 11 animals were recorded.

Cell Type	No Stimulation	8 Hz	10 Hz	12 Hz
Principal Cell	568	456	165	564
Interneuron	83	63	28	80
Spatial Cell	327	246	121	325
Grid Cell	16	16	6	16
Speed Cell-Principal	123	96	41	123
Speed Cell-Interneuron	23	14	11	22
Broadly Tuned HD Cell	265	198	106	265
Sharply Tuned HD Cell	50	46	6	50

Figure 3.2. Spatial patterns are not altered in the mEC during paced theta oscillations.

(a) Mice implanted with tetrodes in mEC were trained to randomly forage in an open field for approximately four sessions per day with the beginning and last session being a no stimulation session. (b) There was no change to the average firing rate of mEC principal cells during any stimulation frequency. (c) Trajectory and rate maps for two example spatial cells recorded across four sessions. (d) There was no change to the spatial information (left) or within-session correlation (right). (e) Trajectory and rate maps for two example grid cells recorded across four sessions. (f) There was no change to the gridness score (left) or the spatial information of grid cells (right).

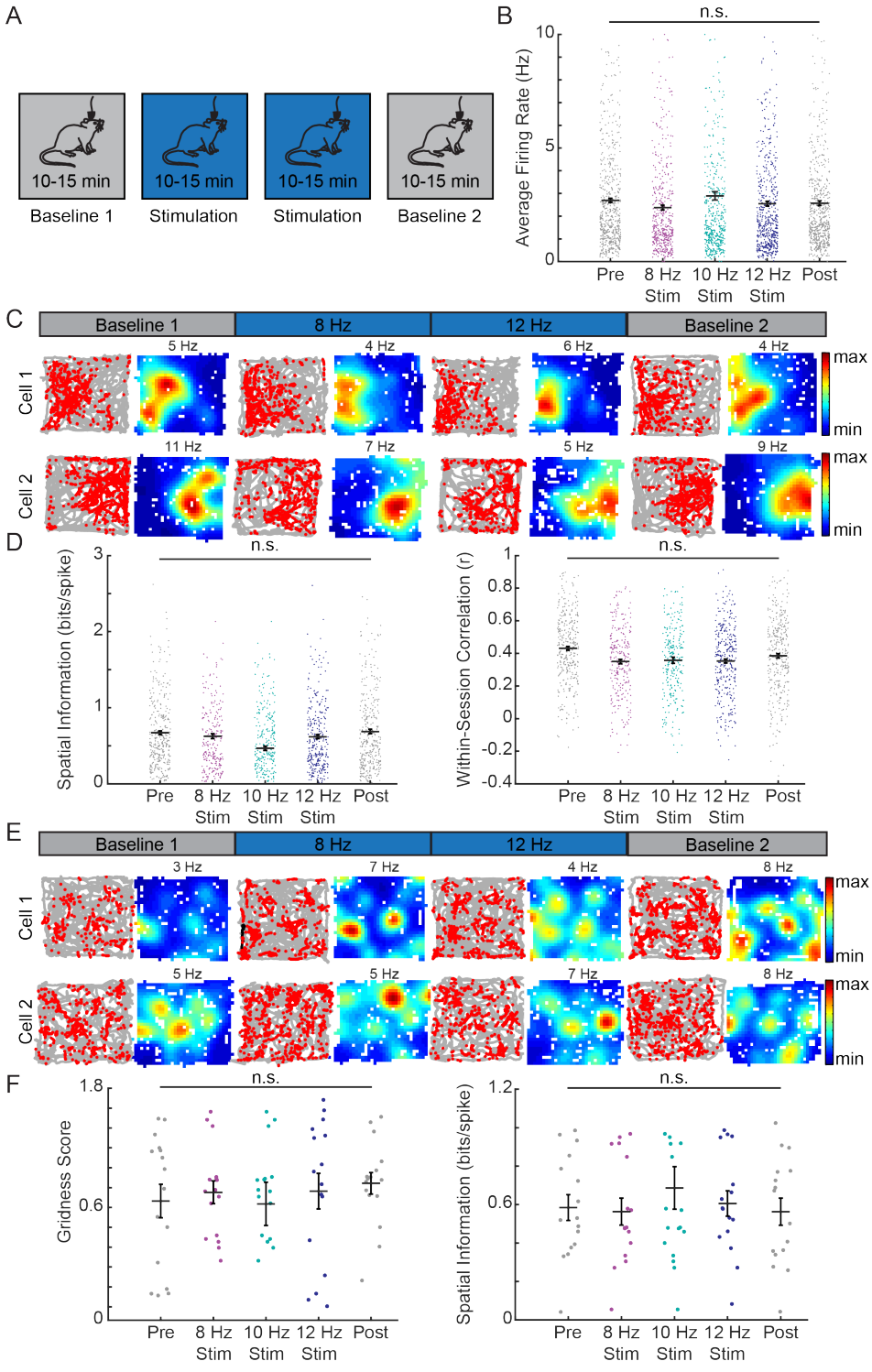
A
10-15 min
Baseline 1
10-15 min
Stimulation
10-15 min
Stimulation
10-15 min
Baseline 2
B
n.s.
Average Firing Rate (Hz)
10
5
0
Pre
8 Hz Stim
10 Hz Stim
12 Hz Stim
Post
C
Baseline 1
8 Hz
12 Hz
Baseline 2
Cell 1
5 Hz
4 Hz
6 Hz
4 Hz
max
min
Cell 2
11 Hz
7 Hz
5 Hz
9 Hz
max
min
D
n.s.
Spatial Information (bits/spike)
3
2
1
0
Pre
8 Hz Stim
10 Hz Stim
12 Hz Stim
Post
n.s.
Within-Session Correlation (r)
1
0.8
0.6
0.4
0.2
0
-0.2
-0.4
Pre
8 Hz Stim
10 Hz Stim
12 Hz Stim
Post
E
Baseline 1
8 Hz
12 Hz
Baseline 2
Cell 1
3 Hz
7 Hz
4 Hz
8 Hz
max
min
Cell 2
5 Hz
5 Hz
7 Hz
8 Hz
max
min
F
n.s.
Gridness Score
1.8
0.6
0
Pre
8 Hz Stim
10 Hz Stim
12 Hz Stim
Post
n.s.
Spatial Information (bits/spike)
1.2
0.6
0
Pre
8 Hz Stim
10 Hz Stim
12 Hz Stim
Post

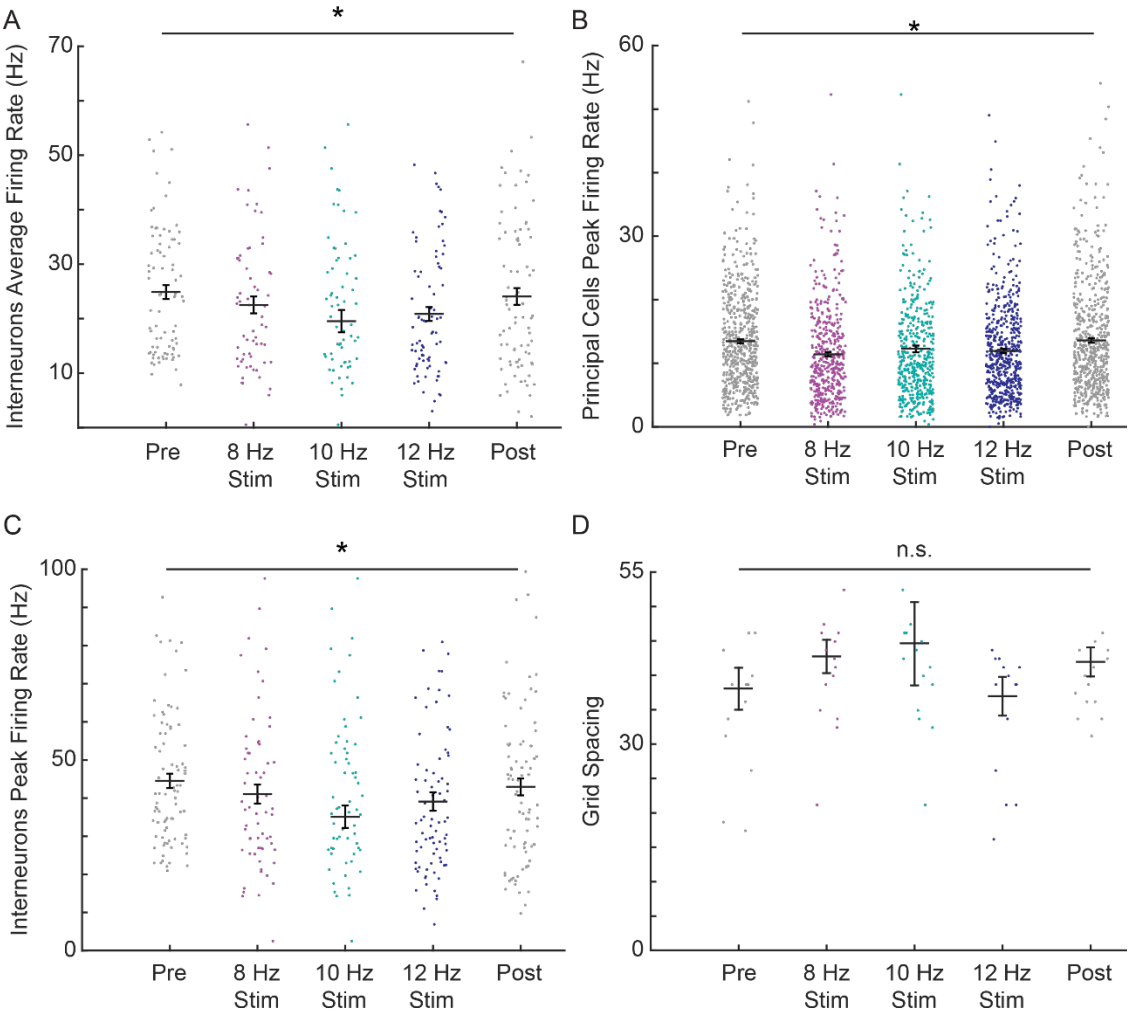

Figure 3.3. Optogenetic theta pacing effects on the firing statistics of mEC cells.

(a) There was a significant decrease in the average firing rate of interneurons. (b) There was a significant decrease in the peak firing rate of principal cells. (c) There was a significant decrease in the peak firing rate of interneurons. (d) There was no change in the spacing of grid cells. *p<0.05. *p<0.05.

Speed coding and head direction coding are not altered during paced theta oscillations

We next looked at speed coding of mEC speed cells during no stimulation and stimulation conditions (Figure 3.4A). It has previously been reported that both principal cells and interneurons can be identified as speed cells (Kropff et al 2015). We therefore separated speed cells into speed modulated principal cells (Figure 3.4B, left) and speed modulated interneurons (Figure 3.4B, right) and measured the changes in speed score during paced theta oscillations. There was no change in the speed coding in speed principal cells (Figure 3.4B, left; $F_{(4,52)}$=0.53, P=0.63) or speed interneurons (Figure 3.4, right; $F_{(4,4)}$=0.33, P=0.85). We next looked at head direction (HD) coding and divided HD cells into broadly tuned cells and sharply tuned cells. There was no effect on sharply tuned cells ($F_{(4,4)}$=0.33, P=0.37) but an effect on broadly tuned cells ($F_{(4,188)}$=7.92, P=0.002).

Figure 3.4. Speed cells are not altered in the mEC during paced theta oscillations.

(a) Two example speed cells recorded across four sessions. Running speed (cm/s) was correlated with the instantaneous firing rate (Hz). (b) There was no difference in speed score at any stimulation frequency for speed modulated principal cells (left) or speed modulated interneurons (right). (c) Example mean resultant length of identified HD cells. (d) There was a significant change in HD length for broadly tuned HD cells but not for sharply tuned HD cells. *$p<0.05$.

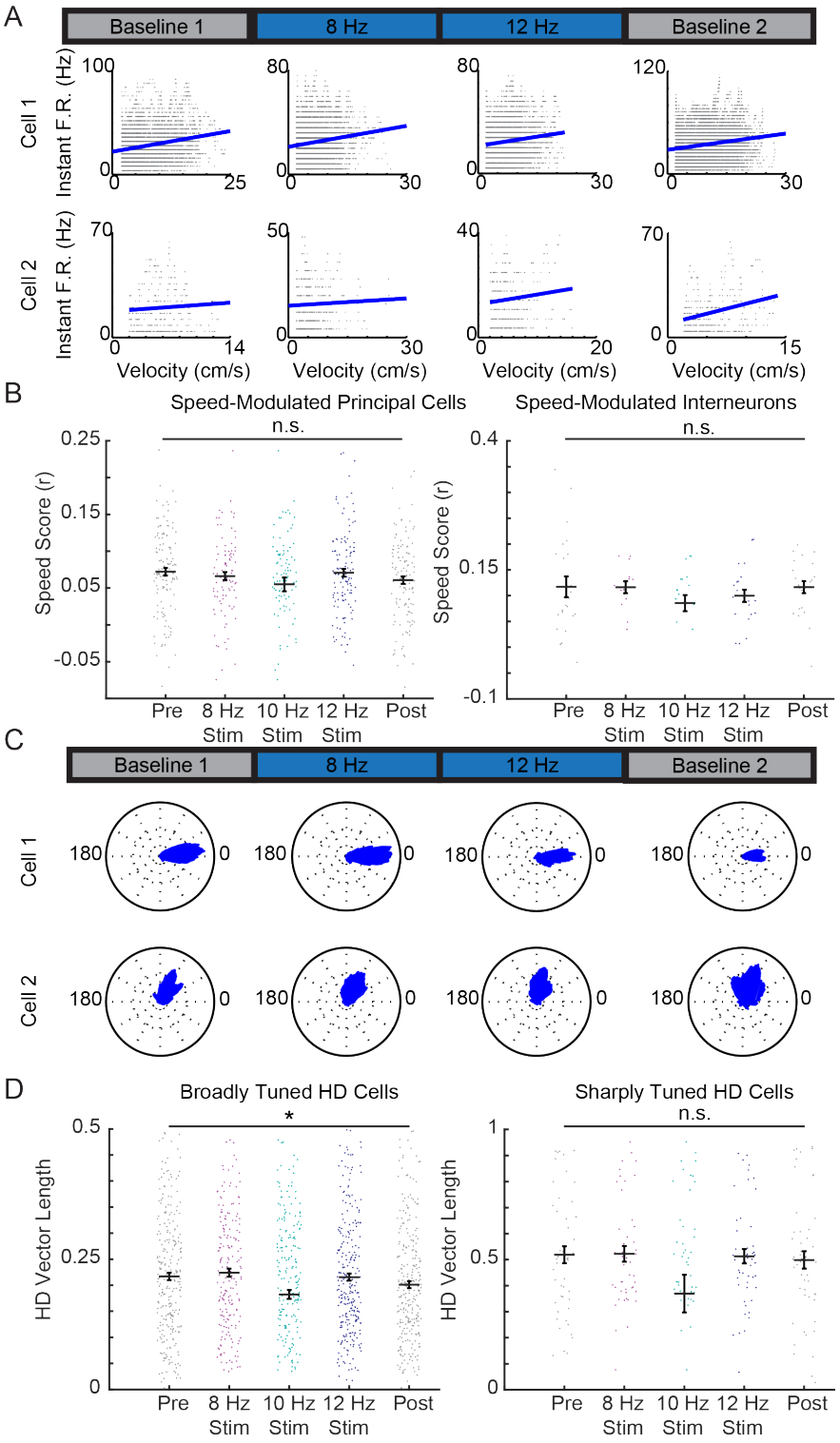
A
Baseline 1
8 Hz
12 Hz
Baseline 2
Cell 1
Cell 2
Instant F.R. (Hz)
Velocity (cm/s)
B
Speed-Modulated Principal Cells
Speed-Modulated Interneurons
n.s.
Speed Score (r)
Pre
8 Hz Stim
10 Hz Stim
12 Hz Stim
Post
C
D
Broadly Tuned HD Cells
Sharply Tuned HD Cells
*
HD Vector Length

Discussion

Previous research has shown that inactivation of the MS and subsequent reduction of theta amplitude has a selective effect on reducing the spatial firing of grid cells in the mEC while other HC place cells and mEC defined spatial non-grid cells, head direction cells, and speed cell types remained completely intact (Brandon et al 2011, Koenig et al 2011, Hinman et al 2016).

Interestingly, our data presented here show that there were no alterations to spatial coding in either the HC or mEC when the frequency of theta oscillations in the mEC or HC was optogenetically manipulated and shifted outside of the endogenous range. Inactivations of the MS cause a large reduction not only in theta amplitude, but to firing rates of principal cells in the entorhino-hippocampal circuit (Brandon et al 2011, Koenig et al 2011, Wang et al 2015, Hinman et al 2016). This suggests that the change in the spatial periodicity of grid cells during MS inactivation could possibly be due to a reduction in excitation to the mEC and HC and not to changes in theta oscillations or the coupling between the animal's running speed and theta frequency.

Importantly, our manipulation used in this experiment did not result in any reduction to the average firing rates of mEC and HC principal cells. Interestingly, we did not see any changes to spatial non-grid cells, head directional cells, or speed coding during accelerated ($\leq$ 10 Hz) theta oscillations when the endogenous theta frequency (6-9 Hz) was lowered. Overall, our results showed that manipulations to endogenous theta frequency did not alter spatial coding or other cell types in the mEC or HC even though

the spike timing and oscillatory frequencies of these cells is significantly altered and oscillates outside of the 6-9 Hz range.

Future experiments will need to examine the role of other cell populations within the MS in generating the firing patterns of grid cells in the mEC. Although it has been hypothesized that the reduction of theta in the MS reduces the coupling between running speed and theta frequency (Jeewajee et al 2008), our manipulations used here to manipulate theta frequency remove the speed modulation of theta frequency. Nonetheless, grid cells maintained their spatial periodicity and speed cells also remained speed modulated as seen previously (Hinman et al 2016).

The smaller glutamatergic cell population within the MS has also showed an ability to slightly alter the frequency of theta oscillations and alter the running speed of animals when these cells are rhythmically activated (Fuhrmann et al 2015). Although the role that these glutamatergic cells play in running speed is now known, their role in grid cell firing is unknown.

It has also been proposed that the large population of muscarinic cholinergic cells in the MS, which project to both principal cells and interneurons in the HC and mEC, may be providing a strong input that regulates grid cell firing. Systemetic injections of scopolamine, a muscarinic acetylcholine antagonist, reduces the spatial periodicity of mEC grid cells (Newman et al 2014). However, because this injection was done systemically and therefore given throughout the brain and body nonspecifically, there is no way of knowing whether manipulating the cholinergic cells in the MS would change the spatial periodicity of mEC grid cells.

Future experiments will also need to examine the role of theta frequency on the coordination of large ensembles of hippocampal place cells. Place cells organize into sequential firing patterns within each theta cycle for overlapping place fields. Previous research has shown that inactivations to the MS cause disruptions to the coordinated sequential firing patterns of hippocampal place cells (Wang et al 2015). Optogenetically shifting the frequency of theta oscillations while performing high density recordings of CA1 cells with overlapping place fields could address this issue.

It has generally been assumed that brain oscillation patterns in multiple frequency bands are necessary for cognitive processes and regulating the spike timing of cells. Here we show that brain circuits within the mEC and HC can tolerate a wide range of perturbations of oscillatory patterns and that these changes did not alter spatial coding of defined cell types in the mEC and HC. While it is already widely recognized that correlative results need to be cautiously interpreted, our data add that manipulations of oscillations also need to be thoroughly examined because they often have effects beyond the directly targeted patterns.

Acknowledgements

Chapter 3, in full, is material that is unpublished and being prepared for publication. It is coauthored by Quirk, Clare R., Zutshi, Ipshita, Srikanth, Sunandha, Wright, Morgan K., Parsey, Darian F., Devico Marciano, Naomie, Liu, Stanley, Fu,

Maylin L., Leutgeb, Jill K., and Leutgeb, Stefan. The dissertation author was the primary researcher and author of this material.

Chapter IV.

Disruption of endogenous theta frequency disrupts spatial working memory

Abstract

Theta oscillations in the medial entorhinal cortex (mEC) and hippocampus (HC) have been hypothesized to coordinating the precise spike timing within the mEC-HC circuit that contributes to the formation of episodic memories. Inactivation of the MS results in a substantial reduction in the amplitude of theta oscillations and, consequently, profound memory impairments in tasks that require the intact function of HC and mEC. We tested how rhythmic control of the timing of theta frequency by optogenetic stimulation of medial septum (MS) parvalbumin (PV) cells would alter spatial working memory in a task that requires the HC and mEC. We found that MS PV stimulation entrained theta for extended periods of time, making this technique a reliable way to manipulate theta oscillations during a memory task. We found that stimulating MS PV cells outside of the 6-9 Hz range by accelerating theta to frequencies of 10, 12, and 20 Hz resulted in significant memory impairments. We further demonstrated that rhythmic stimulation at 8 Hz, a frequency within the endogenous range, did not alter memory performance. We next controlled for the effects of viral expression and light stimulation

on the behavioral results and found no effect in animals injected with ChR2 and stimulated with green light stimulation or in animals injected with a control GFP vector and stimulated with blue light. We finally demonstrate that by restricting the stimulation to distinct periods of the task resulted in a selective memory deficit when oscillatory patterns were accelerated on the return arm. These results demonstrate that the precise endogenous pacing of theta oscillations is critical in hippocampal and mEC-dependent memory and that this deficit occurs during periods of memory encoding. Overall, these results demonstrate a role for endogenously paced theta oscillations in spatial working memory that are as critical as the intact function of the HC and mEC.

Introduction

Theta oscillations have long been hypothesized to play a critical role in memory formation (Hasselmo 2005). Disrupting theta by inactivating or lesioning the MS during hippocampal-dependent memory tasks severely impairs performance (Winson 1978, Chrobak et al 1989, Brioni et al 1990, Mizumori et al. 1990, Givens and Olten 1994, Leutgeb and Mizumori 1999, Wang et al 2015). It has been suggested that this deficit is due to alterations in spike timing of cells in the HC and mEC in the absence of theta (Mizumori et al. 1990, Leutgeb and Mizumori 1999, Wang et al 2015).

Selective lesions to either the GABAergic or cholinergic cell populations in the MS do not, or only mildly impair spatial memory. Combined lesions of both however, result in a severe memory deficit in hippocampal-dependent memory tasks such as the

Morris water maze (Pang et al 2001, Smith and Pang 2005). Other reports suggest that inactivating either cell type is sufficient to cause a memory deficit in a working memory task (Chrobak et al 1992, Bunce et al 2004). The differences seen in these studies is most likely due to differences in methods of inactivations or lesions and which behavioral task was used.

Although silencing the MS is accompanied by severe memory deficits, this deficit can be rescued using electrical stimulation of the MS if the stimulation frequency is theta rhythmic. Inactivation of MS during the Morris water maze impaired learning but could be restored by rhythmic theta stimulation at 7.7 Hz of the fornix (McNaughton et al 2006). In an animal model of traumatic brain injury, rats showed attenuated theta oscillations and deficits in the Barnes maze following lateral fluid percussion that was rescued by stimulation of the MS at 7.7 Hz one minute prior to training (Lee et al 2013) while non rhythmic stimulation did not improve memory. In a brightness discrimination training task, stimulation at 7 Hz applied five minutes after training improved performance while stimulation of 100 Hz significantly impaired retention of the task (Wetzel et al 1977). Interestingly, theta oscillation frequency is also altered in animal models of Alzheimer's disease (Goutagny et al 2013).

Overall, these results strongly point to a role for theta oscillations generated from the MS in hippocampal-dependent memory. However, these experiments also cause drastic changes in the firing statistics of neuronal populations (Brandon et al 2011; Koenig et al 2011; Wang et al 2015), making it difficult to know whether the effect on

memory is due to a reduction in theta oscillations or a loss of excitation within the network.

Methods

Subjects

Twenty three parvalbumin-cre (129p2-Pvalbtm1(cre)arbr/j, Jackson Labs) mice (n=17 male, n=6 female) weighing between 25-35 grams, were used as subjects. Mice were experimentally naïve and housed individually in Plexiglass cages on an inverse 12 hr light/dark cycle (lights off at 8 am). All training and testing was conducted during the dark phase. Mice were restricted to 85% of their *ad libitum* weight and given full access to water. All procedures were conducted in accordance with the University of California, San Diego Institutional Animal Care and Use Committee.

Surgery

Mice were first injected with one of two viral vectors. Fourteen mice were injected with a viral vector containing the light-driven ion pump, Channelrhodopsin (AAV.EF1α.DIO.ChR2.eYFP) and six mice were injected with a control viral vector (AAV.EF1α.DIO.eGFP). Three additional mice were injected with the light-driven ion pump (AAV.EF1αFLEX.oChIEF.mcitrine) and were grouped for all analysis with the ChR2 group. For simplicity, this group was called "ChR2". Viral vectors were provided by Dr. Byungkook Lim's laboratory (University of California, San Diego). Mice were

anesthetized with isoflurane (induction: 2.5%; maintenance 0.5-2%) and mounted in a stereotaxic frame (David Kopf Instruments, Model 1900). The scalp was cleaned and retracted using a midline incision and the skull was leveled between bregma and lambda. A hole was drilled over the MS to make a small craniotomy (+1.0mm A/P, -0.7mm M/L) and 750 nL of virus was injected at a rate of 100 nL/min at two locations (400 nL, +1.0mm A/P, -0.7mm M/L, -4.8mm D/V; 350 nL, +1.0mm A/P, -0.7mm M/L, -4.2mm D/V) through a glass pipette using a microsyringe pump (Micro4, UMP3 UltraMicroPump, World Precision Instruments). The pipette was left in place for 5 minutes after the injection before being slowly retracted. Mice were sutured and allowed to recover for a minimum of 7 days.

Mice were implanted with an optic fiber over the medial septal area (MS) and either a four or eight-tetrode microdrive aimed at the medial entorhinal cortex (mEC) or dorsal CA1 region of the hippocampus (HC). Three mice were implanted with a 16-channel linear silicon probe (NeuroNexus CM16) in CA1. Mice were anesthetized with isoflurane (induction: 2.5%; maintenance 0.5-2%). The scalp was cleaned and retracted using a midline incision and the skull was leveled between bregma and lambda. Five holes were drilled in the skull to attach anchor screws and dental cement to secure the implant. A hole was drilled over the MS (+1mm A/P, -0.7 M/L, -3.7 D/V) and the optic fiber was implanted with a 10° medial-lateral angle. A ground screw was placed over the cortex. The skull was removed using a craniotomy over the HC (-2.25mm A/P, +2.0mm M/L) or MEC (from lambda; -0.9mm A/P, +3.8mm M/L, at an 8° angle anterior-posterior), the dura was removed and tetrodes were placed once they have just entered the

brain. The microdrive was then cemented to the rest of the implant. Postoperative care was administered as needed for five to seven days until mice fully recovered. Any mice in which the shift in peak theta was not observed, were not trained on the figure 8 maze and were not included in the experiment.

Behavior

Mice were trained on a delayed spatial alternation task. The room was lit with a single dim light source, and the environmental cues were kept stable. The behavioral task was performed on a figure-8 maze that was 50 cm above the ground with 75 cm return and stem arms and 25 cm choice arms, all with 5cm wide runway. Delay zones were on the first 25 cm of return arm, created with wooden barriers. Small plastic cups were filled with task reward and placed hidden underneath the maze under the food reward zone to avoid olfactory guidance. After each animal used the maze, the maze was thoroughly cleaned with water and dish soap to prevent odor accumulation altering behavior. Mice were trained on the task in a series of incremental stages over approximately six weeks. Mice were given chocolate sprinkles (Betty Crocker, Parlor Perfect Chocolate Sprinkles) as a food reward for each correct choice. In the first stage, mice were habituated to the maze, in which they were allowed to freely explore for 15 minutes and to forage for food on the maze. Second, mice were trained for three days in a "forced alternation" task where barriers were placed at both ends of the maze, alternating between left and right arms. This forced the animals to run in one direction in a figure-8 pattern in order to receive a food reward for 40 trials. Third, mice were trained to run continuously without

barriers for 80 trials until mice reached a criterion performance of 2 out of 3 consecutive days of ≤80% correct (8 ± 2 sessions). Fourth, delays of 2 s or 10 s were introduced on the central arm in between trials. Mice were trained once daily for 60 trials with an equivalent number of 0, 2, and 10 s delay trials until mice reached a performance of ≤ 80% correct for 2 out of 3 consecutive days (15 ± 5 sessions).

After recovering from surgery, mice were food restricted and retrained on the task until reaching a criterion of 2 out of 3 consecutive sessions at 80% correct performance. Tetrodes were slowly turned down into the cell layer over the course of retraining.

Electrophysiological recordings

Local field potential (LFP) signals were recorded using the chronically implanted four or eight-tetrode (bundles of four 17 μm platinum-iridium (90/10%) wires, California Fine Wire Company) microdrives (Anikeeva et al 2012). Tetrodes were stabilized using an optic fiber (200 μm core, Thor Labs, 0.50 NA multimode fiber) that was glued to a zirconia ferrule (Precision Fiber Products, 230 μm). Electrode tips were plated with platinum to reduce electrode impedances to between 150-250 kΩ at 1 kHz. Recording tetrodes were targeted to the CA1 pyramidal layer or to the dorsal MEC. A preamplifier, tether, and a 32-channel digital data acquisition system (Neuralynx, Inc.) was used. LFP was sampled at 32,000 Hz and filtered between 1 and 1,000 Hz.

Laser stimulation

Light was delivered to the MS using a 473 nm wavelength Blue DPSS Laser System through an optic fiber patch cord (Doric Lenses, MFP_200/240/1100-0.22_10m_FC-ZF1.25(F), 200 μm core, 0.22 NA) to a custom optic fiber implant. The custom fiber optic implant was made using an optic fiber (200 μm core, Thor Labs, 0.50 NA multimode fiber) that was glued to a zirconia ferrule (Precision Fiber Products, 230 μm). The final optic fiber was sanded down to allow maximum light through the fiber and cut to a length of 4 mm. Control green stimulation was delivered through a 532 nm wavelength Green DPSS Laser. The output intensity was adjusted to between 9.0 and 12.0 mW.

Light was delivered at a 50% duty cycle at frequencies of 8, 10, 12, and 20 Hz. Each subject was tested once per day for 60 total trials in 6 blocks of 10 trials. Laser stimulation was delivered on alternating blocks so animals received an equal number of trials for each delay condition (0, 2, or 10 s) and for each stimulation condition for a total of 30 “no stimulation” and 30 “stimulation” trials each day. Restricting stimulation to different regions of the maze was done by defining the x and y coordinates of the maze and dividing the maze into separate zones. The x and y coordinates of the animal’s position data were collected using Neuralynx Cheetah Software and was then passed into MATLAB. A custom MATLAB script was used to calculate the median-x and median-y coordinates of the LEDs while the animals were running on the maze. The script then determined whether the animal was occupying one of the targeted zones. Once animals entered a targeted zone, MATLAB would instruct the Neuralynx Cheetah software to

turn on the laser stimulation and was turned off once the MATLAB script determined the animals exited the zone.

Histological procedures

Mice were perfused with 0.1 M phosphate-buffered saline (PBS) followed by 4% paraformaldehyde in PBS solution. Brains were post-fixed for 24 hours in 4% paraformaldehyde and then cryoprotected in 30% sucrose solution for 2 days. Brains were then frozen and sliced into 40 μm coronal sections for the MS and HC and 40 μm sagittal sections for the MEC on a sliding microtome. Sections were mounted on electrostatic slides and sections of the MS were coverslipped with Fluoroshield with DAPI (Sigma-Aldrich). Sections of the HC or MEC were mounted on electrostatic slides and stained with cresyl violet and coverslipped with Permount (Fisher Scientific, SP15500) to visualize recording locations. Slides were imaged using a virtual slide microscope (Olympus, VS120).

Statistics

All behavior statistics were done using IBM SPSS Statistics version 23. Details of which tests are used were described with the results. No statistical tests were used for predetermining sample sizes, but our sample size is similar to other studies. For all comparisons between stimulation compared to no stimulation conditions were done using paired comparisons or using repeated-measures. Tests for normality were performed and if normality could be assumed, we used paired two-tailed t-tests. When normality could

not be assumed, we used Wilcoxin signed rank tests. For all repeated measures ANOVAs, sphericity was not assumed but accessed using Mauchly's test for sphericity. If sphericity could not be assumed, Greenhouse-Geisser was used.

Results

Pacing of theta oscillations by MS-PV stimulation can be sustained over extended periods during behavioral testing

Given that we observed multiple forms of disruption of oscillatory patterns at any of the stimulation frequencies, we proceeded to analyze whether altered timing of these oscillatory patterns impairs spatial alternation, which has been shown to depend on hippocampus and mEC when a working memory component is introduced by imposing a delay (Ainge et al 2007, Pioli et al 2014, Sabariego et al 2019). We injected mice with ChR2/oCHIEF or a control GFP vector into the MS. We found all mice had robust and restricted viral expression in the MS (Figure 4.1).

Mice were then implanted with an optic fiber over the MS and a microdrive or silicon probe into the mEC or HC. We found electrode tracks were located within the target regions of all mice (Figure 4.2).

Figure 4.1. Viral expression in the MS was strong and restricted to the MS in all animals.

ChR2-YFP and control GFP expression was confirmed the MS in all mice. Mice 07, 19, 38, 39, 45, 47 were injected with ChR2-YFP and mice 40, 41, 42, 43, 51, 52 were injected with control GFP. The white dashed line demarcates the border of the MS. Images were counterstained with DAPI (blue). All scale bars are 250 μm.

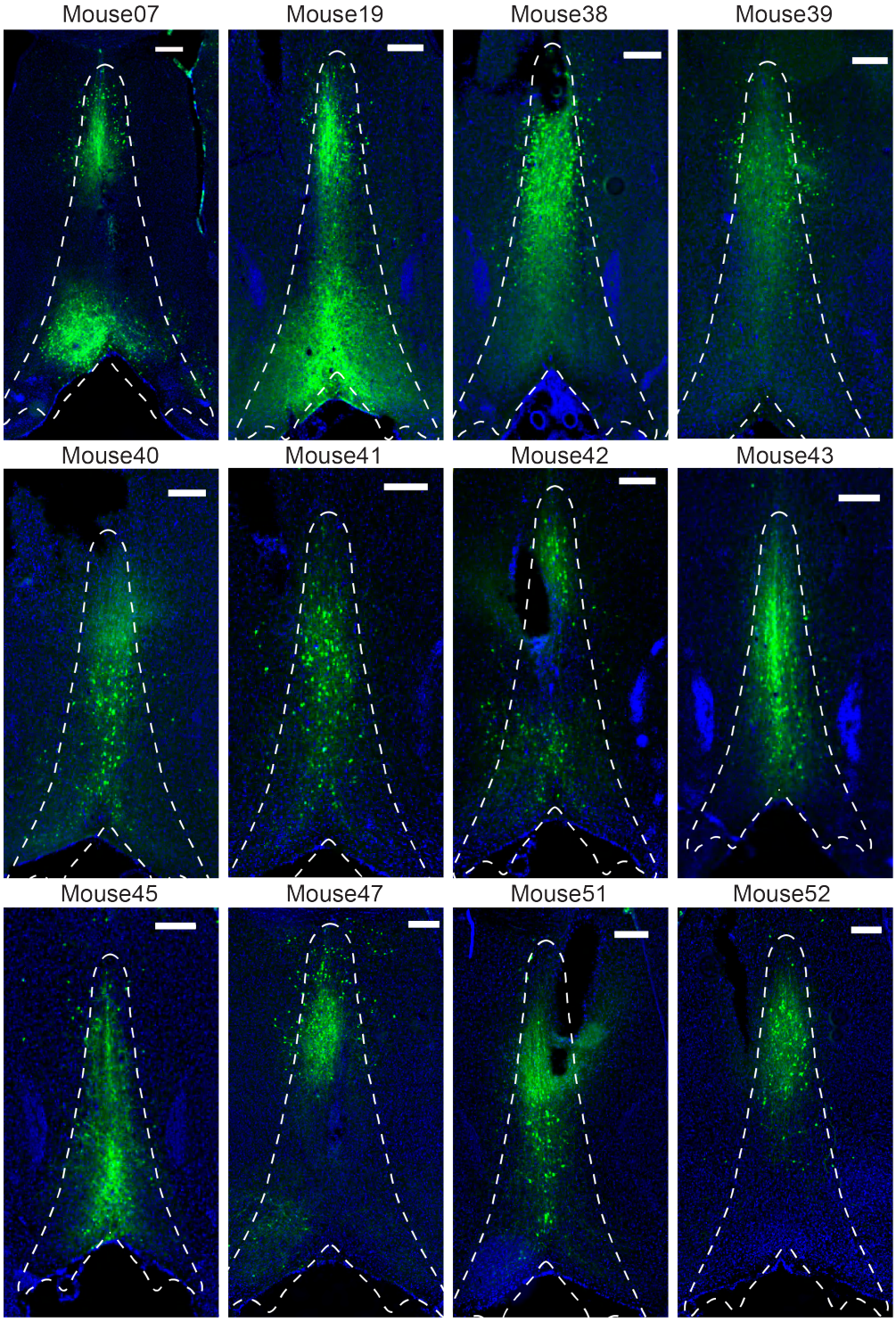
Mouse07
Mouse19
Mouse38
Mouse39
Mouse40
Mouse41
Mouse42
Mouse43
Mouse45
Mouse47
Mouse51
Mouse52

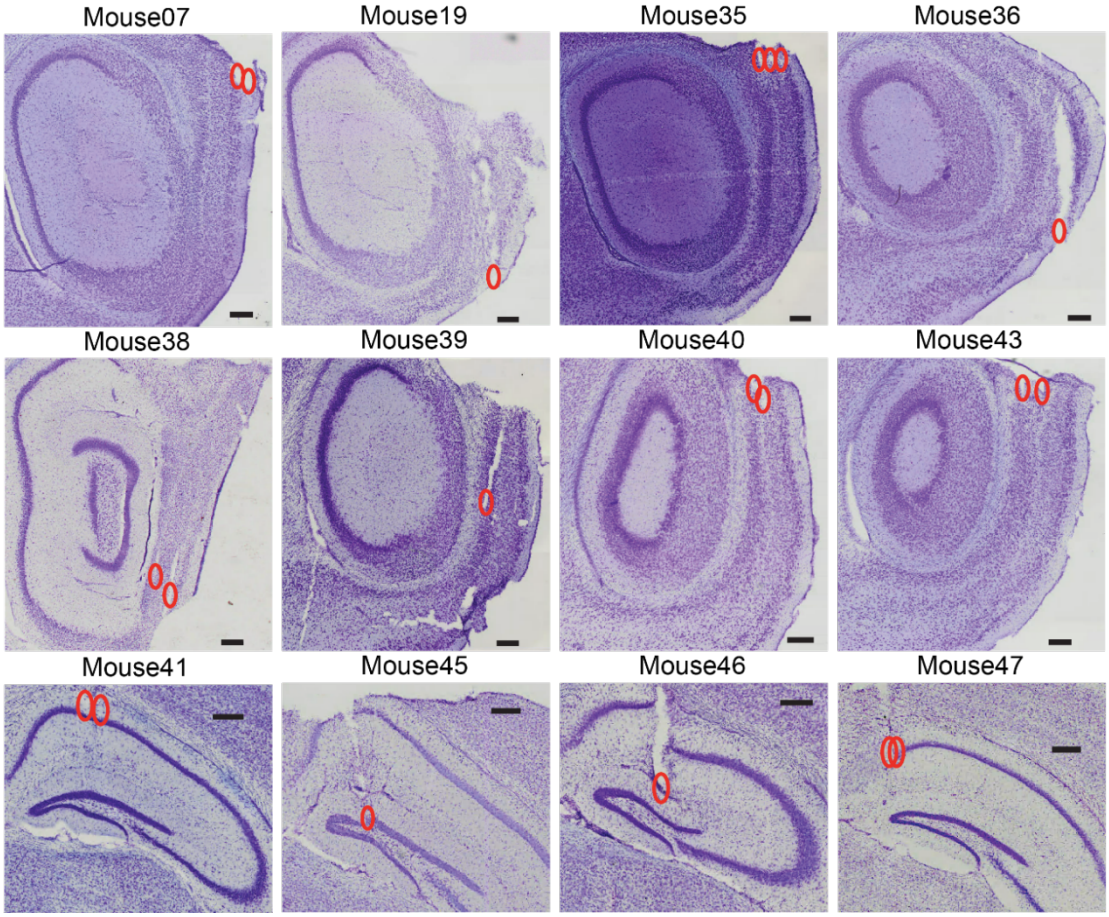

Figure 4.2. Tetrode tracks were localized in the targeted HC and mEC regions in all mice.

Tetrode tracks were visualized in the target recording locations in all animals. Red circles indicate the recording locations for each animal. All scale bars are 250 μm.

Mice were trained on a delayed spatial alternation task in a figure-8 shaped maze. To receive a food reward, they continuously alternated between left and right arms on a trial-by-trial basis (Figure 4.3A). Once mice were trained on the continuous and delayed versions of the task, optogenetic stimulation was performed at 8, 10, 12, and 20 Hz on half of all trials on alternating blocks. At the beginning of each simulation black, the peak theta frequency immediately shifted to the stimulation frequency, and stimulation effectiveness did not diminish over a period of minutes (Figure 4.3B). Theta oscillations immediately returned to their endogenous range after cessation of stimulation (Figure 4.3B).

Figure 4.3. Shifting Endogenous Theta Frequency to ≥10 Hz Disrupts Spatial Working Memory.

(a) Mice injected with either ChR2 or oCHIEF (n=17) or GFP (n=6) were trained on a delayed spatial alternation task in which they ran on a figure-8 maze alternating between left and right arms to receive a food reward with delays of 0 s, 2 s, or 10 s imposed on the central arm for an equal number of trials. (b) Once mice learned the task, optogenetic stimulation occurred on half on all trials on alternating blocks with one stimulation being used each day and repeated for 8, 10, 12, and 20 Hz. Example session for 12 Hz stimulation design (bottom) and corresponding time-frequency spectrogram shows theta immediately shifted to the stimulation frequency and reduced the endogenous 6-9 Hz theta oscillation for the entire period of stimulation (blue lines). (c) Stimulating outside the endogenous theta range at 10, 12, or 20 Hz in ChR2 animals (top) significantly impaired performance on 2 s and 10 s delays while stimulating within the theta range at 8 Hz did not alter performance relative to no stimulation (*$p<0.05$). There was no effect of any stimulation at any delay in GFP animals (bottom). (d) Optogenetic stimulation at 12 Hz was restricted to specific zones of the figure 8 maze. 12 Hz stimulation was targeted to the stem arm, reward arms, stem and reward arms, and return arms. Mice were tested on 60 trials on alternating blocks of no stimulation and targeted stimulation to one selected zone. (e) There was no significant effect on memory performance during stimulation on the stem, reward, or stem and reward conditions for any delay. Stimulation on the return arms resulted in a significant decrease in performance during the 10 s delay trials and a trend towards significant decrease on the 2 s delay trials.

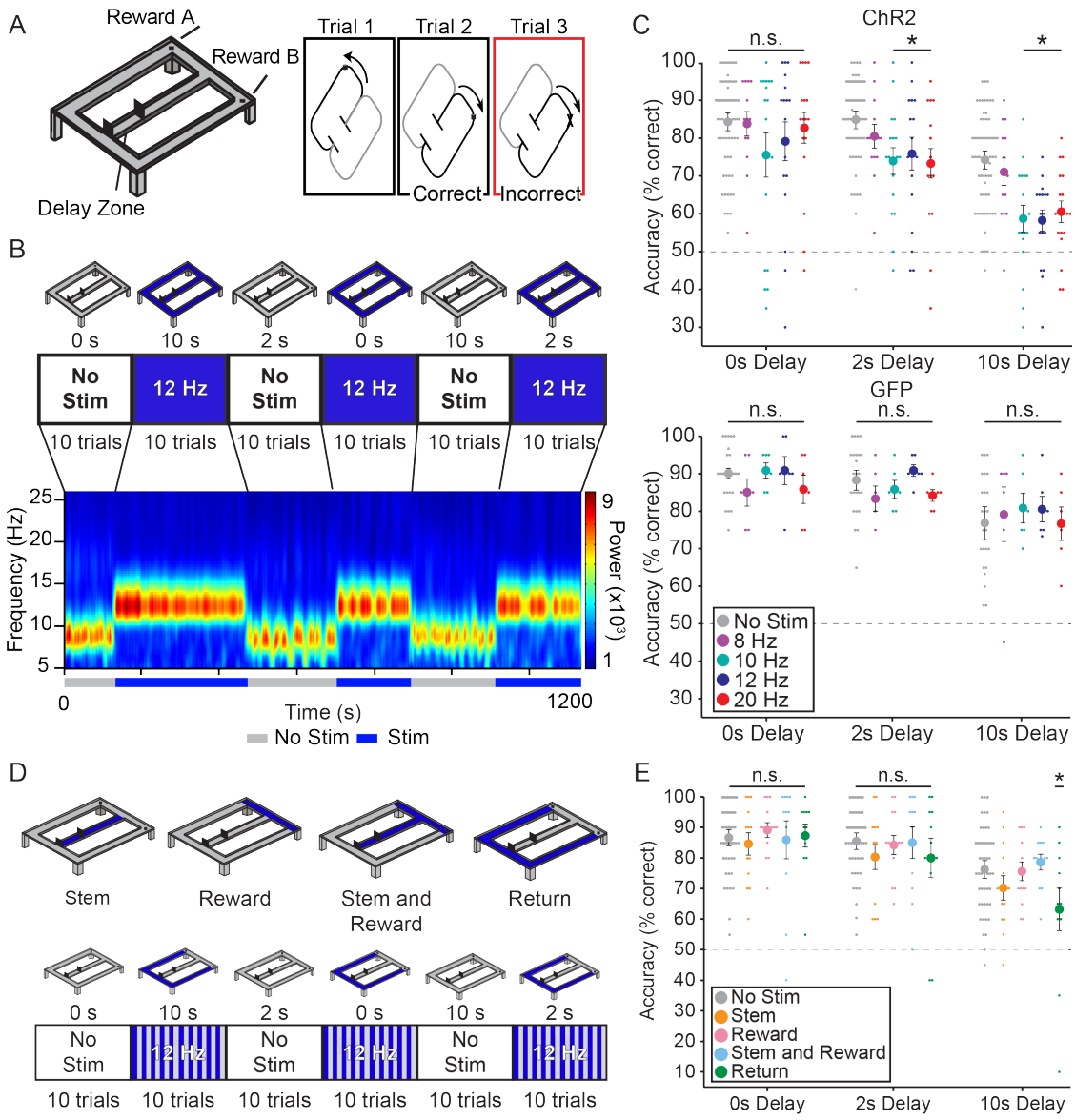
A
Reward A
Reward B
Delay Zone
Trial 1
Trial 2
Trial 3
Correct
Incorrect
B
0 s
10 s
2 s
0 s
10 s
2 s
No Stim
12 Hz
No Stim
12 Hz
No Stim
12 Hz
10 trials
10 trials
10 trials
10 trials
10 trials
10 trials
Frequency (Hz)
25
20
15
10
5
9
1
Power (x10³)
0
1200
Time (s)
No Stim
Stim
C
ChR2
n.s.
*
*
Accuracy (% correct)
100
90
80
70
60
50
40
30
0s Delay
2s Delay
10s Delay
GFP
n.s.
n.s.
n.s.
No Stim
8 Hz
10 Hz
12 Hz
20 Hz
D
Stem
Reward
Stem and Reward
Return
0 s
10 s
2 s
0 s
10 s
2 s
No Stim
12 Hz
No Stim
12 Hz
No Stim
12 Hz
10 trials
10 trials
10 trials
10 trials
10 trials
10 trials
E
n.s.
n.s.
*
Accuracy (% correct)
No Stim
Stem
Reward
Stem and Reward
Return
0s Delay
2s Delay
10s Delay

We found that the peak LFP frequency shifted in every session for every mouse in both the mEC (Figure 4.4A) and HC (Figure 4.4B) at all stimulation frequencies while animals were performing the figure-8 maze task.

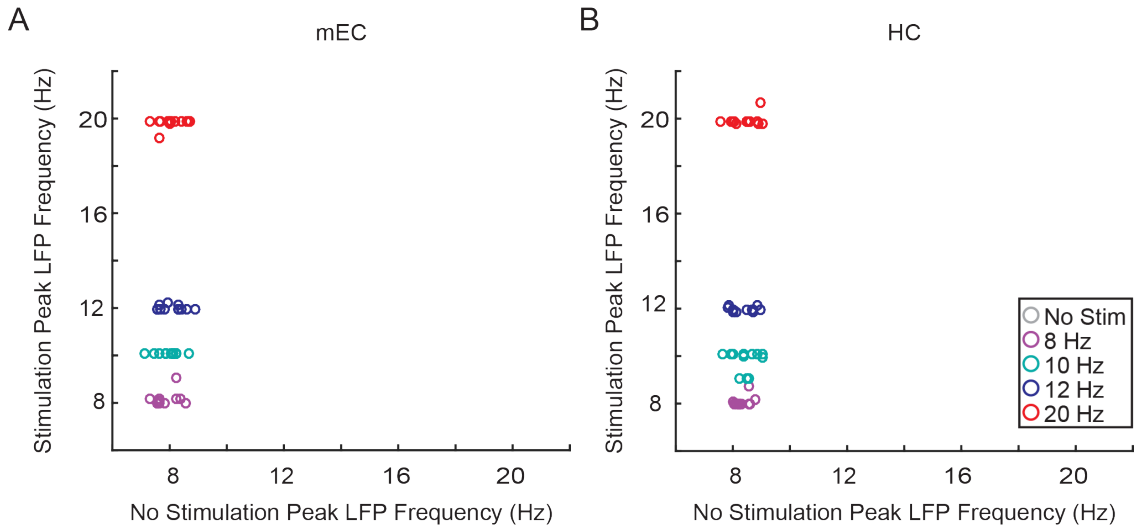

Figure 4.4. The peak LFP frequency was shifted to the stimulation frequency in all mice.

(a) The peak LFP frequency shifted to the stimulation frequency in all mice on the figure-8 maze in the mEC. Each dot represents one mouse. (b) Same as in (a) but for mice implanted with electrodes in the HC.

Figure 4.5. Example recordings while ChR2 and GFP animals performed the spatial alternation task.

Example time-frequency wavelet spectrograms of example recordings from six different mice. The top 4 mice (outlined in blue) were injected with ChR2 and the bottom 2 mice (outlined in green) were injected with the control GFP vector. Grey and blue lines under the x axis of the plot indicate the time during which there was no stimulation and stimulation, respectively, at each frequency while mice ran 60 trials on the figure-8 maze. Rhythmic stimulation of MS PV cells in ChR2 mice controls the frequency of theta oscillations in both the mEC (top 2 rows) and the HC (rows 3 and 4). The bottom GFP control plots show no change in theta frequency during light stimulation.

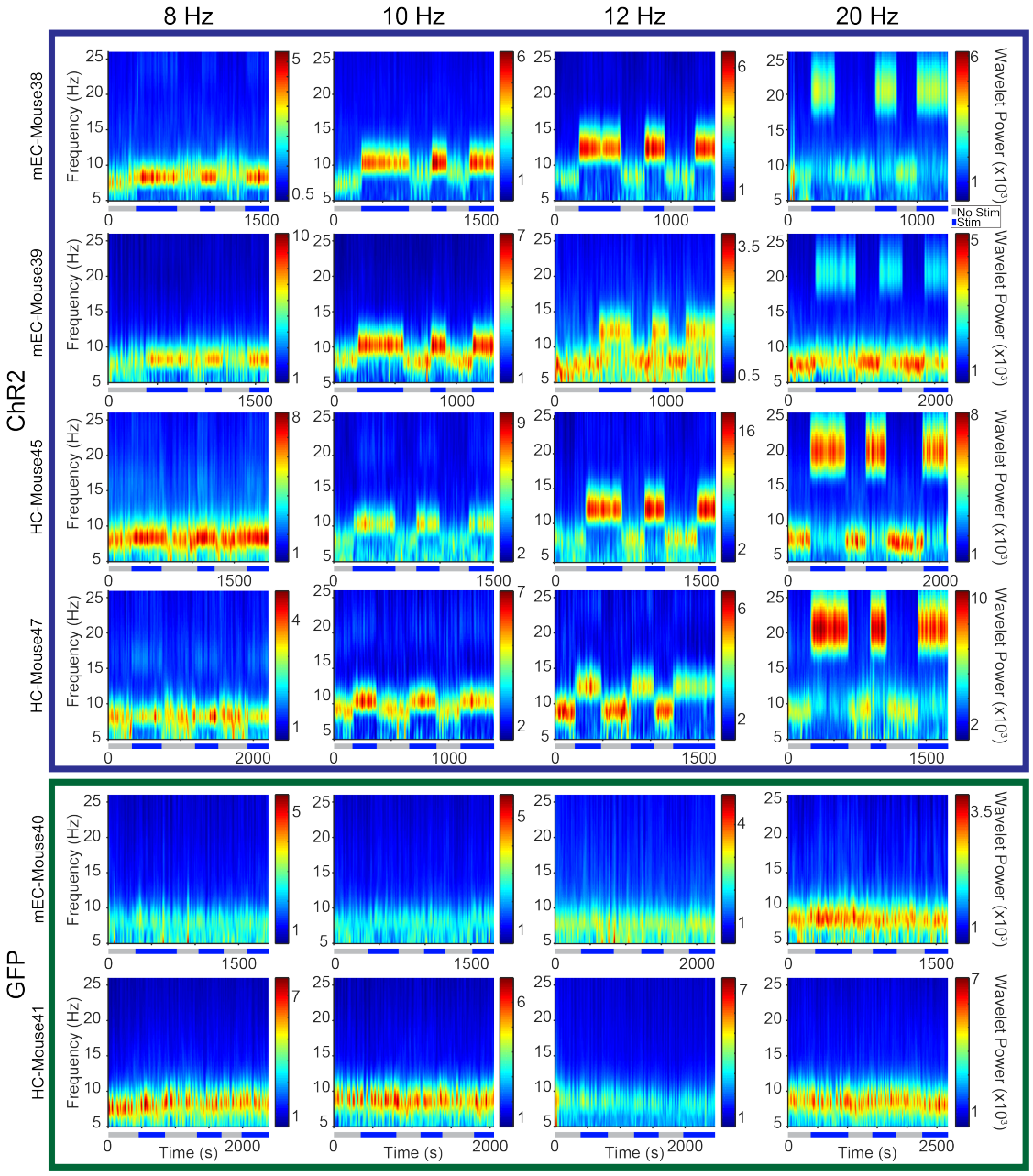
8 Hz
10 Hz
12 Hz
20 Hz
ChR2
GFP
mEC-Mouse38
mEC-Mouse39
HC-Mouse45
HC-Mouse47
mEC-Mouse40
HC-Mouse41
Frequency (Hz)
Wavelet Power (x10³)
No Stim
Stim
Time (s)

Stimulating MS PV cells increases mid-gamma amplitude in mEC and HC in both ChR2 and GFP animals

Previous studies have provided evidence that multiple oscillatory patterns occur during cognitive processes and theta and gamma oscillations co-occur in the HC and mEC (Colgin et al 2009, Schomburg et al 2014). We therefore examined whether gamma oscillations in the mEC or HC were altered during accelerated theta frequency. We examined the amplitude within the 50-120 Hz frequency range in the mEC and HC and compared the amplitude between no stimulation and stimulation periods at each stimulation frequency.

To estimate the average amplitude, we used an FFT to calculate the power and then calculated the area under the curve. We found a significant effect of stimulation on gamma amplitude in the mEC ChR2 animals (Figure 4.6; $F_{(1,10)}$=33.09, P<0.001), but no effect of frequency stimulated ($F_{(3,30)}$=0.70, P=0.56) and no interaction between stimulation and frequency ($F_{(3,30)}$=0.33, P=0.80). Similarly, we found a significant effect of stimulation on gamma amplitude in the HC ChR2 animals ($F_{(1,11)}$=13.71, P=0.003), but no effect of frequency stimulated ($F_{(3,33)}$=0.075, P=0.92) and no interaction between stimulation and frequency ($F_{(3,33)}$=1.29, P=0.30). However, we also found the same effect on gamma amplitude in GFP animals in the mEC with a significant effect of stimulation on gamma amplitude ($F_{(1,10)}$=33.09, P<0.001), but no effect of frequency stimulated ($F_{(3,30)}$=0.70, P=0.56) and no interaction between stimulation and frequency ($F_{(3,30)}$=0.33, P=0.80). We found the same effect in the HC in animals injected with GFP with a significant effect of stimulation on gamma amplitude (Figure 4.6; $F_{(1,7)}$=6.42, P=0.039),

but no effect of frequency stimulated ($F_{(3,21)}$=0.74, P=0.54) and no interaction between stimulation and frequency ($F_{(3,21)}$=1.25, P=0.32). This suggests that the increase in gamma amplitude is due to light stimulation rather than to changes in theta frequency. Note that this does not need to be a direct effect of light on brain physiology but that this effect could also be mediated by the animal seeing the light, which could in turn alter oscillations in the gamma frequency range.

Figure 4.6. Gamma oscillation amplitude was increased in the HC and mEC in both ChR2 and GFP animals.

To analyze whether theta and gamma (50-120 Hz) oscillations were altered by shifting the endogenous theta frequency, we calculated theta and gamma amplitude while animals were performing the figure 8 maze and compared theta and gamma amplitude for each stimulation condition in mEC-ChR2, mEC-GFP, HC-ChR2, and HC-GFP animals. There was an increase in gamma amplitude for all stimulation frequencies in mEC-ChR2, mEC-GFP, HC-ChR2, and HC-GFP animals. These results suggest that the increase in gamma amplitude is due to the light stimulation rather than the shifting of theta oscillations.

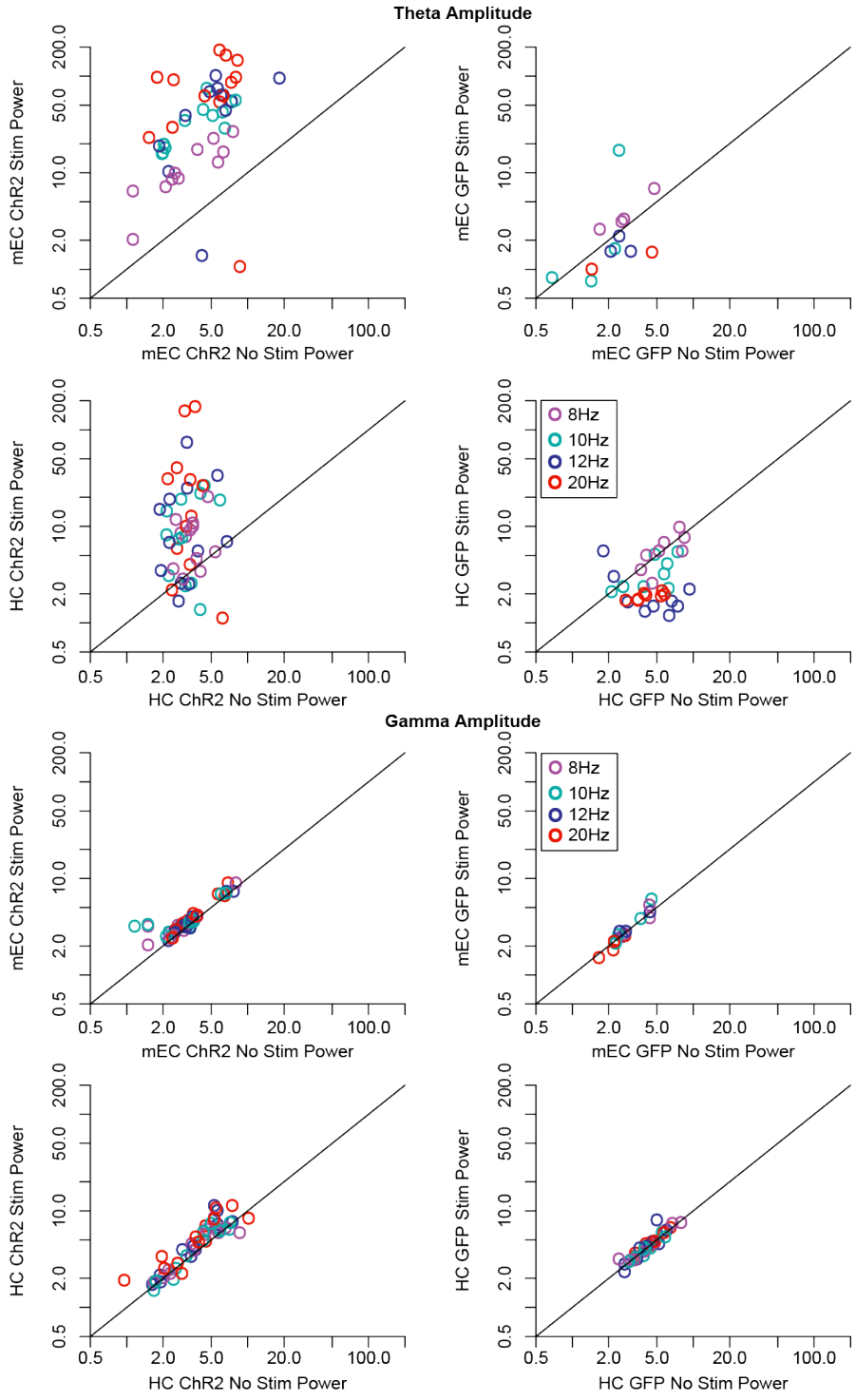
Theta Amplitude
mEC ChR2 Stim Power
mEC ChR2 No Stim Power
mEC GFP Stim Power
mEC GFP No Stim Power
HC ChR2 Stim Power
HC ChR2 No Stim Power
HC GFP Stim Power
HC GFP No Stim Power
8Hz
10Hz
12Hz
20Hz
Gamma Amplitude
0.5
2.0
5.0
20.0
100.0
200.0
50.0
10.0

Shifting the oscillation frequency to ≥ 10 Hz resulted in a hippocampal-dependent working memory impairment

During testing, mice performed significantly above chance at all delays during "no stimulation" conditions (one sample t-test against chance (50%), $p<0.001$). We next compared all behavioral performance between "no stimulation" and "stimulation" conditions using a paired two-tailed t-test. There was no significant difference between no stimulation and stimulation at any frequency for the 0 s delay (Fig 4C; $t_{ChR2\_8Hz(12)}=1.39$, *P=0.19;* $t_{ChR2\_10Hz(16)}=1.92$, *P=0.072;* $t_{ChR2\_12Hz(16)}=0.90$, *P=0.38;* $t_{ChR2\_20Hz(16)}=0.24$, *P=0.81*), consistent with previous evidence that the HC and mEC is not necessary for performance of the task without delay (Sabariego et al 2019).

We found that stimulating at 10, 12, and 20 Hz significantly impaired memory performance on 2 s (Fig 4C; $t_{ChR2\_10Hz(16)}=3.03$, *P=0.008;* $t_{ChR2\_12Hz(16)}=4.18$, *P=0.001;* $t_{ChR2\_20Hz(16)}=3.93$, *P=0.001*) and 10 s delay trials (Fig 4C, top; $t_{ChR2\_10Hz(16)}=3.90$, *P=0.001;* $t_{ChR2\_12Hz(16)}=5.50$, *P<0.001;* $t_{ChR2\_20Hz(16)}=4.61$, *P<0.001*). Stimulating at 8 Hz did not result in a memory impairment across either the 2 s ($t_{ChR2\_8Hz(12)}=1.49$, *P=0.16*) or the 10 s delay ($t_{ChR2\_8Hz(12)}=-0.53$, *P=0.60*). A three-way repeated-measures ANOVA revealed a significant interaction between stimulation, delay, and frequency ($F_{(6,72)}=4.67$, $P<0.001$) in animals injected with ChR2.

We next controlled for any behavioral perturbation that could have been caused by the light stimulation. First, animals injected with ChR2 were tested while stimulation with green light (532 nm) was delivered. This wavelength is known to only weakly activate ChR2. Next, animals injected with a cre-dependent GFP vector

(AAV.EF1a.DIO.eGFP) received blue light stimulation (473 nm). For the ChR2-green group, there were no significant difference in performance between no stimulation and stimulation for 0 s ($t_{ChR2Green\_10Hz(8)}$=-0.66, *P=0.53;* $t_{ChR2Green\_12Hz(8)}$=-0.64, *P=0.54;* $t_{ChR2Green\_20Hz(8)}$ =0.00, *P=1.00*), 2 s ($t_{ChR2Green\_10Hz(8)}$=1.89, *P=0.096;* $t_{ChR2Green\_12Hz(8)}$=0.46, *P=0.66;* $t_{ChR2Green\_20Hz(8)}$ =1.46, *P=0.18*), or 10 s ($t_{ChR2Green\_10Hz(8)}$=-2.22, *P=0.058;* $t_{ChR2Green\_12Hz(8)}$=-0.17, *P=0.87;* $t_{ChR2Green\_20Hz(8)}$ =-0.58, *P=0.58*).

Similarly for the GFP group, there were no significant differences in performance between no stimulation and stimulation for 0 s (Fig 4C, bottom; $t_{GFP\_8Hz(5)}$=1.75, *P=0.14;* $t_{GFP\_10Hz(5)}$=0.00, *P=1.00;* $t_{GFP\_12Hz(5)}$=-0.39, *P=0.71;* $t_{GFP\_20Hz(5)}$ =0.88, *P=0.42*), 2 s ($t_{GFP\_8Hz(5)}$=1.23, *P=0.27;* $t_{GFP\_10Hz(5)}$=0.44, *P=0.68;* $t_{GFP\_12Hz(5)}$=-0.45, *P=0.67;* $t_{GFP\_20Hz(5)}$ =0.61, *P=0.57*), and 10 s delay ($t_{GFP\_8Hz(5)}$=-0.65, *P=0.54;* $t_{GFP\_10Hz(5)}$=-0.76, *P=0.48;* $t_{GFP\_12Hz(5)}$=-0.88, *P=0.42;* $t_{GFP\_20Hz(5)}$ =0.52, *P=0.62*). A three-way repeated-measures ANOVA revealed there was no significant interaction of stimulation, delay, and frequency for ChR2 animals stimulated with green light (ChR2-green: $F_{(4,32)}$=0.88, P=0.48) or in GFP animals that received blue stimulation (GFP-blue: $F_{(3.41,17.03)}$=0.38, P=0.79). These results demonstrate that behavioral impairments were due to disruption in the timing of endogenously paced theta oscillations and not due to behavioral perturbation by light stimulation.

Figure 4.7. Change in behavioral performance for all animals and all stimulation conditions.

(a) Behavioral performance of each animal (n=17) for each delay condition during no stimulation and stimulation sessions. Each dot represents an individual animal and the average of the sessions for that animal. The black line connects the behavioral performance of each animal for the statistical comparison. Stimulating at 10, 12, and 20 Hz impaired performance during the 2 s and 10 s delay condition. (b) In 9 of the 17 ChR2 animals used from panel (a), we performed control green light (532 nm wavelength) 10, 12, and 20 Hz stimulation. There were no significant changes in performance for any stimulation frequency or delay. (c) In 6 mice, we injected a control vector and performed the same experimental protocol used in (a). There were no effects on performance at any delay for any stimulation condition. (d) In 12 of the ChR2 mice used from panel (a), we performed targeted 12 Hz stimulation in different zones of the maze. There was a significant impairment during stimulation on the return arm during the 10 s delay.

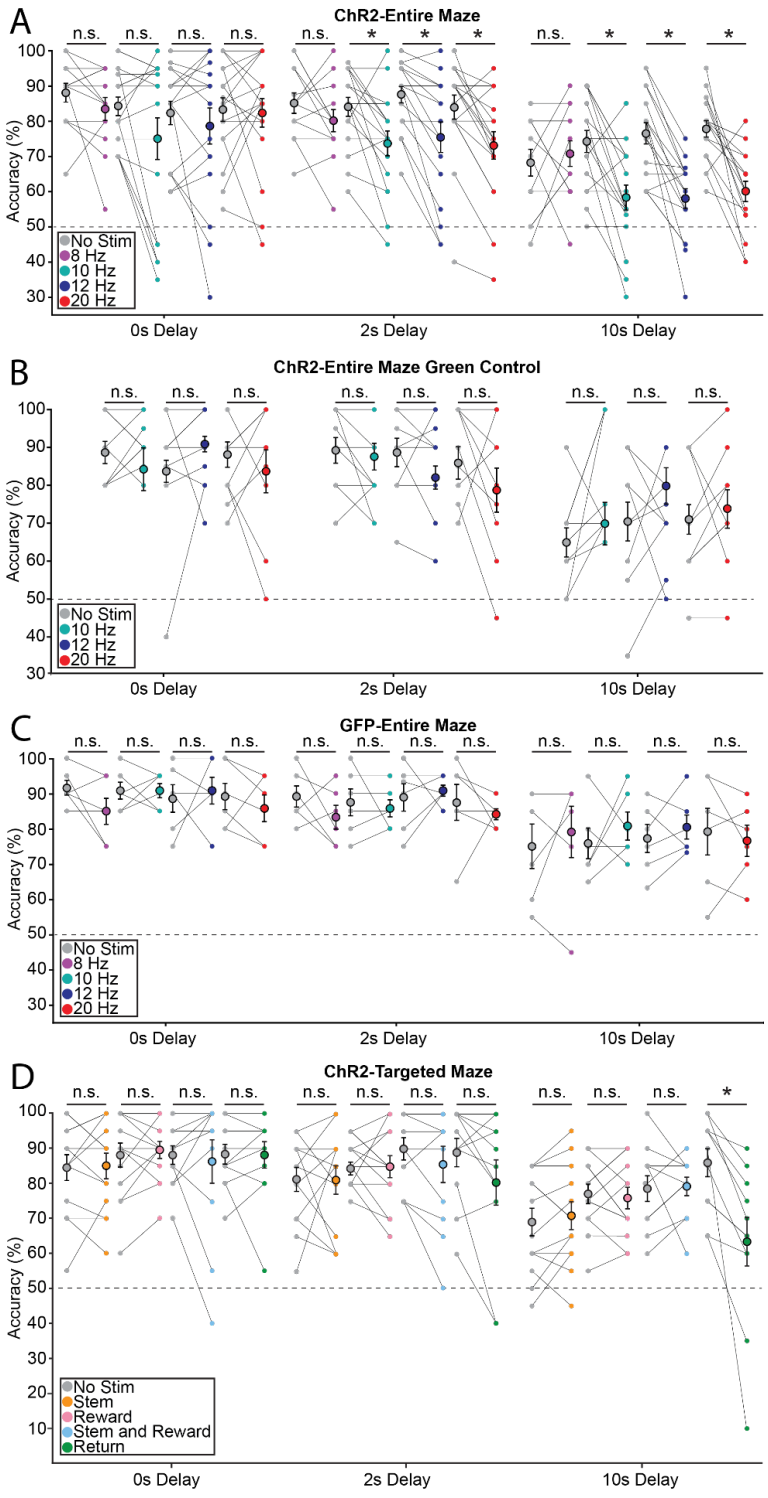
A
ChR2-Entire Maze
n.s.
*
Accuracy (%)
No Stim
8 Hz
10 Hz
12 Hz
20 Hz
0s Delay
2s Delay
10s Delay
B
ChR2-Entire Maze Green Control
No Stim
10 Hz
12 Hz
20 Hz
C
GFP-Entire Maze
D
ChR2-Targeted Maze
Stem
Reward
Stem and Reward
Return

Targeted shifting of theta oscillations on the return arm selectively impairs memory

In order to test whether altered theta oscillation frequency was critical during different periods of the memory task (e.g., encoding and retrieval), we performed stimulation during different periods of the spatial alternation task by targeting 12 Hz stimulation to different zones of the maze (i.e., reward arms, stem arm, return arms, or combined stem and reward arms, Figure 4.3D). We were able to reliably shift the peak theta frequency to 12 Hz in the targeted zone for each condition at each delay. We found that only stimulation on return arms impaired working memory performance at the 10s delay (Figure 4.3E; $t_{(10)}$=3.50, P=0.006), a trend towards significance on the 2s delay (Figure 4.3E; $t_{(10)}$=1.97, P=0.077), and no effect on the 0s delay (Figure 4.3E; $t_{(10)}$=.16, P=0.88).

There were no significant effects from any other targeted stimulation conditions on the 0s (Figure 4.3E; $t_{ChR2\_Reward(12)}$=-0.63, *P=0.54;* $t_{ChR2\_Stem(12)}$=-0.14, *P=0.89;* $t_{ChR2\_StemandReward(10)}$=0.38, *P=0.71*), 2s (Figure 4.3E; $t_{ChR2\_Reward(12)}$=0.81, *P=0.44;* $t_{ChR2\_Stem(12)}$=0.083, *P=0.94;* $t_{ChR2\_StemandReward(10)}$=1.61, *P=0.14*), or 10s delay (Figure 4.3E; $t_{ChR2\_Reward(12)}$=0.43, *P=0.67;* $t_{ChR2\_Stem(12)}$=-0.92, *P=0.38;* $t_{ChR2\_StemandReward(10)}$=-.13 *P=0.90*). Further there was a significant interaction of stimulation, delay, and region stimulated ($F_{(6,60)}$=3.25, P=0.008). The deficit seen on the return arm stimulation suggests a potential deficit in memory encoding.

In the spatial alternation task, a successful trial depends on the correct encoding of the previous trajectory. This could possibly be done by distinct representations of the left or right return arms (Sabariego et al 2019). While the animal is on the return arm, the

animal is well positioned to be encoding information on either the left or right arm. These results suggest that endogenously paced theta oscillations may have a preferential role in encoding the information that the mouse is currently experiencing on either the right or the left arm. Interestingly, there was no effect on performance when any other zone of the maze was stimulated including the stem arm when the animal no longer has any indication of whether they were just on the left or right arm and has to use the memory from the previous trial to make a correct choice.

Figure 4.5. Stimulation efficacy in targeted zones.

We analyzed the efficacy of stimulation in each zone of the maze in the conditions where we stimulated in the entire maze (rows 1, 3, and 5) and when we stimulated in targeted zones of the maze (rows 2, 4, and 6) for each delay. We were able to shift theta frequency in each of the different stimulation frequencies in all zones during all delays. We were also able to shift the frequency of theta to 12 Hz in the targeted zone but no effects were observed in the non-targeted zones.

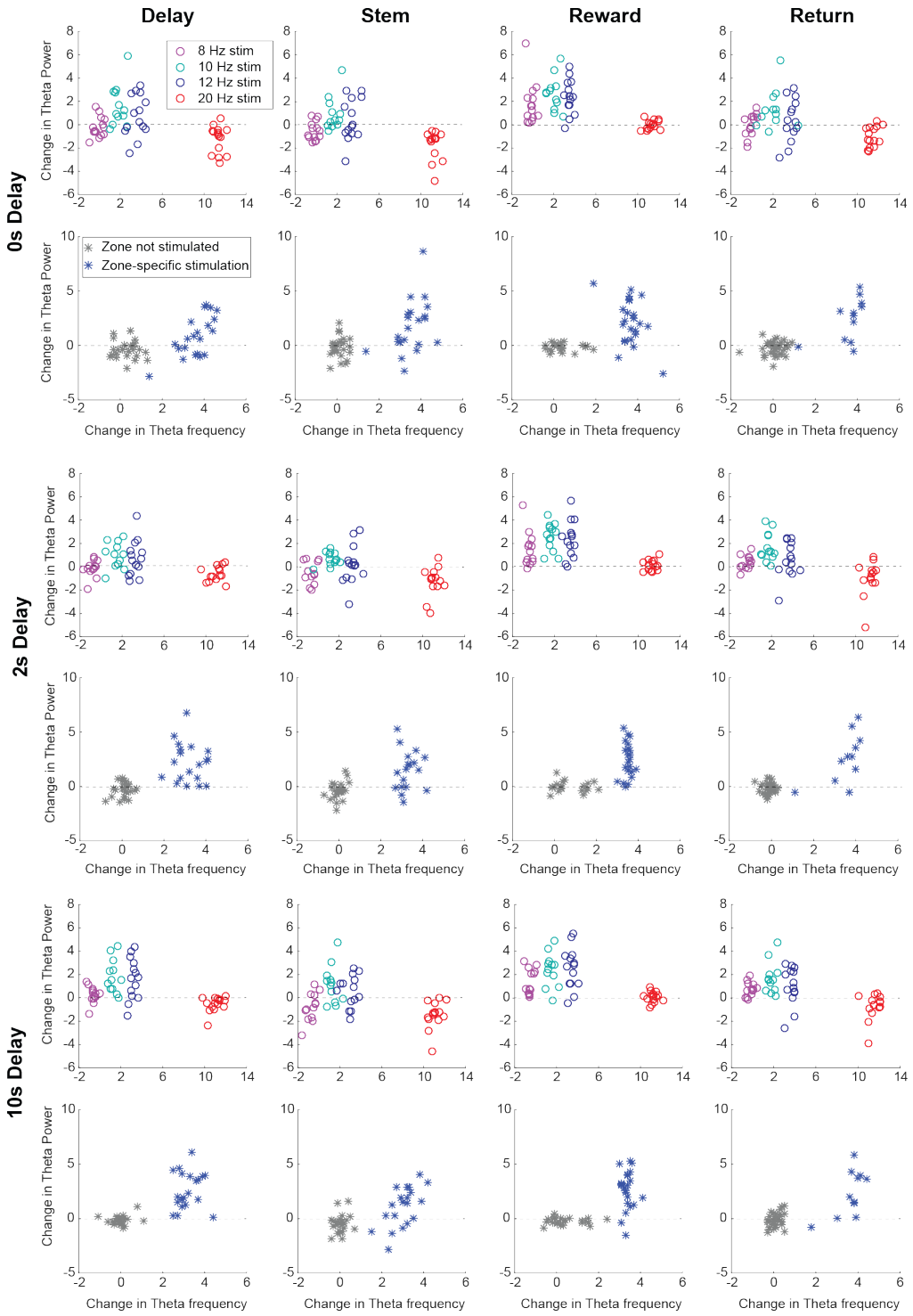
Delay
Stem
Reward
Return
0s Delay
2s Delay
10s Delay
8 Hz stim
10 Hz stim
12 Hz stim
20 Hz stim
Zone not stimulated
Zone-specific stimulation
Change in Theta Power
Change in Theta frequency

Discussion

Here we investigated whether the precise timing of theta oscillatory frequency was required for performance of a hippocampal-dependent memory task. As previously reported (Bender et al 2015, Fuhrmann et al 2015, Justus et al 2017, Zutshi et al 2018), we were able to precisely control the frequency of HC theta oscillations by optogenetically activating MS PV cells and show here that the mEC is not only directly paced but that the pathway through mEC continues to make a major contribution to hippocampal theta during pacing. Although the increase in mEC theta modulation of principal cells was already evident with 8 Hz stimulation, we demonstrated that at least a small deviation ($\leq$ 2 Hz) from the endogenous theta range to 10 Hz or greater was required to cause a severe memory impairment. Importantly, these findings demonstrate a role for theta rhythm in memory that coincides with changes in the spike timing of cells in the mEC-HC circuit.

Due to the precise temporal precision of optogenetics used here, we were able to demonstrate that the circuit tolerated a large range of perturbations to the mEC-HC circuit, such as an increase in amplitude of mEC principal cells and a shift in the intrinsic frequency of both mEC and HC principal cells, as long as the optogenetic perturbation remained within the endogenous (6-9 Hz) theta range. In particular, we found that causing profound perturbations of oscillatory patterns were without behavioral consequences when limited to behavioral phases during which memory needed to be retained and a choice needed to be selected. While these data further support a long-

hypothesized role for theta in memory encoding, they also show that other aspects of memory processing are highly tolerant to major disruptions of oscillatory patterns. Oscillatory patterns however are not always necessary for memory encoding. Memory can be reinstated during contextual fear conditioning without altering the oscillations within the network (Ramirez et al 2013). Taken together, our findings demonstrate for the first time that medial septal control of theta oscillations is stronger in the mEC than HC and that the excessive drive of entorhino-hippocampal oscillatory patterns outside of the endogenous theta range causes selective impairments in the encoding of episodic memory in mice.

While it has been hypothesized that theta oscillations contribute to the coordinated spike timing important for episodic memory, our findings presented here establish a critical role for cellular oscillatory timing in memory encoding. This is the first study that has demonstrated a role for oscillatory timing in memory without also causing other downstream effects including reductions in excitation and disruptions to spatial coding.

Acknowledgements

Chapter 4, in full, is material that is unpublished and being prepared for publication. It is coauthored by Quirk, Clare R., Zutshi, Ipshita, Srikanth, Sunandha, Wright, Morgan K., Parsey, Darian F., Devico Marciano, Naomie, Liu, Stanley, Fu,

Maylin L., Leutgeb, Jill K., and Leutgeb, Stefan. The dissertation author was the primary researcher and author of this material.

Chapter V.

Overall Conclusions

In this dissertation, we examined the role of endogenously paced theta oscillations in the entorhino-hippocampal circuit in regulating the spike timing of cells in HC and mEC and the role of this precisely controlled oscillatory frequency in spatial working memory. In chapters II and III we examined the role of oscillatory timing of theta oscillations in the spike timing of HC and mEC cells and the effect on spatial coding. We found that many cells within the mEC-HC circuit fired rhythmically in the same frequency range of theta oscillations and showed spatial tuning when exploring an environment. Interestingly, we found that the primary theta modulated input to CA1 originates from the mEC and that mEC cells are more strongly entrained to MS PV stimulation than HC cells were. We found that both brain regions systematically shifted their peak frequencies toward the stimulation frequency and generated oscillation frequencies that were well outside the endogenous range, which during baseline conditions was generally below 10 Hz, when theta was accelerated and paced at 10 and 12 Hz.

In chapter IV, we tested whether changes to oscillatory timing in theta oscillations had a role in spatial working memory in a delayed alternation task that has been shown to depend on the intact function of both HC and mEC (Ainge et al 2007, Sabariego et al

2019). We found that shifting theta oscillations to 10 Hz or higher caused a severe memory impairment while stimulating within the endogenous range at 8 Hz did not cause any impairments in memory. Thus, we demonstrated that even a small deviation from the endogenous range ($\leq$ 2 Hz) was sufficient to cause a severe memory impairment. When we further restricted this optogenetically accelerated oscillatory frequency to different periods of the delayed spatial alternation task, we found that only accelerated theta frequency impaired performance on the return arm. These results suggest that the precise timing of theta oscillations is specifically critical during periods of memory encoding during hippocampal dependent tasks.

Importantly, these findings demonstrate a role for theta rhythm in memory that coincides with changes in the spike timing of cells in the mEC-HC circuit. Due to the precise temporal precision of optogenetics used here, we were able to demonstrate that the circuit tolerated a large range of perturbations of oscillatory patterns, such as an increase in amplitude of mEC cells and increases in gamma amplitude, as long as the perturbation remained within the endogenous theta range. In particular, we found that even more profound perturbation of oscillatory patterns were without behavioral consequences when limited to behavioral phases during which memory needed to be retained and a choice needed to be selected (i.e., stem arm). While these data confirm a long-hypothesized role for theta in episodic memory encoding, they also show that other aspects of memory processing including memory retrieval are highly tolerant to major disruptions of oscillatory patterns in the mEC-HC circuit.

Taken together, our findings demonstrate that medial septal control of theta oscillations resulted in stronger changes to the spike timing of cells in the mEC than the HC and that the excessive drive of medial entorhinal and hippocampal oscillatory patterns outside of the endogenous theta range (6-9 Hz) causes selective impairments in the encoding of episodic memories by altering the spike timing of cells within the mEC and HC while leaving spatial, directional, and speed coding intact. This is the first study that has demonstrated a role for oscillatory timing in memory without also causing other downstream effects including reductions in excitation and disruptions to spatial coding.

Chapter 5, in full, is material that is unpublished and being prepared for publication. It is coauthored by Quirk, Clare R., Zutshi, Ipshita, Srikanth, Sunandha, Wright, Morgan K., Parsey, Darian F., Devico Marciano, Naomie, Liu, Stanley, Fu, Maylin L., Leutgeb, Jill K., and Leutgeb, Stefan. The dissertation author was the primary researcher and author of this material.

REFERENCES

Ainge, J.A., van der Meer, M.A., Langston, R.F., and Wood, E.R. (2007). Exploring the role of context-dependent hippocampal activity in spatial alternation behavior. *Hippocampus* 17(10): 988-1002.

Allen, K., Gil, M., Resnik, E., Toader, O., Seeburg, P., and Monyer, H. (2014). Impaired path integration and grid cell spatial periodicity in mice lacking GluA1-containing AMPA receptors. *Journal of Neuroscience* 34(18): 6245-6259.

Alonso, A. and Kohler, C. (1984). A study of the reciprocal connections between the septum and the entorhinal area using anterograde and retrograde axonal transport methods in the rat brain. *Journal of Comparative Neurology* 225: 327–343.

Amaral, D.G. and Witter, M.P. (1989). The three-dimensional organization of the hippocampal formation: a review of anatomical data. *Neuroscience* 31(3): 57-91.

Aoki, Y., Igata, H., Ikegaya, Y., and Sasaki, T. (2019). The integration of goal-directed signals onto spatial maps of hippocampal place cells. *Cell Reports* 27: 1516-1527.

Anikeeva, P., Andalman, A.S., Witten, I., Warden, M., Goshen, I., Grosenick, L., Gunaydin, L.A., Frank, L.M., and Deisseroth, K. (2012). Optetrode: a multichannel readout for optogenetic control in freely moving mice. *Nature Neuroscience 15*: 163–170.

Barry, C., Hayman, R., Burgess, N., and Jeffery, K.J. (2007). Experience-dependent rescaling of entorhinal grids. *Nature Neuroscience* 10: 682–684.

Beason-Held, L.L., Rosene, D.L., Killiany, R.J., and Moss, M.B. (1999). Hippocampal formation lesions produce memory impairment in the rhesus monkey. *Hippocampus* 9(5): 562-574.

Benchenane K., Peyrache, A., Khamassi, M., Tierney, P.L., Gioanni, Y., Battaglia, F.P., and Wiener, S.I. (2010). Coherent theta oscillations and reorganization of spike timing in the hippocampal-prefrontal network upon learning. *Neuron* 66(6): 921-936.

Bender, F., Gorbati, M., Cadavieco, M.C., Denisova, N., Gao, X., Holman, C., Korotkova, T., and Ponomarenko, A. (2015). Theta oscillations regulate the speed of locomotion via a hippocampus to lateral septum pathway. *Nature Communications* 6: 8521.

Blumberg, B.J., Flynn, S.P., Barriere, S.J., Mouchati, P.R., Scott, R.C., Holmes, G.L., and Barry, J.M. (2016). Efficacy of nonselective optogenetic control of the medial septum over hippocampal oscillations: the influence of speed and implications for cognitive enhancement. *Physiological Reports* 4(23).

Boccara, C.N., Sargolini, F., Thoresen, V.H., Solstad, T., Witter, M.P., Moser, E.I., and Moser, M.B. (2010). Grid cells in pre- and parasubiculum. *Nature Neuroscience* 13(8): 987-994.

Bonnevie, T., Dunn, B., Fyhn, M., Hafting, T., Derdikman, D., Kubie, J.L., Roudi, Y., Moser, E.I., and Moser, M.B. (2013). Grid cells require excitatory drive from the hippocampus. *Nature Neuroscience* 16: 309-317.

Borhegyi, Z., Magloczky, Z., Acsady, L., and Freund, T.F. (1997). The supramammillary nucleus innervates cholinergic and GABAergic neurons in the medial septum-diagonal band of broca complex. *Neuroscience* 82(4): 1053-1065.

Borhegyi, Z., Varga, V., Szilagyi, N., Fabo, D., and Freund, T.F. (2004). Phase segregation of medial septal GABAergic neurons during hippocampal theta activity. *Journal of Neuroscience* 24(39): 8470-8479.

Bragin, A., Jando, G., Nadasdy, Z., Hetke, J., Wise, K., and Buzsaki, G. (1995). Gamma (40- 100 Hz) oscillation in the hippocampus of the behaving rat. *Journal of Neuroscience* 15(1 Pt 1): 47-60.

Brandon, M.P., Bogaard, A.R., Libby, C.P., Connerney, M.A., Gupta, K., and Hasselmo, M.E. (2011). Reduction of theta rhythm dissociates grid cell spatial periodicity from directional tuning. *Science* 332(6029): 595-599.

Brandon, M.P., Koenig, J., and Leutgeb, S. (2014 a). Parallel and convergent processing in grid cell, head-direction cell, boundary cell, and place cell networks. *Wiley Interdisciplinary Reviews: Cognitive Science* 5: 207-219.

Brandon, M.P., Koenig, J., Leutgeb, J.K., and Leutgeb, S. (2014 b). New and distinct hippocampal place codes are generated in a new environment during septal inactivation. *Neuron* 82: 789-796.

Brun, V.H., Solstad, T., Kjelstrup, K.B., Fyhn, M., Witter, M.P., Moser, E.I., and Moser, M.B. (2008). Progressive increase in grid scale from dorsal to ventral medial entorhinal cortex. *Hippocampus* 18: 1200-1212.

Buetfering, C., Allen, K., and Monyer, H. (2014). Parvalbumin interneurons provide grid cell driven recurrent inhibition in the medial entorhinal cortex. *Nature Neuroscience* 17: 710-718.

Bunce, J.G., Sabolek, H.R., and Chrobak, J.J. (2004). Intraseptal infusion of the cholinergic agonist carbachol impairs delayed-non-match-to-sample radial arm maze performance in the rat. *Hippocampus* 14: 450-459.

Burgess, N., Barry, C., and O'Keefe, J. (2007). An oscillatory interference model of grid cell firing. *Hippocampus* 17: 801-812.

Burgess, N. (2008). Grid cells and theta as oscillatory interference: theory and predictions. *Hippocampus* 18: 1157-1174.

Buzsaki, G., Leung, L.W., and Vanderwolf, C.H. (1983). Cellular bases of hippocampal EEG in the behaving rat. *Brain Research* 287(2): 139-171.

Buzsaki, G. (2002). Theta oscillations in the hippocampus. *Neuron* 33(3): 325-240.

Buzsaki, G., and Drauguhn, A. (2004). Neuronal oscillations in cortical networks. *Science* 304(5679): 1926-1929.

Buzsaki, G. (2015). Hippocampal sharp wave-ripple: a cognitive biomarker for episodic memory and planning. *Hippocampus* 25: 1073-1188.

Chen, G., Manson, D., Cacucci, F., and Wills, T.J. (2016). Absense of visual input results in the disruption of grid cell firing in the mouse. *Current Biology* 26: 2335-2342.

Chevaleyre, V. and Siegelbaum, S.A. (2010). Strong CA2 pyramidal neuron synapses define a powerful disynaptic cortico-hippocampal loop. *Neuron* 66: 560-572.

Chrobak, J.J., Stackman, R.W., and Walsh, T.J. (1989). Intraseptal administration of muscimol produces dose-dependent memory impairments in the rat. *Behavioral Neural Biology* 52(3): 357-369.

Chrobak, J.J., and Napier, T.C. (1992). Antagonism of GABAergic transmission within the septum disrupts working/episodic memory in the rat. *Neuroscience* 47(4): 833-841.

Colgin, L.L., Denninger, T., Fyhn, M., Hafting, T., Bonnevie, T., Jensen, O., Moser, M.B., and Moser, E.I. (2009). Frequency of gamma oscillations routes flow of information in the hippocampus. *Nature* 462(7271): 353-357.

Colgin, L.L. and Moser, E.I. (2010). Gamma oscillations in the hippocampus. *Physiology 25*(5): 319-329.

Colgin, L.L. (2016). Rhythms of the hippocampal network. *Nature Reviews Neuroscience* 17: 239-249.

Dannenberg, H., Pabst, M., Braganza, O., Schoch, S., Niediek, J., Bayraktar, M., Mormann, F., and Beck, H. (2015). Synergy of direct and indirect cholinergic septo-hippocampal pathways coordinates firing in hippocampal networks. *Journal of Neuroscience* 35(22): 8394-8410.

Deshmukh, S.S., Yoganarasimha, D., Voicu, H., and Knierim, J.J. (2010). Theta modulation in the medial and the lateral entorhinal cortices. *Journal of Neurophysiology* 104(2): 994-1006.

Diehl, G.W., Hon, O.J., Leutgeb, S., and Leutgeb, J.K. (2017). Grid and non-grid cells in medial entorhinal cortex represent spatial location and environmental features with complementary coding schemes. *Neuron* 94: 83-92.

Diehl, G.W., Hon, O.J., Leutgeb, S., and Leutgeb, J.K. (2019). Stability of medial entorhinal cortex representations over time. *Hippocampus* 29(3): 284-302.

Domnisoru, C., Kinkhabwala, A.A., and Tank, D.W. (2013). Membrane potential dynamics of grid cells. *Nature* 495: 199-204.

Dragoi, G., Carpi, D., Reece, M., Csicsvari, J., and Buzsaki, G. (1999). Interactions between hippocampus and medial septum during sharp waves and theta oscillation in the behaving rat. *Journal of Neuroscience* 19(14): 6191-6199.

Dragoi, G., and Buzsaki, G. (2006). Temporal encoding of place sequences by hippocampal cell assemblies. *Neuron* 50: 145-157.

Eichenbaum, H., Fortin, N.J., Ergorul, C., Wright, S.P., and Agster, K.L. (2005). Episodic recollection in animals: "If it walks like a duck and quacks like a duck...". *Learning and Motivation* 36(2):

Ferbinteanu, J., and Shapiro, M.L. (2003). Prospective and retrospective memory coding in the hippocampus. *Neuron* 40(6): 1227-1239.

Freund, T.F., and Antal, M. (1988). GABA-containing neurons in the septum control inhibitory interneurons in the hippocampus. *Nature* 336: 170-173.

Freund, T.F. (1989). GABAergic septohippocampal neurons contain parvalbumin. *Brain Research* 478(2): 375-381.

Fuchs, E.C., Neitz, A., Pinna, R., Melzer, S., Caputi, A., and Monyer, H. (2016). Local and distant input controlling excitation in layer II of the medial entorhinal cortex. *Neuron* 89(1): 194-208.

Fuhrmann, F., Justus, D., Sosulina, L., Kaneko, H., Beutel, T., Friedrichs, D., Schoch, S., Schwarz, M.K., Fuhrmann, M., and Remy, S. (2015). Locomotion, theta oscillations, and the speed-correlated firing of hippocampal neurons are controlled by a medial septal glutamatergic circuit. *Neuron* 86(5): 1253-1264.

Fyhn, M., Molden, S., S., Witter, M.P., Moser, E.I., and Moser, M.B. (2004). Spatial representation in the entorhinal cortex. *Science* 305(5688): 1258-1264.

Fyhn, M., Hafting, T., Treves, A., Moser, M.B., and and Moser, E.I. (2007). Hippocampal remapping and grid realignment in entorhinal cortex. *Nature* 446: 190-194.

Fyhn, M., Hafting, T., Witter, M.P., Moser, E.I., and Moser, M.B. (2008). Grid cells in mice. *Hippocampus* 18: 1230-1238.

Geisler, C., Diba, K., Pastalkova, E., Mizuseki, K., Royer, S., and Buzsaki, G. (2010). Temporal delays among place cells determine the frequency of population theta oscillations in the hippocampus. *Proceedings of the National Academy of Science U S A* 107(17): 7957-7962.

Gil, M., Ancau, M., Schlesiger, M.I., Neitz, A., Allen, K., De Marco, R.J., and Monyer, H. (2018). Impaired path integration in mice with disrupted grid cell firing. *Nature Neuroscience* 21: 81-91.

Giocomo, L.M., Moser, M.B., and Moser, E.I. (2011). Computational models of grid cells. *Neuron* 71(4): 589-603.

Giocomo, L.M., Stensola, T., Bonnevie, T., Van Cauter, T., Moser, M.B., and Moser, E.I. (2014). Topography of head direction cells in medial entorhinal cortex. *Current Biology* 24(3): 252-262.

Givens, B., and Olton, D.S. (1994). Local modulation of basal forebrain: effects on working and reference memory. *Journal of Neuroscience* 14(6): 3578-3587.

Gogolak, G., Stumpf, C., Petsche, H., and Sterc, J. (1968). The firing pattern of septal neurons and the form of the hippocampal theta wave. *Brain Research* 7(2): 201-207.

Gonzalez-Sulser, A., Parthier, D., Candela, A., McClure, C., Pastoll, H., Garden, D., Surmeli, G., and Nolan, M.F. (2014). GABAergic projections from the medial septum selectively inhibit interneurons in the medial entorhinal cortex. *Journal of Neuroscience* 34: 16739–16743.

Goutagny, R., Gu, N., Cavanagh, C., Jackson, J., Chabot, J.G., Quirion, R., Krantic, S., and Williams, S. (2013). Alterations in hippocampal network oscillations and theta-

gamma coupling arise before Aβ overproduction in a mouse model of Alzheimer's disease. *European Journal of Neuroscience* 37: 1896–1902.

Gu, Y., Lewallen, S., Kinkhabwala, A.A., Domnisoru, C., Yoon, K., Gauthier, J.L., Fiete, I.R., and Tank, D.W. (2018). A map-like organization of grid cells in the medial entorhinal cortex. *Cell* 175(3): 736-750.

Hafting, T., Fyhn, M., Molden, S., Moser, M., and Moser, E.I. (2005). Microstructure of a spatial map in the entorhinal cortex. *Nature* 436: 801-806.

Hafting, T., Fyhn, M., Bonnevie, T., Moser, M., and Moser, E.I. (2008). Hippocampus-independent phase precession in entorhinal grid cells. *Nature* 453: 1248-1252.

Hales, J.B., Schlesiger, M.I., Leutgeb, J.K., Squire, L.R., Leutgeb, S., and Clark, R.E. (2014). Medial entorhinal cortex lesions only partially disrupt hippocampal place cells and hippocampus-dependent place memory. *Cell Rep* 9:893-901.

Hales, J.B., Vincze, J.L., Reitz, N.T., Ocampo, A.C., Leutgeb, S., and Clark, R.E. (2018). Recent and remote retrograde memory deficit in rats with medial entorhinal cortex lesions. *Neurobiology of Learning and Memory* 155: 157-163.

Hallock, H.L., Wang, A., and Griffin, A.L. (2016). Ventral midline thalamus is critical for hippocampal-prefrontal synchrony and spatial working memory. *Journal of Neuroscience* 36(32): 8372-8389.

Harvey, C.D., Collman, F., Dombeck, D.A., and Tank, D.W. (2009). Intracellular dynamics of hippocampal place cells during virtual navigation. *Nature* 461(7266): 941-946.

Hasselmo, M.E. (2005). What is the function of hippocampal theta rhythm? Linking behavior data to phasic properties of field potential and unit recording data. *Hippocampus* 15(7): 936-949.

Hasselmo, M.E. (2008). Grid cell mechanisms and function: contributions of entorhinal persistent spiking and phase resetting. *Hippocampus* 18: 1213-1229.

Hinman, J.R., Brandon, M.P., Climer, J.R., Chapman, G.W., and Hasselmo, M.E. (2016). Multiple running speed signals in medial entorhinal cortex. *Neuron* 91: 666-679.

Jacobs, J., Weidemann, C.T., Miller, J.F., Solway, A., Burke, J.F., Wei, X.X., Suthana, N., Sperling, M.R., Sharan, A.D., Fried, I., and Kahana, M.J. (2013). Direct recordings of grid-like neuronal activity in human spatial navigation. *Nature Neuroscience* 16(9): 1188-1190.

Jadhav, S.P., Kemere, C., German, P.W., and Frank, L.M. (2012). Awake hippocampal sharp-wave ripples support spatial memory. *Science* 336: 1454–1458.

Jeewajee, A., Barry, C., O'Keefe, J., and Burgess, N. (2008). Grid cells and theta as oscillatory interference: electrophysiological data from freely moving rats. *Hippocampus* 18: 1175-1185.

Joshi, A., Salib, M., Viney, T.J., Dupret, D., and Somogyi, P. (2017). Behavior-dependent activity and synaptic organization of septo-hippocampal GABAergic neurons selectively targeting the hippocampal CA3 area. *Neuron* 96:1342-1357.

Jung, M.W., Wiener, S.I., and McNaughton, B.L. (1994). Comparison of spatial firing characteristics of units in dorsal and ventral hippocampus of the rat. *Journal of Neuroscience* 14(12): 7347-7356.

Justus, D., Dalugge, D., Bothe, S., Fuhrmann, F., Hannes, C., Kaneko, H., Friedrichs, D., Sosulina, L., Schwarz, I., Elliott, D.A., Schoch, S., Bradke, F., Schwarz, M.K., and Remy, S. (2017). Glutamatergic synaptic integration of locomotion speed via septoentorhinal projections. *Nature Neuroscience* 20(1): 16-19.

Jutras, M.P., Fries, P., and Buffalo, E.A. (2009). Gamma-band synchronization in the macaque hippocampus and memory formation. *Journal of Neuroscience* 29: 12521–12531.

Kamondi, A., Acsady, L., Wang, X.J., and Buzsaki, G. (1998). Theta oscillations in somata and dendrites of hippocampal pyramidal cells in vivo: activity-dependent phase-precession of action potentials. *Hippocampus* 8(3): 244-261.

Kennedy, P.J., and Shapiro, M.L. (2009). Motivational states activate distinct hippocampal representations to guide goal-directed behaviors. *Proceedings of the National Academy of Science U S A* 106(26): 10805-10810.

Killian, N.J., Jutras, M.J., and Buffalo, E.A. (2012). A map of visual space in the primate entorhinal cortex. *Nature* 491(7426): 761-764.

King, C., Reece, M., and O'Keefe, J. (1998). The rhythmicity of cells of the medial septum/diagonal band of Broca in the awake freely moving rate: relationships with behaviour and hippocampal theta. *European Journal of Neuroscience* 10(2): 464-477.

Kjelstrup, K.B., Solstad, T., Brun, V.H., Hafting, T., Leutgeb, S., Witter, M.P., Moser, E.I., and Moser, M.B. (2008). Finite scale of spatial representation in the hippocampus. *Science* 321(5885): 140-143.

Knierim, J.J. (2002). Dynamic interactions between local surface cues, distal landmarks, and intrinsic circuitry in hippocampal place cells. *Journal of Neuroscience* 22: 6254-6264.

Koenig, J., Linder, A.N., Leutgeb, J.K., and Leutgeb, S. (2011). The spatial periodicity of grid cells is not sustained during reduced theta oscillations. *Science* 332(6029): 592-595.

Kramis, R., Vanderwolf, C.H., and Bland, B.H. (1975). Two types of hippocampal rhythmical slow activity in both the rabbit and the rat: Relations to behavior and effects of atropine, diethyl ether, urethane, and pentobarbital. *Experimental Neurology* 49(1.1): 58–85.

Kraus, B.J., Robinson, R.J., White, J.A., Eichenbaum, H., and Hasselmo, M.E. (2013). Hippocampal "time cells": time versus path integration. *Neuron* 78: 1090-1101.

Kraus, B.J., Brandon, M.P., Robinson, R.J. 2nd, Connerney, M.A., Hasselmo, M.E., and Eichenbaum, H. (2015). During running in place, grid cells, integrate elapsed time and distance run. *Neuron* 88(3): 578-589.

Kropff, E., Carmichael, J.E., Moser, M., and Moser, E.I. (2015). Speed cells in the medial entorhinal cortex. *Nature* 523: 419-424.

Krupic, J., Bauza, M., Burton, S., Barry, C., and O'Keefe, J. (2015). Grid cell symmetry is shaped by environmental geometry. *Nature* 518: 232-235.

Langston, R.F., Ainge, J.A., Couey, J.J., Canto, C.B., Bjerknes, T.L., Witter, M.P., Moser, E.I., and Moser, M.B. (2010). Development of the spatial representation system in the rat. *Science* 328(5985): 1576-1580.

Lee, M.G., Chrobak, J.J., Sik, A., Wiley, R.G., and Buzsaki, G. (1994). Hippocampal theta activity following selective lesion of the septal cholinergic system. *Neuroscience* 62(4): 1033-1047.

Leutgeb, S., and Mizumori, S.J.Y. (1999). Excitotoxic septal lesions result in spatial memory deficits and altered flexibility of hippocampal single-unit representations. *Journal of Neuroscience* 19(15): 6661-6672.

Leutgeb, S., Leutgeb, J.K., Treves, A., Moser, M.B., and Moser, E.I. (2004). Distinct ensemble codes in hippocampal areas CA3 and CA1. *Science* 305(5688): 1295-1298.

Leutgeb, S., Leutgeb, J.K., Barnes, C.A., Moser, E.I., McNaughton, B.L., and Moser, M.B. (2005). Independent codes for spatial and episodic memory in hippocampal neuronal ensembles. *Science* 309(5734): 619-623.

MacDonald, C.J., Lepage, K.Q., Eden, U.T., and Eichenbaum, H. (2011). Hippocampal "time cells" bridge the gap in memory for discontiguous events. *Neuron* 71(4): 737-749.

Mahut, M., Zola-Morgan, S., and Moss, M. (1982). Hippocampal resections impair associative learning and recognition memory in the monkey. *Journal of Neuroscience* 2(9): 1214-1220.

Malkova, L., and Mishkin, M. (2003). One-trial memory for object-place associations after separate lesions of hippocampus and posterior parahippocampal region in the monkey. *Journal of Neuroscience* 23(5): 1956-1965.

Manns, J.R., Zilli, E.A., Ong, K.C., Hasselmo, M.E., and Eichenbaum, H. (2007). Hippocampal CA1 spiking during encoding and retrieval: Relation to theta phase. *Neurobiology of Learning and Memory* 87(1): 9-20.

McNaughton, B.L., Barnes, C.A., Gerrard, J.L., Gothard, K., Jung, M.W., Knierim, J.J., Kudrimoti, H., Qin, Y., Skaggs, W.E., Suster, M., and Weaver, K.L. (1996). Deciphering the hippocampal polyglot: the hippocampus as a path integration system. *Journal of Experimental Biology* 199(Pt 1): 173-185.

McNaughton, B.L., Battaglia, F.P., Jensen, O., Moser, E.I., and Moser, M.B. (2006 a). Path integration and the neural basis of the 'cognitive map'. *Nature Reviews Neuroscience* 7: 663-678.

McNaughton, N., Ruan, M., and Woodnorth, M.A. (2006 b). Restoring theta-like rhythmicity in rats restores initial learning in the Morris water maze. *Hippocampus* 16(12): 1102-1110.

Mehta, M.R., Lee, A.K., and Wilson, M.A. (2002). Role of experience and oscillations in transforming a rate code into a temporal code. *Nature* 417(6890): 741-746.

Melzer, S., Michael, M., Caputi, A., Eliava, M., Fuchs, E.C., Whittington, M.A., and Monyer, H. (2012). Long-range-projecting GABAergic neurons modulate inhibition in hippocampus and entorhinal cortex. *Science* 335(6075): 1506-1510.

Miao, C., Cao, Q., Moser, M.B., and Moser, E.I. (2017). Parvalbumin and somatostatin interneurons control different space-coding networks in the medial entorhinal cortex. *Cell* 171(3): 507-521.

Mishkin, M. (1978). Memory in monkeys severely impaired by combined but not by separate removal of amygdala and hippocampus. *Nature* 273(5660): 297-298.

Mitchell, S.J., and Ranck, J.B. Jr. (1980). Generation of theta rhythm in medial entorhinal cortex of freely moving rats. *Brain Research* 189(1): 49-66.

Mitchell, S.J., Rawlins, J.N., Steward, O., and Olton, D.S. (1982). Medial septal area lesions disrupt theta rhythm and cholinergic staining in medial entorhinal cortex and produce impaired radial arm maze behavior in rats. *Journal of Neuroscience* 2(3): 292-302.

Mizumori, S.J.Y., Perez, G.M., Alvarado, M.C., Barnes, C.A., and McNaughton, B.L. (1990). Reversible inactivation of the medial septum differentially affects two forms of learning in rats. *Brain Research*, 528: 12-20.

Morris, R.G.M., Garrud, P., Rawlins, J.N.P., and O'Keefe, J. (1982). Place navigation impaired in rats with hippocampal lesions. *Nature* 297: 681-683.

Moss, M., Mahut, H., and Zola-Morgan, S. (1981). Concurrent discrimination learning of monkeys after hippocampal, entorhinal, or fornix lesions. *Journal of Neuroscience* 1(3): 227-240.

Muller, R.U., and Kubie, J.L. (1987). The effects of changes in the environment on the spatial firing of hippocampal complex-spike cells. *Journal of Neuroscience* 7(7): 1951–1968.

Muller, R.U., Bostock, E., Taube, J.S., and Kubie, J.L. (1994). On the directional firing properties of hippocampal place cells. *Journal of Neuroscience* 14 (12): 7235-7251.

Nakazawa, K., Quirk, M.C., Chitwood, R.A., Watanabe, M., Yeckel, M.F., Sun, L.D., Kato, A., Carr, C.A., Johnston, D., Wilson, M.A., Tonegawa, S. (2002). Requirement for hippocampal CA3 NMDA receptors in associative memory recall. *Science* 297(5579): 211-218.

Newman, E.L., Gillet, S.N., Climer, J.R., and Hasselmo, M.E. (2013). Cholinergic blockade reduces theta-gamma phase amplitude coupling and speed modulation of theta-frequency consistent with behavioral effects on encoding. *Journal of Neuroscience* 33(50): 19635-19646.

Newman, E.L., Climer, J.R., and Hasselmo, M.E. (2014). Grid cell spatial tuning reduced following systemic muscarinic receptor blockade. *Hippocampus* 24(6): 642-655.

O'Keefe, J. (1976). Place units in the hippocampus of the freely moving rat. *Experimental Neurology* 51(1): 78-109.

O'Keefe, J., and Reece, M.L. (1993). Phase relationship between hippocampal place units and the EEG theta rhythm. *Hippocampus* 3(3): 317-330.

Pang, K.C.H., Nocera, R., Secor, A.J., and Yoder, R.M. (2001). GABAergic septohippocampal neurons are not necessary for spatial memory. *Hippocampus* 11: 814-827.

Parkinson, J.K., Murray, E.A., and Mishkin, M. (1988). A selective mnemonic role for the hippocampus in monkeys: memory for the location of objects. *Journal of Neuroscience* 8(11): 4159-4167.

Parron, C., Poucet, B., and Save, E. (2004). Entorhinal cortex lesions impair the use of distal but not proximal landmarks during place navigation in the rat. *Behavioral Brain Research* 154(2): 345-352.

Pastalkova, E., Itskov, V., Amarasingham, A., and Buzsaki, G. (2008). Internally generated cell assembly sequences in the rat hippocampus. *Science* 321 (5894): 1322-1327.

Pastoll, H., Solanka, L., van Rossum, M.C.W, and Nolan, M.F. (2013). Feedback inhibition enables theta-nested gamma oscillations and grid firing fields. *Neuron* 77: 141-154.

Penfield, W. (1952). Memory mechanisms. *American Medical Association Archive of Neurology and Psychiatry* 67(2): 178-198.

Penfield, W., and Milner, B. (1958). Memory deficit produced by bilateral lesions in the hippocampal zone. *American Medical Association Archive of Neurology and Psychiatry* 79(5): 475-497.

Perez-Escobar, J.A., Kornienko, O., Latuske, P., Kohler, L., and Allen, K. (2016). Visual landmarks sharpen grid cell metric and confer context specificity to neurons of the medial entorhinal cortex. *Elife* 5. pii: e16937. doi: 10.7554/eLife.16937.

Petsche, H., Stumpf, C., and Gogolak, G. (1962). The significance of the rabbit's septum as a relay station between the midbrain and the hippocampus. I. The control of hippocampus arousal activity by the septum cells. *Electroencephalography and Clinical Neurophysiology* 14: 202-211.

Place, R., Farovik, A., Brockman, M., and Eichenbaum, H. (2016). Bidirectional prefrontal-hippocampal interactions support context-guided memory. *Nature Neuroscience* 19(8): 992-994.

Quirk, G.J., Muller, R.U., Kubie, J.L., and Ranck, J.B. Jr. (1992). The positional firing properties of medial entorhinal neurons: description and comparison with hippocampal place cells. *Journal of Neuroscience* 12(5): 1945-1963.

Racine, R.J., and Kimble, D.P. (1965). Hippocampal lesions and delayed alternation in the rat. *Psychonomic Science* 3(1-12): 285-286.

Ramirez, S., Liu, X., Lin, P.A., Suh, J., Pignatelli, M., Redondo, R.L., Ryan, T.J., and Tonegawa, S. (2013). Creating a false memory in the hippocampus. *Science* 341(6144): 387-391.

Raudies, F., Brandon, M.P., Chapman, G.W., and Hasselmo, M.E. (2015). Head direction is coded more strongly than movement direction in a population of entorhinal neurons. *Brain Research* 1621: 355-367.

Remondes, M., and Wilson, M.A. (2013). Cingulate-hippocamus coherence and trajectory coding in a sequential choice task. *Neuron* 80: 1277-1289.

Robinson, J., Manseau, F., Ducharme, G., Amilhon, B., Vigneault, E., El Mestikawy, S., and Williams, S. (2016). Optogenetic activation of septal glutamatergic neurons drive hippocampal theta rhythms. *Journal of Neuroscience* 36 (10): 3016-3023.

Robinson, N.T.M., Priestley, J.B., Rueckemann, J.W., Garcia, A.D., Smeglin, V.A., Marino, F.A., and Eichenbaum, H. (2017). Medial entorhinal cortex selectively supports temporal coding by hippocampal neurons. *Neuron* 94(3): 677-688.

Rolls, E.T., and Kesner, R.P. (2006). A computational theory of hippocampal function, and empirical tests of the theory. *Progress in Neurobiology* 79(1): 1-48.

Sabariego, M., Schnonwald, A., Boublil, B.L., Zimmerman, D.T., Ahmadi, S., Gonzalez, N., Leibold, C., Clark, R.E., Leutgeb, J.K., and Leutgeb, S. (2019). Time cells in the hippocampus are neither dependent on mEC inputs nor necessary for spatial working memory. *Neuron* 102(6): 1235-1248.

Sargolini, F., Fyhn, M., Hafting, T., McNaughton, B.L., Witter, M.P., Moser, M.B., and Moser, E.I. (2006). Conjunctive representation of position, direction, and velocity in entorhinal cortex. *Science* 312(5774): 758-762.

Schlesiger, M.I., Cannova, C.C., Boublil, B.L., Hales, J.B., Mankin, E.A., Brandon, M.P., Leutgeb, J.K., Leibold, C., and Leutgeb, S. (2015). The medial entorhinal cortex is necessary for temporal organization of hippocampal neuronal activity. *Nature Neuroscience* 18(8): 1123-1132.

Schmitzer-Torbert, N., Jackson, J., Henze, D., Harris, K., and Redish, A.D. (2005). Quantitative measures of cluster quality for use in extracellular recordings. *Neuroscience* 131(1): 1-11.

Schomburg, E.W., Fernandez-Ruiz, A., Mizuseki, K., Berenyi, A., Anastassiou, C.A., Koch, C., and Buzsaki, G. (2014). Theta phase segregation of input-specific gamma patterns in entorhinal-hippocampal networks. *Neuron* 84(2): 470-485.

Scoville, W.B., and Milner, B. (1957). Loss of recent memory after bilateral hippocampal lesions. *Journal of Neurology, Neurosurgery, and Physiciatry* 20(1): 11-21.

Shirvalkar, P.R., Rapp, P.R., and Shapiro, M.L. (2010). Bidirectional changes to hippocampal theta-gamma comodulation predict memory for recent spatial episodes. *Proceedings of the National Academy of Science U S A* 107(15): 7054-7059.

Siegle, J.H., and Wilson, M.A. (2014). Enhancement of encoding and retrieval functions through theta phase-specific manipulation of hippocampus. *Elife* 3:e03061.

Skaggs, W.E., and McNaughton, B.L. (1996). Replay of neuronal firing sequences in rat hippocampus during sleep following spatial experience. *Science* 271(5257): 1870-1873.

Skaggs, W.E., McNaughton, B.L., Wilson, M.A., and Barnes, C.A. (1996). Theta phase precession in hippocampal neuronal populations and the compression of temporal sequences. *Hippocampus* 6: 149-172.

Smith, H.R., and Pang, K.C.H. (2005). Orexin-saporin lesions of the medial septum impair spatial memory. *Neuroscience* 132: 261-271.

Solstad, T., Boccara, C.N., Kropff, E., Moser, M.B., and Moser, E.I. (2008). Representation of geometric borders in the entorhinal cortex. *Science* 322(5909): 1865-1868.

Squire, L.R., and Zola-Morgan, S. (1991). The medial temporal lobe memory system. *Science* 253(5026): 1380-1386.

Squire, L.R. (1992). Declarative and nondeclarative memory: multiple brain systems supporting learning and memory. *Journal of Cognitive Neuroscience* 4(3): 232-243.

Steffenach, H.A., Witter, M., Moser, M.B., and Moser, E.I. (2005). Spatial memory in the rat requires the dorsolateral band of the entorhinal cortex. *Neuron* 45 (2): 301-313.

Steward, O., and Scoville, S.A. (1976). Cells of origin of entorhinal cortical afferents to the hippocampus and fascia dentata of the rat. *Journal of Comparative Neurology* 169(3): 347-370.

Stewart, M., and Fox, S.E. (1990). Do septal neurons pace the hippocampal theta rhythm? *Trends in Neuroscience* 13(5): 163-169.

van Strien, N.M., Cappaert, N.L., and Witter, M.P. (2009). The anatomy of memory: an interactive overview of the parahippocampal-hippocampal network. *Nature Reviews Neuroscience* 10(4): 272-282.

Sun, C., Kitamura, T., Yamamoto, J., Martin, J., Pignatelli, M.,Kitch, L.J., Schnitzer, M.J., and Tonegawa, S. (2015). Distinct speed dependence of entorhinal island and ocean cells, including respective grid cells. *Proceedings of the National Academy of Science U S A* 112(30): 9466-9471.

Taube, J.S., Muller, R.U., and Ranck, J.B. Jr. (1990). Head-direction cells recorded from the postsubiculum in freely moving rats. I. Description and quantitative analysis. *Journal of Neuroscience* 10(2): 420-435.

Taube, J.S. (2007). The head direction signal: origins and sensory-motor integration. *Annual Review of Neuroscience* 30: 181-207.

Toth, K., Borhegyi, Z., and Freund, T.F. (1993). Postsynaptic targets of GABAergic hippocampal neurons in the medial septum-diagonal band of broca complex. *Journal of Neuroscience* 13(9): 3712-3724.

Tort, A.B.L., Komorowski, R.W., Manns, J.R., Kopell, N.J., and Eichenbaum, H. (2009). Theta-gamma coupling increases during the learning of item-context associations. *Proceedings of the National Academy of Science U S A* 106 (49): 20942-20947.

Tulving, E. (1972). Episodic and semantic memory. *Organization of memory 1*: 381-403.

Unal, G., Joshi, A., Viney, T.J., Kis, V., and Somogyi, P. (2015). Synaptic targets of medial septal projections in the hippocampus and extrahippocampal cortices of the mouse. *Journal of Neuroscience* 35(48): 15812-15826.

Vandecasteele, M., Varga, V., Berenyi, A., Papp, E., Bartho, P., Venance, L., Freund, T.F., and Buzsaki, G. (2014). Optogenetic activation of septal cholinergic neurons suppresses sharp wave ripples and enhances theta oscillations in the hippocampus. *Proceedings of the National Academy of Science U S A* 111 (37): 13535-13540.

Vanderwolf, C.H. (1969). Hippocampal electrical activity and voluntary movement in the rat. *Electroencephalography and Clinical Neurophysiology* 26(4): 407-18.

Wang Y., Romani, S., Lustig, B., Leonardo, A., and Pastalkova, E. (2015). Theta sequences are essential for internally generated hippocampal firing fields. *Nature Neuroscience* 18(2): 282-288.

Wetzel, W., Ott, T., and Amtthies, H. (1977). Post-training hippocampal rhythmic slow activity ("theta") elicited by septal stimulation improves memory consolidation in rats. *Behavioral Biology* 21(1):32-40.

Wills, T.J., Cacucci, F., Burgess, N., and O'Keefe, J. (2010). Development of the hippocampal cognitive map in preweanling rats. *Science* 328: 1573-1576.

Winson, J. (1978). Loss of hippocampal theta rhythm results in spatial memory deficit in the rat. *Science* 201(4351): 160-163.

Winter, S.S., Clark, B.J., and Taube, J.S. (2015). Spatial navigation. Disruption of the head direction cell network impairs the parahippocampal grid cell signal. *Science* 347(6224): 870-874.

Winter, S.S., Mehlman, M.L., Clark B.J., and Taube, J.S. (2015). Passive transport disrupts grid signals in the parahippocampal cortex. *Current Biology* 25 (19): 2493-2502.

Witter, M.P., Griffioen, A.W., Jorritsma-Byham, B., and Krijnen, J.L. (1988). Entorhinal projections to the hippocampal CA1 region in the rat: an underestimated pathway. *Neuroscience Letters* 85(2): 193-198.

Witter, M.P. (2007). The performant path: projections from the entorhinal cortex to the dentate gyrus. *Progress in Brain Research* 163: 43-61.

Wood, E.R., Dudchenko, P.A., Robitsek, R.J., Eichenbaum, H. (2000). Hippocampal neurons encode information about different types of memory episodes occurring in the same location. *Neuron* 27(3): 623-633.

Yamamoto, J., Suh, J., Takeuchi, D., and Tonegawa, S. (2014). Successful execution of working memory linked to synchronized high-frequency gamma oscillations. *Cell* 157: 845-857.

Yartsev, M.M., Witter, M.P., and Ulanovsky, N. (2011). Grid cells without theta oscillations in the entorhinal cortex of bats. *Nature* 479 (7371): 103-107.

Yeckel, M.F., and Berger, T.W. (1990). Feedforward excitation of the hippocampus by afferents from the entorhinal cortex: Redefinition of the role of the trisynaptic pathway. *Proceedings of the National Academy of Science* 87: 5832-5836.

Yoder, R.M., and Pang, K.C.H. (2005). Involvement of GABAergic and cholinergic medial septal neurons in hippocampal theta rhythm. *Hippocampus* 15: 381-392.

Zhang, S.J., Ye, J., Miao, C., Tsao, A., Cerniauskas, I., Ledergerber, D., Moser, M.B., and Moser, E.I. (2013). Optogenetic dissection of entorhinal-hippocampal functional connectivity. *Science* 340(6128): 1232627.

Zheng, C., Bieri, K.W., Hwaun, E., and Colgin, L.L. (2016). Fast gamma rhythms in the hippocampus promote encoding of novel object-place pairings. *eNeuro* 3(2). ENEURO.0001-16.2016.

Zola-Morgan, S., Squire, L.R., and Amaral, G.G. (1986). Human amnesia and the medial temporal region enduring memory impairment following a bilateral lesion limited to field CA1 of the hippocampus. *Journal of Neuroscience* 6(10): 1950-2967.

Zutshi, I., Brandon, M.P., Fu, Maylin, L., Donegan, M.L., Leutgeb, J.K., and Leutgeb, S. (2018a). Hippocampal neural circuits respond to optogenetic pacing of theta frequencies by generating accelerated oscillation frequencies. *Current Biology* 28(8): 1179-1188.

Zutshi, I., Fu, M.L., Lilascharoen, V., Leutgeb, J.K., Lim, B., and Leutgeb, S. (2018b). Recurrent circuits within medial entorhinal cortex superficial layers support grid cell firing. *Nature Communications* 9(1): 3701.